Rotor Design and Performance Evaluation of a PM-assisted Reluctance Synchronous Traction Machine

By

Sguda Enock Sibande

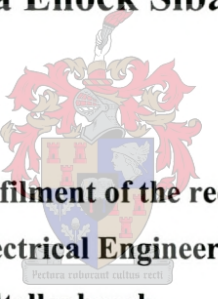

Thesis presented in partial fulfilment of the requirements for the degree of Masters of Science in Electrical Engineering at the University of Stellenbosch

Supervisor: Prof. M.J. Kamper

April 2005

Declaration

I, the undersigned, hereby declare that the work contained in this thesis is my own original work and that I have not previously in its entirety or in part submitted it at any other University for a degree.

Place: Stellenbosch

Thesis abstract

The thesis describes the optimum rotor design and performance of a 110kW Permanent-Magnet assisted (PM-assisted) Reluctance Synchronous traction Machine (RSM) using bonded permanent magnet sheets. Particular attention is given to the performance of the machine drive in the flux-weakening speed region. A detail explanation is given of the finite-element design optimisation, the basic principles of operation and the control-design of the PM-assisted RSM drive. A theoretical torque comparison of the PM-assisted RSM, the standard RSM and the induction machine is also done. The measured and calculated results of the different drives are presented and analysed in detail. It is concluded that the performance of the PM-assisted RSM in terms of torque, voltage and power factor compares favourably well with that of the induction machine in both the constant torque and flux-weakening speed regions. Furthermore, it is shown that the temperature rise of the stator winding of the PM-assisted RSM is lower than that of the RSM with both machines at the same load.

Opsomming

Die tesis beskryf die optimum rotor ontwerp en vermoë van 'n 110 kW Permanent-Pagnet-ondersteunde (PM-ondersteunde) Reluktansie Sinchroon Masjien (RSM) trekkrag aandryfstelsel. Spesifieke aandag word gegee aan die vermoë van die aandryfstelsel in die vloedverswakking spoedgebied. 'n Volledige verduideliking word gegee van die eindige-element ontwerp optimering, die basiese beginses van werking en die beheer-ontwerp van die PM-ondersteunde RSM aandryfstelsel. 'n Teoretiese vergelyking van die draaiumoment-vergelyking van die PM-ondersteunde RSM, die standard RSM en die induksmasjien word gedoen. Die berekende en gemete resultate van die verskillende aandryfstelsels word in detail aangebied en ge-analiseer. Dit is gevind dat die vermoë van die PM-ondersteunde RSM in teme van draaimoment, spanning en arbeidsfaktor gunstig vergelyk met dit van die induksiemasjien in beide die konstante draaimoment en vloedverswakking spoedgebiede. Verder word getoon dat die temperatuur-styging van die statorwinding van die PM-ondersteunde RSM laer is as die van die RSM, met deide masjiene by die selfde las

Acknowledgments

The author wishes to express his gratitude to the following people who have contributed to the success of this project.

Professor M.J Kamper for his sound supervision and extended constant encouragement through the entire project. I would also like to express my sincere appreciation for all his efforts in ensuring the availability of financial resources and in particular from the NRF and Spoornet.

Mr Willie Coetze for his support and encouragement through the entire project.

Dr Rongie Wang for all his theoretical and technical assistance especially on the Finite Element Analysis. I also extend my appreciation to Mr Pieter Fick and Mr Jacko Serdyn for their assistance with the DSP controller.

The mechanical workshop and the SMD for their assistance in assembling the machine and setting the water-cooling system. Mr Francois Rossouw for his genuine assistance in particular with assembling the protection circuit. I also extend my appreciation to the assistance rendered by Mr Andrew Dale regarding programming the EPLD.

To my group members (also bible study fellows), Mr Y Ai and Mr ET Rakgati for their encouragement.

To my family and to all my friends for their continuous support.

To Nonto Mfeka, I sincerely value the courage you have, the time and the support you have given me through all the difficult times I had.

May God be with you all.

Dedications

To my mother.

Table of contents

List of Figures:

Tables

Glossary

θ	Rotor angle, **rad**
ϕ	Current angle, **deg**
γ	Torque angle, **deg**
μ	Equivalent permeability, **H/m**
λ_s	Stator space phasor flux linkage, **Wb**
λ_d, λ_q	*d* and *q*-axis fundamental stator flux linkage components, **Wb**
λ_{abc}	Instantaneous values of total flux linkages of phases *a*, *b* and *c*, **Wb**
λ_{abc1}	Instantaneous values of fundamental total flux linkages of phases *a*, *b* and *c*, **Wb**
λ_{abc3}	Instantaneous values of 3rd harmonic flux linkages of phases *a*, b, *c*, **Wb**
λ_0	Instantaneous value of zero sequence flux linkages of phases *a*, *b*, *c*, **Wb**
λ_{pm}	Permanent magnet flux component, **Wb**
σ	RSM inductance ratio (L_d / L_q)
σ_m	PM assisted rotor RSM inductance ratio (L_d / L_q)
ω_e	Electrical speed, **rad/s**
ω_m	Mechanical speed, **rad/s**
ν	RSM current ratio (I_q/I_d)
ν_m	PM assister rotor RSM current ratio (I_q/I_d)
ζ	Integration variable
$\beta_{eq}, \beta_m, \beta_L$	Equivalent, mechanical and load friction coefficients respectively
L_d	*d*-axis inductance, **H**
M_d	*d*-axis mutual inductance, **H**
L_q	*q*-axis inductance, **H**
M_q	*q*-axis mutual inductance, **H**
L_m	The inductance due to permanent magnets, **H**
K	skew factor
V_d	Steady state *d*-axis voltage, **V**
V_q	Steady state *q*-axis voltage, **V**
V_s	Space phasor of stator voltage, **V∠rad**

$\mathbf{V_s}$	Peak phasor of stator voltage amplitude
E_d	*d*-axis speed voltage, **V**
E_q	*q*-axis speed voltage, **V**
L_e	Leakage inductance
R_c	Per phase core resistance, **Ω**
R_s	Per phase stator resistance, **Ω**
I_d	*d*-axis current, **A**
I_q	*q*-axis current, **A**
T	Torque, **Nm**
P	Number of pole pairs
P_{cu}	Copper losses, **W**
P_f	Power factor
P_{fm}	PM assisted rotor RSM power factor
I_s	Space phasor of stator current, **A∠rad**
$\mathbf{I_{sl}}$	Peak phasor current amplitude
J_m, J_L	Mechanical and load inertia coefficients
J_{eq}	Equivalent inertia coefficient
H_c	Coercive force
H_m	PM magnetic field strength, **At/m**
H_g	Magnetic field strength in the air gap , **At/m**
S	Apparent power, **VA**
l	Axial stack length, **m**
l_e	Average coil end length, **m**
n_a	Number of parallel circuits
A_{cu}	Active stator slot copper area, $\mathbf{m^2}$
z	Number of conductors per slot
$\frac{A_{cu}}{z}$	Stator conductor active copper area
ρ_{20}	Copper resistivity at 20^0C
N_{ph}	Number of turns in series
B_{mt}, B_{my}	The maximum flux densities in the teeth and yoke respectively, $\mathbf{Wb/m^2}$
M_t, M_y	The iron masses of the teeth and yoke respectively, $\mathbf{Wb/m^2}$

List of abbreviations

IM	Induction machine
RSM	Reluctance synchronous machine
PM-assisted RSM/PM-RSM	Permanent magnet assisted reluctance synchronous machine
FEA	Finite element analysis
PF	Power factor
PF-M	Measured power factor
SMD	Central mechanical services
RTD	Resistance temperature detector
Pm	Input power into the machine
Pdc	Inverter DC input power

Definition of terms as used in the thesis

Base speed (1200 rpm)	The speed obtained under given conditions when full traction motor supply voltage is reached
Rated speed (1500 rpm)	The speed at a guaranteed rating of a machine
Maximum working speed	The highest rotational speed assigned to the traction motor by the manufacture
Maximum test speed (2800 rpm)	The highest test rotational speed

1. INTRODUCTION

THE distinct features of induction machines (IM) such as low cost, good performance over wide speed range and robust design have made them popular in variable speed ac drive. Despite these attractive advantages induction machines exhibits higher winding losses and requires relative complicated controllers. These inherent disadvantages of the IM has sought research in alternate direction with a goal of finding an electric motor configuration and the corresponding controller to yield:

- High torque density
- Low winding losses per torque
- High kW/kVA ratio
- Fast torque and speed dynamics
- Wide speed range control
- Simplicity and robustness of motion controller and
- Low overall cost and weight

A series of recent research has shown that distributed anisotropy rotor reluctance synchronous machines (RSM) and drives with advanced control are promising candidates to meet the above mentioned goals in variable speed drives. The RSM is an AC machine with a standard, non-salient, three-phase stator and an unexcited rotor with magnetic asymmetry. No windings, brushes or permanent magnets are used on the rotor, which makes the RSM a simple and robust electric machine.

The RSM motor is characterised by low torque density and poor power factor when designed for single-speed, open loop operations. Current research, however, shows that the RSM under current vector control, that is using an inverter and a closed-loop control system, and with an optimum designed stator and rotor has attractive torque and power factor characteristics [1-2].

This thesis focuses on the RSM with normal laminated, cage-less rotors with limited number of punched flux barriers and saturation bridges for traction applications. Axially laminated rotor structures are not considered due to, amongst others, difficult construction. Typical normal laminated RSM rotor cross sections are shown in Fig. 1.1 below.

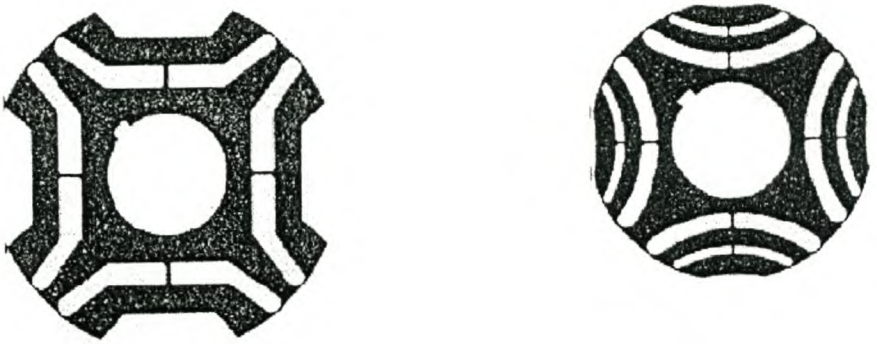

(a) (b)

Figure 1.1. Typical normal laminated RSM rotor structures

1.1 Advantages and disadvantages of RSM traction motors [3]

There are many advantages of using the RSM specifically for traction applications. Without brushes and rotor windings the RSM requires less maintenance and is in principle more reliable than wound-rotor or cage-rotor machines. Without the cage windings, the manufacturing cost of the RSM will also be potentially less on mass production. There are practically little losses on the rotor if it is designed correctly. All the losses are on the stator. The cooling of the machine therefore is in principle much less of a problem than in the case of wound-rotor or cage-rotor machines. The latter is a very important advantage when it comes to traction applications. Bearing currents due to the inverter switching seems also to be less in RSMs than in cage or wound rotor machines [6]. In terms of bearing failure and thus maintenance the latter,

if true, will be an important advantage. Another important advantage of the flux barrier rotor RSM is the relative high torque and power density capability of the machine. This is an advantage in terms of weight and volume for the traction motor. Finally, current vector control or flux and torque control of the RSM is relatively simple, as no rotor parameters have to be identified.

The use of a RSM as a traction motor, however, also has disadvantages. As the RSM is a synchronous machine an inverter is required for each traction machine that is used on the electric vehicle or locomotive. It is not possible, as in the case of asynchronous machines, that one inverter supplies for example two or four traction motors. The main disadvantage of the RSM is the relative low power factor of the machine. It could be typically 75% that of the asynchronous machine. The low power factor affects negatively the kVA rating and thus the cost of the inverter. It will also affect the high speed operating range of the machine. Another disadvantage of the flux barrier rotor RSM is the restriction on the maximum rotational speed of the rotor. The iron pieces of the rotor lamination are held together by means of ribs and webs and these ribs and webs must be as thin as possible to improve the performance of the machine. This disadvantage becomes important in large, high speed RSMs. Finally, it is sometimes mentioned that the RSM needs a small air-gap length to have a good performance. While a small air-gap length improves the performance of the RSM, a large air-gap length affects negatively the performance of the RSM in very much the same way as in asynchronous machines [4]. In this regard, thus there is no particular disadvantage of using the RSM.

1.2 Optimum design of the RSM

To improve the performance of the RSM an overall (stator and rotor) design optimisation is necessary. It is important to note that with the RSM under current vector control a cage-rotor is not necessary [6]. Design optimisations are done using

finite element analysis and optimisation algorithms, to maximise various output performance parameters of the RSM [2]. This evaluates the true performance capability of the RSM.

1.3 Optimum (vector) control of the RSM

Vector control means, in general, separate or decoupled flux linkage and torque control yielding fast torque response and through adequate reference flux linkage-torque relationship, high energy conversion rates [5].

The optimum control of the RSM is equally important to improve the performance of the machine. The special placement of the current in the machine with respect to the rotor can be optimally controlled to ensure, for example, minimum current or minimum apparent power for any load condition [6]. The current angle is defined as the electrical space angle between the current phasor and the rotor *d*-axis. It is varied to minimise the phase current of the RSM for a given torque. In general, the locus of minimum current per torque shows that a constant current angle of about 65^0 can be used for all loads.

Constant current angle control means that the machine is controlled the same way as a series DC machine where the flux changes with the load. The current angle and current amplitude can be controlled to ensure best performance over the entire speed range of the machine. Below base speeds a constant current angle for maximum torque per ampere could be used. For speeds higher than base speed the current angle can be advanced, equivalent to reducing the flux, to minimise the apparent power.

1.4 Performance capability in the medium power range

An important question arises as to what the performance capability of the RSM is in the medium and higher power levels. To investigate this, RSMs were optimised in asynchronous machine frames from 5.5 to 250 kW [3]. The RSMs were optimised for the same amount of copper losses and air-gap lengths as that of standard asynchronous machines. The torque densities of the RSMs and asynchronous machines versus outer diameters were analysed. It was found that the torque density of the RSM increases with frame size and that the RSM outperforms the torque density of the asynchronous machine. On the other hand, it was found that the power factor of the RSM is relatively low compared to the asynchronous machine.

1.5 Problem statement

A comparative study on the performance of the RSM and IM at a 110 kW power level for traction applications was carried out by Germishuizen [7]. The finite element cross sectional diagram of the 110 kW RSM is shown in Fig. 1.2 with the rotor flux barriers, webs and ribs. It was found that the RSM compares favourably well with the IM in terms of torque and voltage in the constant torque region. It was also found that in general, the RSM has a low power factor compared to the IM.

The torque versus speed performance found for the 110 kW RSM and IM is shown in Fig. 1.3 below [7]. It is clear that up to rated speed, which is 1500 rpm, the torque performance of the RSM and IM compares well. However, in the flux-weakening region, the torque of the RSM vastly deteriorates as compared to the IM.

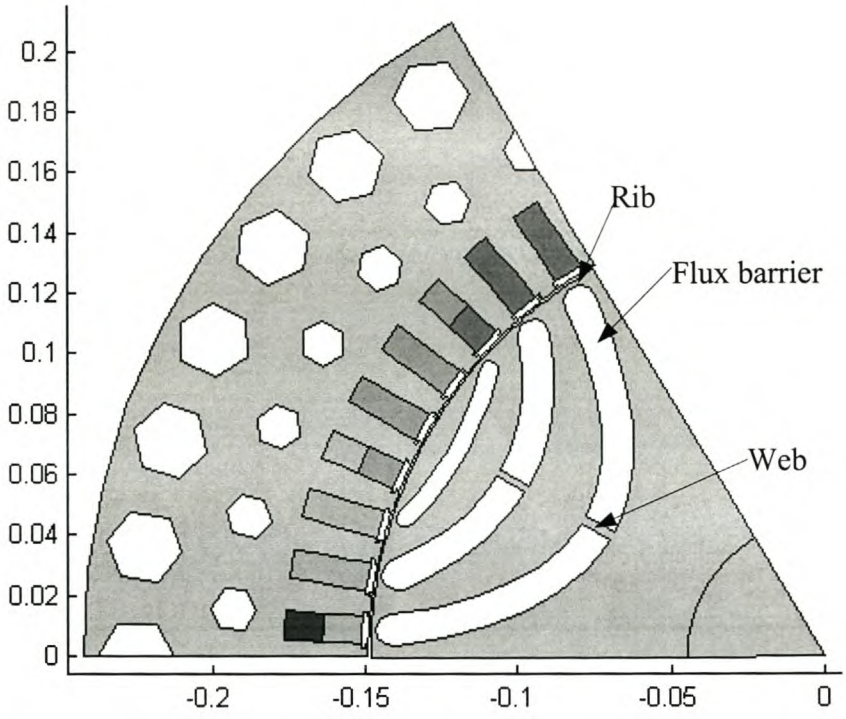

Figure 1.2. Cross sectional diagram of the 110 kW RSM

One reason for the poor torque performance in this region is attributed to the small air-gap of the RSM (0.8 mm) compared to that of the IM (1.5 mm). The small air-gap implies that the flux per pole in the RSM is more than that of the IM. Consequently the induced voltage in the RSM stator is more than that in the IM. The second reason is due to armature reaction (or the demagnetisation effect). The effect of the armature reaction becomes significantly high in the flux-weakening region because the *d*-axis current of the machine is reduced (hence *d*-axis flux) and the rotor iron comes out of saturation. With the rotor iron out of saturation, the *q*-axis flux distorts and reduces the main *d*-axis flux and hence the torque. The effect of armature reaction in the induction machine is relatively small as compared to the RSM.

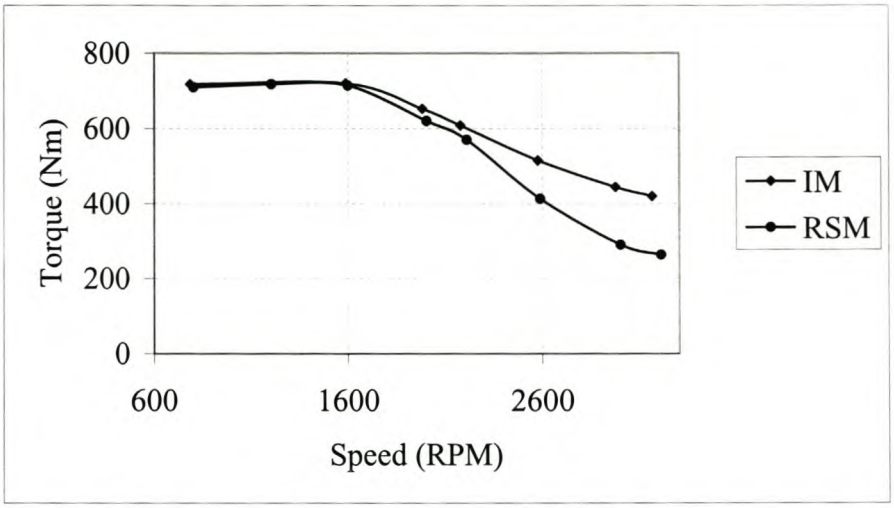

Figure 1.3. Torque-speed characteristics of 110 kW RSM and IM [7]

1.6 Approach to problem

In order to improve the performance of the RSM, especially in the flux weakening operation range, it has been proposed by some researchers that small quantity of PM material may be incorporated into the reluctance rotor to reduce the q-axis magnetic flux and thus increase the magnetic saliency [12, 16-20]. Their research in this regard can be summarised as follows:

- A permanent magnet assisted synchronous reluctance drive is theoretically analysed [12] by designing an appropriate rotor permanent magnet (PM) flux component in order to obtain a drive-matching ratio ($\frac{P}{VA}$) only slightly less than one, without theoretical dependence on the speed range. It is argued that with an appropriate PM flux, the drive current will be high enough to at least allow the infinitesimal flux operating condition. A similar theoretical analysis was later carried out by Boldea [20]. The work of Boldea also concluded that with an appropriate PM material in the RSM, a high operating (flux-weakening) speed region could be attained.

- The effect of adding magnets on L_d and L_q inductance of the RSM was later carried out [18] using the finite element analysis. It was concluded that with PMs on the rotor, the inductance ratio and inductance difference show an increase, which implies an increase of power factor and torque density. A more recent publication [16] also concluded that the RSM with PMs in the rotor results in an improved efficiency and power factor over an IM of the same size.

- The performance evaluation of an RSM with PMs on the rotor for high efficiency and wide speed range was carried out by [11] at a 100 W level. It was concluded that with appropriate PM material, a speed range of up to 5 times base speed and high efficiency could be achieved.

It is important to note that the above-mentioned research has been focused on low power machines in contrast to the 110 kW power level investigation explained in section 1.5 above (see also section 1.1 above).

The objective of this research is to improve the performance parameters of the existing RSM [7] by adding optimum designed PM sheets to the existing rotor so that the machine is comparable to the IM specifically in the flux-weakening region. The performance parameters of concern in this regard are the generating torque and the limited supply voltage and current of the machine. The optimum design of the PM sheets is done using the finite element analysis method directly in an optimisation procedure.

1.7 Thesis layout

The layout of the remainder of the thesis is structured as follows:

Chapter 2: In this chapter the mathematical model of the RSM in the *dq* reference frame is presented and discussed in detail. This chapter also describes the calculation of the performance parameters using finite element analysis method. A brief overview of the finite element analysis and the presentation of the permanent magnets using the current sheet method are also given.

Chapter 3: This chapter focuses on the analysis of the RSM with permanent magnets on the rotor. It discusses and presents the basic principle of operation and the equations of the performance parameters for this machine respectively. It then describes the optimisation of the rotor and lastly presents the finite element optimised structures as well as the calculated performance parameters.

Chapter 4: In this chapter the designs of the digital speed and current PI controllers are presented. Then the practical implementation of these controllers using the DSP digital controller is discussed.

Chapter 5: This chapter describes experimental setup.

Chapter 6: This chapter presents the measured results and machines performance comparison.

Chapter 7: This chapter gives conclusions and recommendations are made for future research.

Chapter 2

2. Mathematical Circuit Modelling of the RSM

This chapter describes the mathematical model of the RSM in the conventional *abc* reference frame and its transformation to the *d* and *q*-axis synchronously rotating reference frame fixed to the rotor using Park's transformation. This chapter also describes the calculation of the performance parameters using 2-dimensional finite element analysis method. A brief overview of the finite element analysis and the presentation of the permanent magnets using the current sheet method in the finite element analysis program are also given.

2.1 Park's transformation

The RSM, like any other electric motor, can be considered to be a system of coupled electric and magnetic circuits. It can be modelled by a network of resistances, self-inductances and mutual inductances. The resulting circuit model of the RSM can be represented by a set of mathematical equations to predict its performance. In general, two model types are employed to represent the RSM. These are the phase coordinate and the space-phasor models.

The solution to the phase-coordinate model of the RSM results in a set of non-linear differential equations with time varying inductance coefficients. The solution to the time variable model often requires the use of numerical methods and the computational effort is often not justified in the study of electric drives. This procedure is therefore generally avoided.

The space phasor model or *dq* complex plane model, for balanced three phase systems, was introduced to obtain a model of an electric motor in which the inductance terms are independent of time or rotor position. This model rotates with the rotor at synchronous speed determined by the frequency of the phase currents. The *d*-axis of the complex plane is chosen to coincide with the minimum reluctance path and the *q*-axis to coincide with the high reluctance path as shown in Fig. 2.1. It is important to note that at steady state, the *dq* components are dc quantities.

Variables in the *abc* reference frame are transformed to the *dq0* reference frame using Park transformation [23]. The relation between the *dqo* and *abc* reference frames is given by

$$f_{qdo} = Kf_{abc} \tag{2.1}$$

These variables (equation 2.1) can represent currents, flux linkages or voltages and are given by

$$(f_{abc})^T = [f_a \quad f_b \quad f_c] \tag{2.2}$$

$$(f_{qdo})^T = [f_q \quad f_d \quad f_o] \tag{2.3}$$

where the superscript *T* represents transpose of the matrix. The transformation matrix is given by

$$K = \frac{2}{3}\begin{bmatrix} \cos(\theta) & \cos(\theta-120) & \cos(\theta+120) \\ \sin(\theta) & \sin(\theta-120) & \sin(\theta+120) \\ 0.5 & 0.5 & 0.5 \end{bmatrix} \tag{2.4}$$

where $$\theta = \int_0^t \omega\xi \, d\xi + \theta(0) \tag{2.5}$$

and ξ is the temporary integration variable.

The corresponding inverse relation is $$f_{abc} = K^{-1} f_{qdo} \tag{2.6}$$

where the inverse matrix is given by

$$K^{-1} = \frac{2}{3}\begin{bmatrix} \cos(\theta) & \sin(\theta) & 1 \\ \cos(\theta - 120) & \sin(\theta - 120) & 1 \\ \cos(\theta + 120) & \sin(\theta + 120) & 1 \end{bmatrix} \tag{2.7}$$

If the rotor rotates at an electrical speed ω_e, then the rotor angle, θ, is defined as the angle between the magnetic axis of phase *a* and the *q*-axis. It is given by

$$\theta = \int_0^t \omega_e \xi d\xi = \alpha_r \tag{2.8}$$

as shown in Fig. 2.1 below.

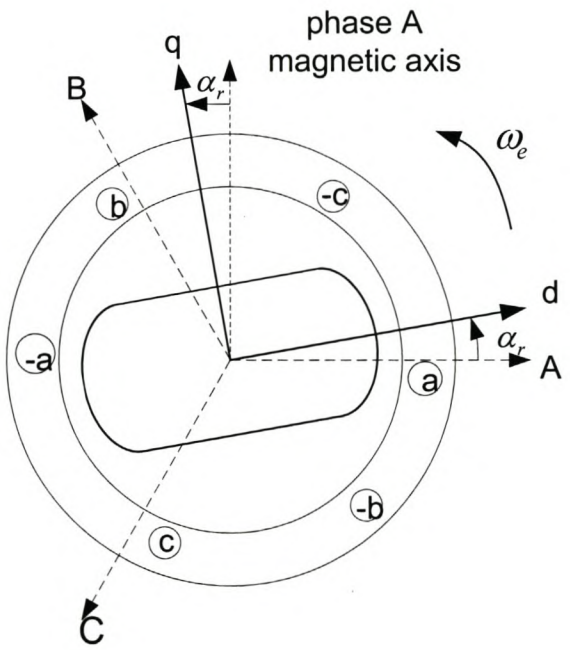

Figure 2.1. Vector diagram of a 2-pole RSM in the *abc* and *dqo* reference frame [21]

2.2 *dq* model of the RSM

The general three phase stator voltage equation of the RSM in the *abc* reference frame is given by

$$v_s = r_s i_s + \frac{d\lambda_s}{dt} \tag{2.9}$$

where

$$v_s = \begin{bmatrix} v_a \\ v_b \\ v_c \end{bmatrix}; \; i_s = \begin{bmatrix} i_a \\ i_b \\ i_c \end{bmatrix}; \; \lambda_s = \begin{bmatrix} \lambda_a \\ \lambda_b \\ \lambda_c \end{bmatrix} \tag{2.10}$$

This equation is then transformed to the *dq0* reference frame using Park's transformation such that

$$v_d = r_s i_d + \frac{d\lambda_d}{dt} - \omega_{re}\lambda_q \tag{2.11}$$

$$v_q = r_s i_q + \frac{d\lambda_q}{dt} - \omega_{re}\lambda_d \tag{2.12}$$

$$v_0 = r_s i_0 + \frac{d\lambda_0}{dt} \tag{2.13}$$

where r_s is the phase resistance and ω_{re} the electrical speed. Assuming a balanced three-phase system, the zero sequence voltage (v_0) is zero.

The *d* and *q*-axis flux linkages are both functions of the *d*-axis current, *q*-axis current and rotor position or else [26]

$$\lambda_d = f(i_d, i_q, \theta) \text{ and } \lambda_q = f(i_q, i_d, \theta) \tag{2.14}$$

These equations can be expanded using the chain rule such that

$$\frac{d\lambda_d}{dt} = \frac{\partial\lambda_d}{\partial i_d}\frac{di_d}{dt} + \frac{\partial\lambda_d}{\partial i_q}\frac{di_q}{dt} + \frac{\partial\lambda_d}{\partial\theta}\frac{d\theta}{dt} \tag{2.15}$$

$$= L'_d \frac{di_d}{dt} + M'_d \frac{di_q}{dt} + \frac{\partial\lambda_d}{\partial\theta}\omega_{re} \tag{2.16}$$

where L'_d and M_d' are the d-axis inductance and mutual inductance respectively, and

$$\frac{d\lambda_q}{dt} = \frac{\partial\lambda_q}{\partial i_q}\frac{di_q}{dt} + \frac{\partial\lambda_q}{\partial i_d}\frac{di_d}{dt} + \frac{\partial\lambda_q}{\partial\theta}\frac{d\theta}{dt} \tag{2.17}$$

$$= L'_q\frac{di_q}{dt} + M'_q\frac{di_d}{dt} + \frac{\partial\lambda_q}{\partial\theta}\omega_{re} \tag{2.18}$$

where L'_q and M_q' are the q-axis mutual inductances respectively.

The effect of the flux linkage variation with rotor position is considered negligible for skewed rotor machines. It has also been reported [8] that for well-designed reluctance machines the flux linkage variation with rotor position is minimal. In this study the machines are not skewed and the effect of flux-linkage variation with rotor position is assumed insignificant and the voltage equations are simplified as shown in equations 2.19 and 2.20 below.

$$v_d = r_s i_d - \omega_{re}\lambda_q + L'_d\frac{di_d}{dt} + M'_d\frac{di_q}{dt} \tag{2.19}$$

$$v_q = r_s i_q + \omega_{re}\lambda_d + L'_q\frac{di_q}{dt} + M'_q\frac{di_d}{dt} \tag{2.20}$$

where $\omega\lambda_d$ *and* $\omega\lambda_q$ are the rotational emf's or speed voltages. These equations can be visualised in block diagram format as shown in Fig. 2.2 below.

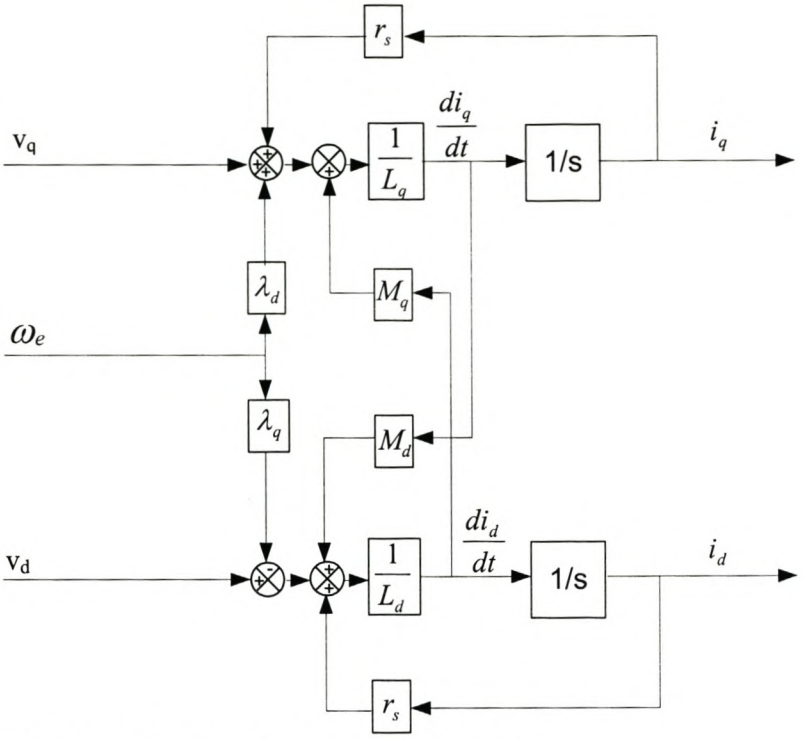

Figure 2.2. Simplified block diagram of the RSM

It is clear from Fig. 2.2 that the *d* and *q*-axis block diagram models of the RSM are interconnected by the speed dependent terms ($\omega\lambda_d$ *and* $\omega\lambda_q$) and the mutual inductance terms.

At steady state, the *d* and *q*-axis current components are pure dc quantities such that

$$\frac{di_q}{dt} = \frac{di_d}{dt} = 0 \tag{2.21}$$

Therefore for steady state analysis, equations 2.19 and 2.20 can be simplified to

$$v_d = r_s i_d - \omega_{re}\lambda_q \tag{2.22}$$

$$v_q = r_s i_q + \omega_{re}\lambda_d \tag{2.23}$$

By assuming that the effect of flux variation with rotor position is negligible, the voltage equations (eq. 2.22 and 2.23) above can be visualised on the schematic diagrams as shown in Fig. 2.3 below.

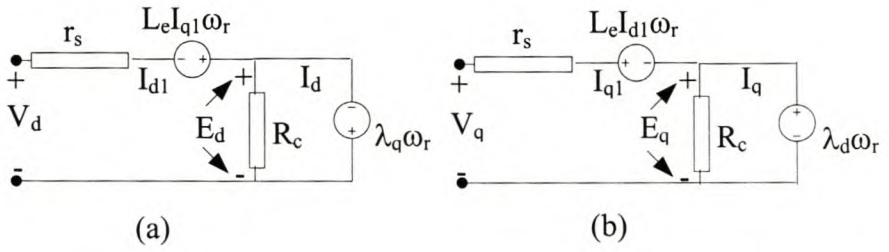

Figure 2.3. Steady state *d*- and *q*-axis equivalent circuit diagrams [10]

2.3 Electromagnetic torque production

The RSM has unequal reluctances along its pole rotor structure due to the magnetic asymmetry of the rotor. As a result, the *d* and *q*-axis inductances are not equal. The inequality in the *d* and *q*-axis inductance gives rise to the torque of the RSM. This torque is called the reluctance torque since it arises due to the difference in reluctance path between the *d* and *q*-axis of the rotor. The vector diagram and the torque equations are given next and are used to explain the torque production in an RSM.

The vector diagram of the RSM in the rotor reference frame is shown in Fig. 2.4. The current and the flux linkage space phasors are at an angle of γ^0 apart and the current space vector is at an angle ϕ^0 from the *d*-axis. These angles are called the toque and current angles respectively. For current angles of either 0 or 90^0, the resultant stator flux would purely have a *d* or *q*-axis component and no torque would be produced. At any other arbitrary angle between 0 and 90^0 as the case in Fig. 2.4, the resultant flux comprises of both the *d* and *q*-axis flux components and the rotor experiences a net

angular torque to position it in the direction of minimum reluctance or the electrically aligned position.

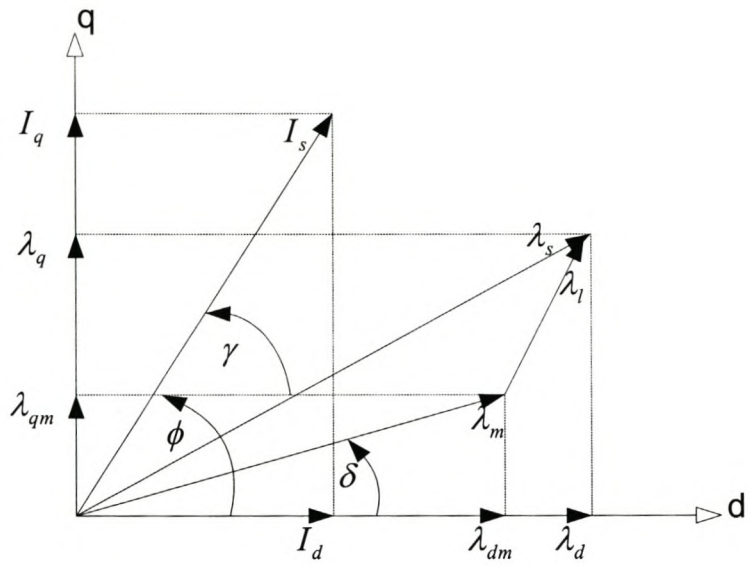

Figure 2.4. Vector diagram in the rotor reference frame

The produced torque is proportional to the cross product between the stator space phasor flux linkage λ_s and the stator current space phasor I_s [3], i.e.

$$T_{em} = k\lambda_s \times I_s \text{ or } T_{em} = k\,\lambda_s\, I_s \sin(\gamma) \tag{2.24}$$

where k is called a torque constant. Equation 2.6 can be expressed in terms of dq components [3] as

$$T_{em} = \frac{3}{2} P\left(\lambda_d I_q - \lambda_q I_d\right) \tag{2.25}$$

where P is the number of pole pairs. The d and q-axis inductances are defined as Ld = λd/Id and Lq = λq/Iq. Substituting the d and q-axis inductance terms into equation 2.25 yields

$$T = \frac{3}{2} P(L_d - L_q) I_d I_q \text{ or else } T = \frac{3}{4} P(L_d - L_q) I_s^2 \sin(2\phi) \tag{2.26}$$

where ϕ is the current space phasor angle, the angle between the current space phasor and the *d*-axis of the rotor, I_d and I_q the *d* and *q*-axis fundamental stator currents, λ_d and λ_q the fundamental stator flux linkage components.

It is clear from equation 2.26 that maximum torque of an RSM could be achieved by ensuring a large inductance difference $(L_d - L_q)$ in the design process.

2.4 Mechanical model

The general mechanical equation for electrical driven systems is given by

$$T_{em} = J_{eq} \frac{d\omega_{rm}}{dt} + \beta_{eq} \omega_{rm} + T_L \tag{2.27}$$

where $$J_{eq} = J_m + J_L \text{ and } \beta_{eq} = \beta_m + \beta_L, \tag{2.29}$$

and J_M and J_L are the inertia of the machine and the load respectively. β_m and β_L are the friction coefficients of the machine and the load respectively. T_m is the mechanical torque and T_L the load torque. The torque balance equation (equations 2.25 and 2.27) can be depicted in a block diagram format as shown in Fig. 2.5 with the operator $\int \frac{d}{dt}$ replaced with its Laplace variable 1/s and *P* is the number of pole pairs.

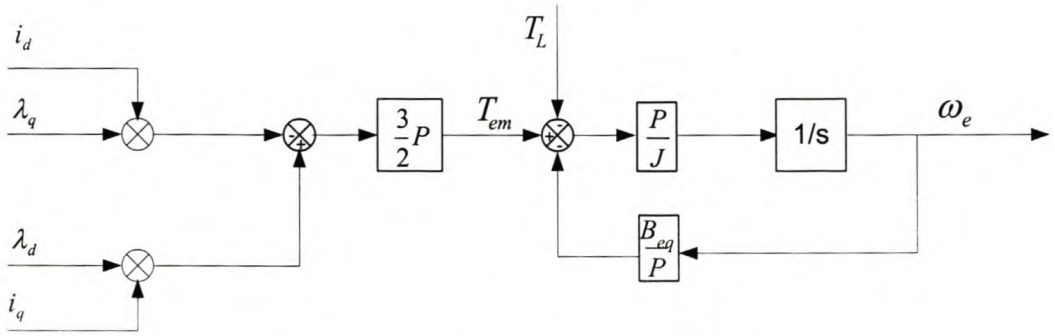

Figure 2.5. Simplified block diagram of RSM-torque and mechanical system

2.5 Finite element analysis

The 2-dimensional finite element (FE) program used in this research is not of commercial variety. The source code of the FE solver is available which makes it possible to invoke the FE field solution for any electrical machine design analysis. The FE program makes use of triangular elements of the first order. Only one pole of the stator and rotor is meshed with one airgap macro element comprising nodals on both sides of the airgap [3]. The Newton-Raphson method is used in finding the solution to the set of non-linear equations.

The FE solution is important in the design of the RSM since it gives accurate calculated results and it takes into account the effects of cross magnetisation and saturation.

2.5.1 Calculation of the equivalent circuit parameters [3]

The FE program makes use of the equivalent circuit parameters (see Fig. 2.3) to calculate the performance parameters (e.g. torque, efficiency, est.) of the machine. This section then describes the calculation of the equivalent circuit parameters and the performance parameters.

The equivalent circuit parameters are the per phase winding resistance ,R_s, core resistance, Rc, and the *d* and *q*-axis flux linkages, λ_d and λ_q, respectively, as shown in Fig. 2.3.

The per phase stator winding resistance is given by

$$R_s = \frac{2N_{ph}\rho_t(l+l_e)}{n_a.\frac{A_{cu}}{z}} \tag{2.30}$$

where ρ_t is the resistivity of copper at temperature t and is given by $\rho_t = \rho_{20}(1+Y_t(t-20))$ [3]. The other variables are defined as:

l	Axial stack length
l_e	Average coil end length
n_a	Number of parallel circuits
A_{cu}	Active stator slot copper area
z	Number of conductors per slot
$\frac{A_{cu}}{z}$	Stator conductor active copper area
ρ_{20}	Copper resistivity at 20^0C
N_{ph}	Number of turns in series per phase

To calculate the flux linkages of the RSM under current control it is necessary to specify the phasor current and the current angle of the machine in the FE software. The corresponding *dq* current components are then calculated from the given phasor current and current angle. The instantaneous three phase currents are calculated from the *dq* currents using the inverse Park transformation. The FE analysis method is then called to calculate the total stator flux linkages excluding the endwinding flux linkage.

The calculated flux linkages versus rotor position will contain harmonics and it is necessary to calculate the fundamental flux linkages. However, if the machine is skewed (see next paragraph), no prominent high frequency slot ripple will be present in the flux linkage wave.

The effect of skew is accounted for in the FE analysis by using a set of unskewed machines. The rotors are displaced by an angle that is a fraction of the total skew. With $(k = 5)$ unskewed machines the phase flux linkages are calculated using the equation

$$[\lambda_{abc}] = \frac{1}{k}\left[\sum_{1}^{k} \lambda_{abc}(\alpha_n)\right] \tag{2.31}$$

These flux linkages will however contain prominent harmonics of the 3rd and less prominent harmonics of the 5th and 7th order respectively. If the less prominent harmonics are ignored, the total flux linkage can be written in terms of the fundamental and the third order harmonics as

$$[\lambda_{abc}] \approx [\lambda_{abc1}] + [\lambda_{abc3}] \tag{2.32}$$

The co-phasal 3rd harmonic flux linkages, including the higher order triplen harmonics can be obtained from the actual three-phase flux linkages as

$$\lambda_{a3} = \lambda_{b3} = \lambda_{c3} = \frac{1}{3}(\lambda_a + \lambda_b + \lambda_c) \tag{2.33}$$

Thus with the actual total phase flux linkages and the 3rd harmonic flux linkages known from the FE analysis, the fundamental total phase flux linkages can be calculated as

$$[\lambda_{abc1}] \approx [\lambda_{abc}] - [\lambda_{abc3}] \tag{2.34}$$

The fundamental total phase flux linkages are necessary for the calculation of the performance parameters in the FE as will be described in the next section. These

fundamental phase flux linkages are then transformed to the *dq* flux linkages using Park's transformation such that

$$\lfloor \lambda_{qd0} \rfloor = \lfloor K_p \rfloor [\lambda_{abc1}] \tag{2.35}$$

The *d* and *q*-axis speed voltages are then determined as

$$E_d = -\lambda_q \omega \text{ and } E_q = \lambda_d \omega \tag{2.36}$$

The core loss resistance ,R_c, is calculated from

$$Rc = \frac{3E_a^2}{P_c} \tag{2.37}$$

The detailed calculation of the iron copper losses is described in [3], and is given by $P_c = cf_1^1(B_{mt}^y M_t + B_{my}^y M_y)$. B_{mt} and B_{my} are the maximum flux densities in the teeth and yoke, M_t and M_y are the iron masses of the teeth and yoke respectively while f_1 is the fundamental supply frequency. $E_a = \sqrt{\frac{E_d^2 + E_q^2}{2}}$ is the rms value of the phase EMF.

2.6 Calculation of performance parameters [6]

With reference to Fig. 2.3 and the calculated equivalent circuit parameters in the previous sub section, the *d* and *q*-axis currents are calculated as

$$I_{d1} = I_d + \frac{E_d}{R_c} \text{ and } I_{q1} = I_q + \frac{E_q}{R_c} \tag{2.38}$$

and the phasor current amplitude as

$$\boldsymbol{I}_{s1} = \sqrt{I_{d1}^2 + I_{q1}^2} \tag{2.39}$$

The *dq* and the voltage amplitude supply voltages are then calculated as

$$V_d = E_d + L_e I_{q1}\omega_r + I_{d1}R_s \ , \ V_q = E_q + L_e I_{d1}\omega_r + I_{q1}R_s \tag{2.40}$$

$$V_s = \sqrt{V_d^2 + V_q^2} \tag{2.41}$$

The power factor is calculated from the known *dq* currents and voltages and can be expressed as [6]

$$P_f = \cos\left(\tan^{-1}\left(\frac{\sigma/\upsilon + \upsilon}{\sigma - 1}\right)\right) \tag{2.42}$$

where $\sigma = \frac{L_d}{L_q}$ and $\upsilon = \frac{I_d}{I_q}$.

The supply apparent power and the copper losses of the RSM are calculated as

$$S = \frac{3}{2}V_s I_{s1} \text{ and } P_{cu} = \frac{3}{2}I_{s1}^2 R_s \tag{2.42}$$

This section focused on the calculation of the performance parameters using the FE analysis software. Since the work presented in this thesis also focuses on the PM assisted rotor RSM, it is important to describe how permanent magnets are represented in the FE software. This description is done in the next sub section.

2.6.1 PM representation in FE software

The representation of non-rectangular and non-linear PM magnetization characteristics in FE calculations is complex. It is however often acceptable to consider the magnets as ideal or linear. The characteristic of linear magnets is shown in Fig. 2.6 below. The operating point is represented by (H_m, B_m).

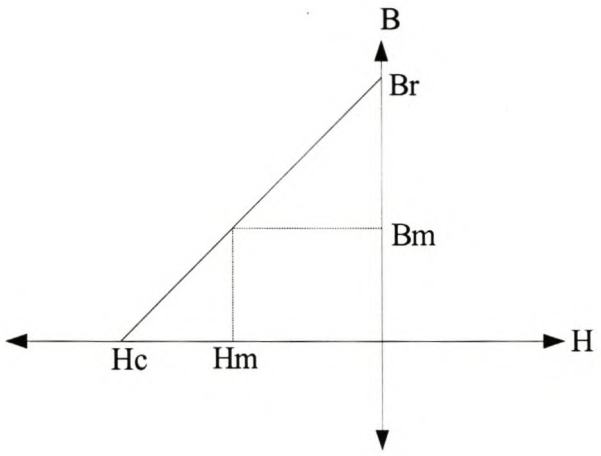

Figure 2.6. Characteristics linear PM

Most of the strong magnetic materials used in electrical machines exhibit a linear magnetisation characteristic in the second quadrant. The machine with PMs is designed to operate in this region, so that even during transients such as short circuits the magnets will not be demagnetised. There are two models that are commonly used to represent PMs in the FE program. These are the magnetisation vector and the equivalent current sheet. Although these methods have a different starting point, they result in the same set of equations. The current sheet equivalent method has an advantage in that a standard FE program without special permanent magnet capability can be used as explained in the next paragraphs.

Consider Fig. 2.7. If we assume that the permeability of the core is infinite, then

$$H_m l + H_g l_g = 0 \tag{2.43}$$

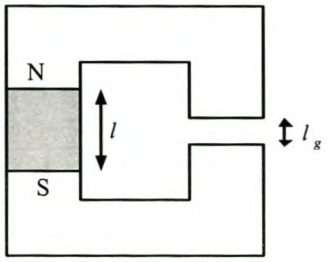

Figure 2.7. Core with permanent magnet

The permanent magnet can be represented by a current sheet (see Fig. 2.8) with a total ampere-turns $NI = H_c l$ and a material of equivalent permeability $\mu = \frac{B_r}{H_c}$. If the iron has infinite permeability then

$$H_m l + H_g l_g = H_c l \tag{2.44}$$

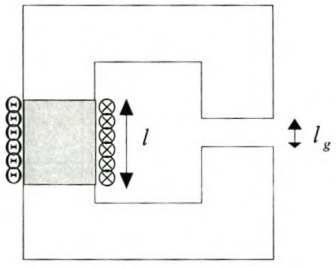

Figure 2.8. Core with current sheets equivalent

The magnetic quantities outside the current sheet are the same as that of the permanent magnet. It can be concluded that the permanent magnets can be represented by current sheets with the same magnetic properties provided that

- The magnets are replaced by a material of permeability of $\mu_{eq} = \frac{B_r}{H_c}$
- Thin current sheets are added along the two sides of the magnet to produce a field in the direction of the magnetisation. The linear current density should be equal to the coercive force (H_c).

2.7 Finite element calculated results

The calculation of the performance parameters in the FE software has been theoretically described in the previous section. In this section the FE calculated results of the 110 kW RSM are presented. The FE calculated results of the PM assisted RSM are given in Chapter 3.

Fig. 2.9 shows the *d*-axis flux linkage for different values of *q*-axis current. The rated current of the RSM is 200 A RMS, and the peak phasor current amplitude, ***Is*** = $\sqrt{(I_d^2+I_q^2)}$, is 280 A. It is clear that the *d*-axis flux decreases as the *q*-axis current is increased from 0 - 280A in steps of 40A. This decrease is due to magnetic coupling between the *d* and *q*-axis circuits.

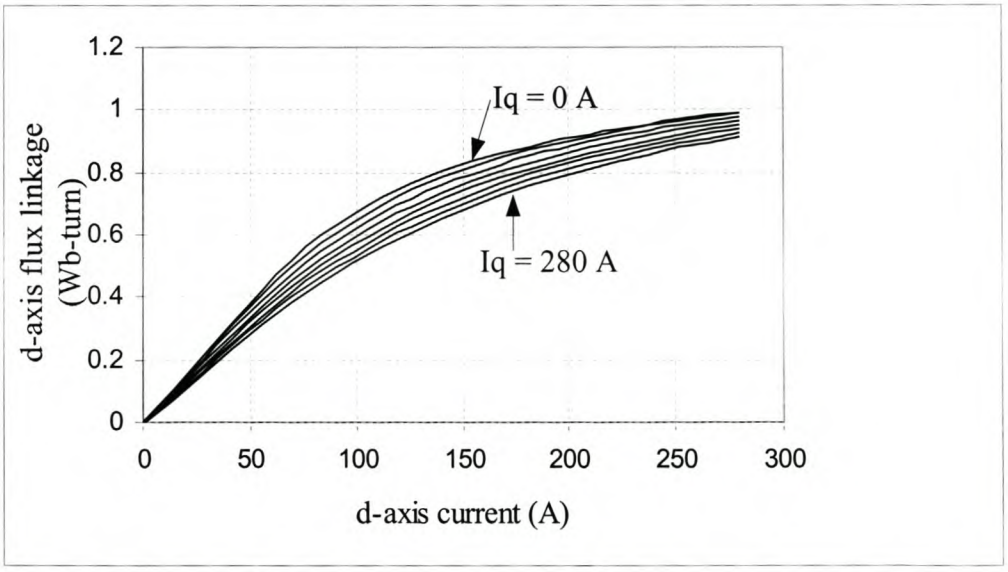

Figure 2.9. *d*-axis flux linkage versus *d*-axis current

The *d*-axis inductance curves are shown in Fig. 2.10 below. These inductances are calculated from the flux-linkages of Fig. 2.9 as $L_d^{'} = \frac{\partial \lambda_d}{di_d}$. The *d*-axis inductances

also decrease as the q-axis current is increased. Again this is due to cross coupling between the d and q-axis circuits. This is significant at low values of Id, but at the rated d-axis current variation of the inductance difference is relatively small as the q-axis current is increased due to saturation of the magnetising flux λ_d.

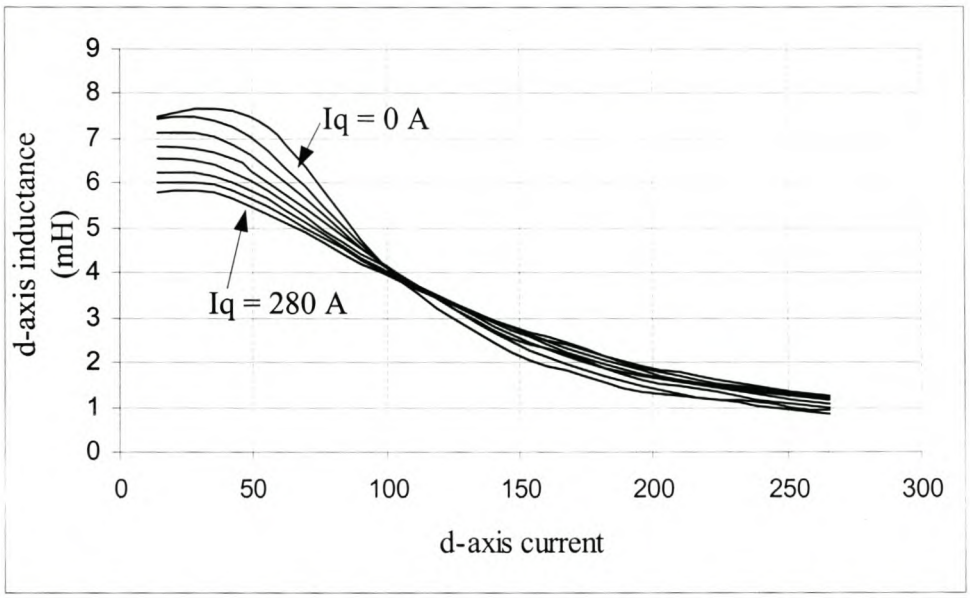

Figure 2.10. d-axis inductance versus d-axis current

The d-axis mutual inductance curve shown in Fig. 2.11 is calculated from $M_d' = \frac{\partial \lambda_d}{\partial i_q}$.

It is important to note that the mutual inductance has a negative polarity at all current values and therefore has a reducing characteristic in the d-axis voltage shown in Fig. 2.3. However, the influence of the d and q-axis mutual inductances is zero with the machine in steady state (equation 2.19) due to the fact that all currents are assumed constant.

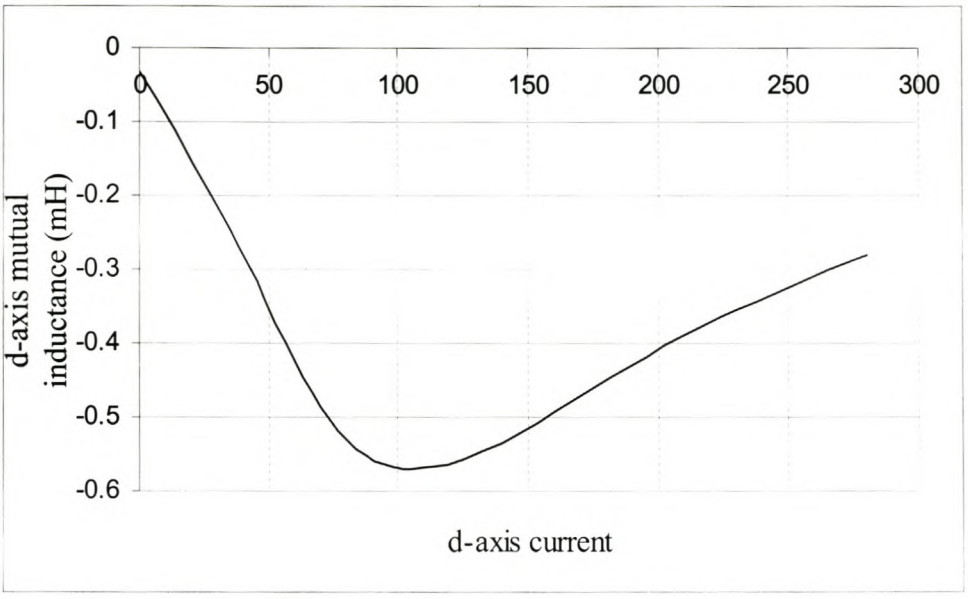

Figure 2.11. *d*-axis mutual inductance versus *d*-axis current

The *q*-axis flux linkage curves are shown in Fig. 2.12 for different values of the *d*-axis current. Similarly, due to cross coupling, the *q*-axis flux linkages decrease as the *d*-axis current is increased from 0 – 280 A as shown in Fig. 2.12.

Fig. 2.13 below shows the calculated *q*-axis inductances for different values of the *d*-axis current. It is clear from Fig. 2.13 that at low values of the *q*-axis current, the *q*-axis inductances are greatly negatively affected by the variation of the *d*-axis current. Again at rated values of the *q*-axis current, the inductance difference is relatively small as the *d*-axis current is increased due to saturation in the *q*-axis flux λ_q.

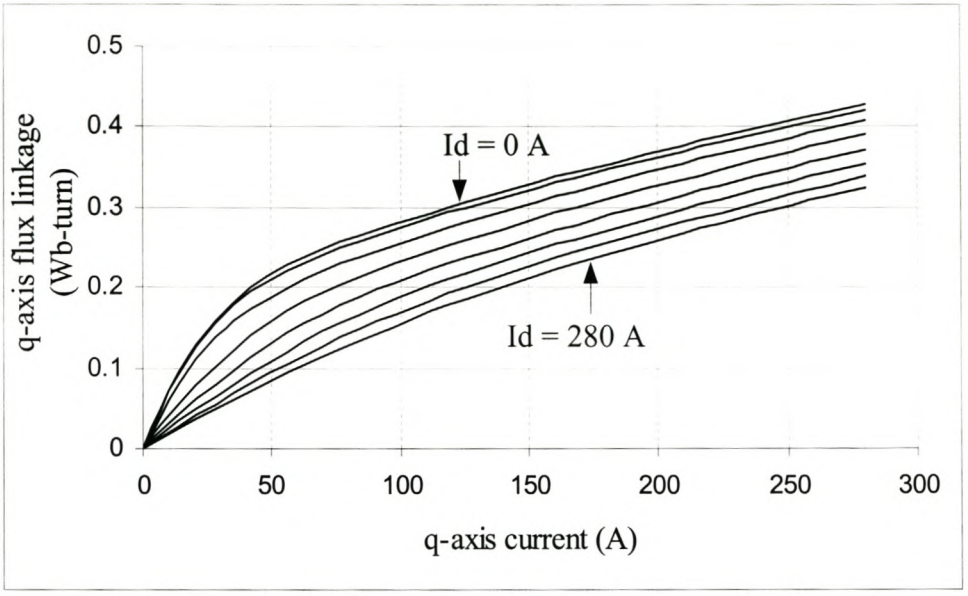

Figure 2.12. *q*-axis flux linkage versus *q*-axis current

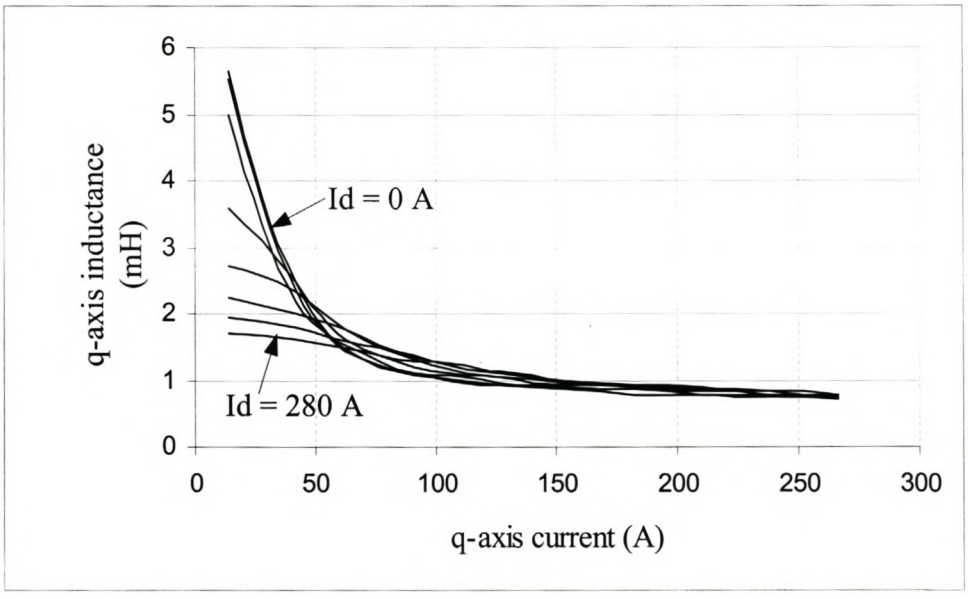

Figure 2.13. *q*-axis inductance versus *q*-axis current

The q-axis mutual inductance curve shown in Fig. 2.14 is calculated from $M_q' = \frac{\partial \lambda_q}{\partial i_d}$.

It is important to note that the q-axis mutual inductance also has a negative polarity at all current values and therefore has a reducing characteristic in the q-axis voltage as shown in Fig. 2.14. Again, the influence of the q-axis mutual inductance is zero with the machine in steady state due to constant q-axis current (see equation 2.20).

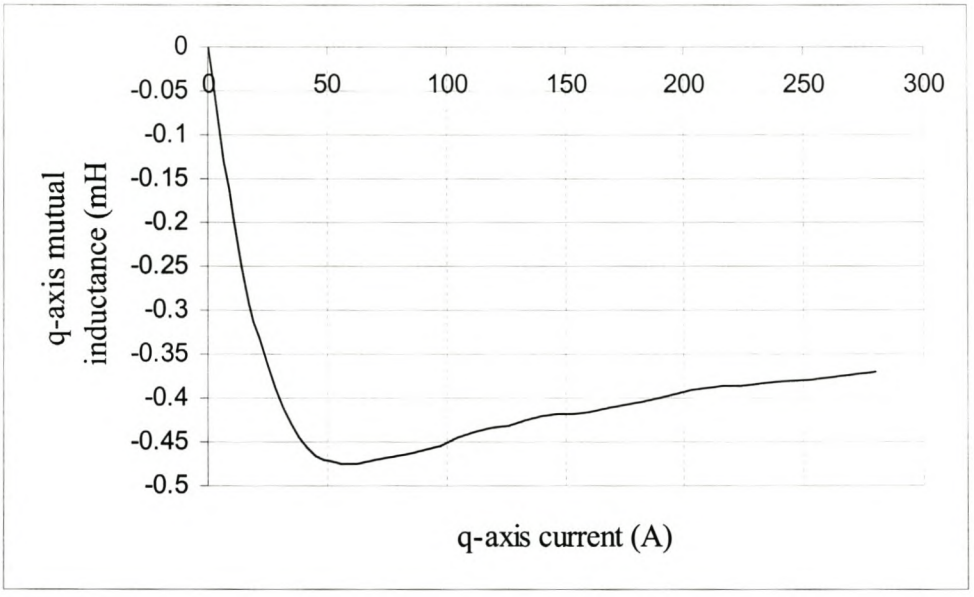

Figure 2.14. q-axis mutual inductance versus q-axis current

Chapter 3

3. Modelling of the Permanent-Magnet-Assisted RSM

In this chapter the basic principles of the Permanent magnet assisted RSM (PM-assisted RSM) are described. The steady state vector diagram, torque equations, voltage equations, design optimisation and finite element results are presented and explained in detail.

3.1 Physical model of PM-assisted RSM

The aim of this section is to describe the basic principle of operation of the RSM with permanent magnets added to the rotor. Fig. 3.1 below shows the cross-sectional diagram of a salient 2-pole RSM with permanent magnets on the q-axis of the rotor. In this figure the magnets are represented by the dark marked lines and the arrows indicate their magnetic polarity.

The fictious q-axis stator coil (indicated as Sq) on the d-axis of the rotor produces q-axis flux and the fictious d-axis stator coil (indicated as Sd) on the q-axis of the rotor produces d-axis flux as shown in the figure. Positive current in a coil is represented by a cross and negative current by a dash. It then follows from magnetic field theory that positive d and q-axis stator flux flows along the positive conventional d and q-axis of the rotor respectively, as indicated in Fig. 3.1. Since the magnets are to reduce the main stator q-axis flux, their magnetic polarity is in opposite direction to the main q-axis stator flux also shown in Fig. 3.1. However, if negative current is injected to get negative torque or during motor regen, the stator q-axis flux will complement the permanent magnet sheet flux. To avoid this phenomenon, the machine is controlled such that the q-axis current remains positive and only the d-axis current is allowed to

go negative. This control strategy is known as constant current angle control and is shown in Fig. 3.2. It implies that the phasor current, *Is*, is kept positive but the current angle, ϕ, is advanced to the second quadrant to get negative *d*-axis current as shown in Fig. 3.2.

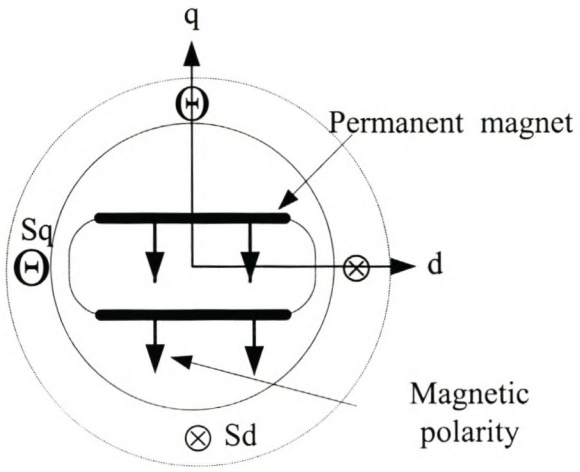

Figure 3.1. Cross section of an RSM with PMs on the *q*-axis of the rotor

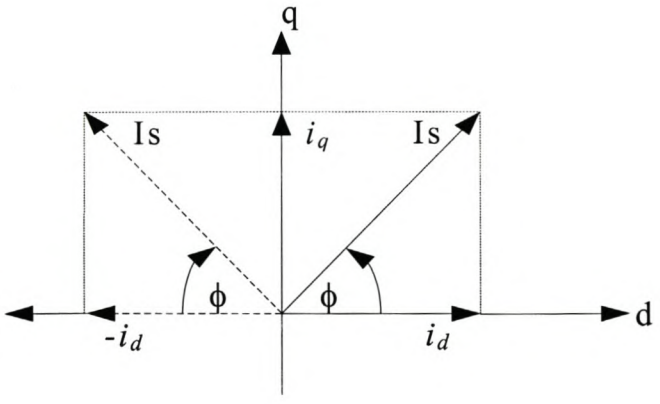

Figure 3.2. Simple current control scheme of the PM-assisted RSM (dotted lines indicate negative torque or regeneration)

3.1.1 Voltage equations and equivalent circuits

The general *d* and *q*-axis voltage equations are given as

$$v_d = r_s i_d + \frac{d\lambda_d}{dt} - \omega_{re}\lambda_q'$$

or (3.1)

$$v_d = r_s i_d - \omega_{re}\lambda_q + \omega_{re}\lambda_{pm}$$

$$v_q = r_s i_q + \frac{d\lambda_q}{dt} + \omega_{re}\lambda_d \quad (3.2)$$

where $\lambda_q' = \lambda_q - \lambda_{pm}$ and λ_{pm} is the flux due to PM sheets (see Fig. 3.1).

The flux linkages (λ_d and λ_q') are both functions of the *d*-axis current, i_d, *q*-axis current, i_q, fictious *q*-axis current (due to permanent magnet sheets) i_f and the rotor position, θ, as shown by equations 3.3 and 3.4 below, respectively.

$$\lambda_d = f(i_d, i_q, i_f, \theta) \quad (3.3)$$

$$\lambda_q' = f(i_q, i_d, i_f, \theta) \quad (3.4)$$

The rate of change of the flux linkages $\frac{\partial\lambda_d}{dt}$ and $\frac{\partial\lambda_q'}{dt}$ are expanded using the chain rule such that

$$\frac{d\lambda_d}{dt} = \frac{\partial\lambda_d}{\partial i_d}\frac{di_d}{dt} + \frac{\partial\lambda_d}{\partial i_q}\frac{di_q}{dt} + \frac{\partial\lambda_d}{\partial i_f}\frac{di_f}{dt} + \frac{\partial\lambda_d}{\partial\theta}\frac{d\theta}{dt} \quad (3.5)$$

$$\frac{d\lambda_q'}{dt} = \frac{\partial\lambda_q'}{\partial i_q}\frac{di_q}{dt} + \frac{\partial\lambda_q'}{\partial i_d}\frac{di_d}{dt} + \frac{\partial\lambda_q'}{\partial i_f}\frac{di_f}{dt} + \frac{\partial\lambda_q'}{\partial\theta}\frac{d\theta}{dt} \quad (3.6)$$

Since the permanent magnet sheet current is constant, the contribution of the terms $\frac{\partial \lambda_d}{\partial i_f}\frac{di_f}{dt}$ and $\frac{\partial \lambda_q^{'}}{\partial i_f}\frac{di_f}{dt}$ are disregarded in the flux linkage equations above and the voltage equations above are derived as

$$v_d = r_s i_d - \omega_{re}\lambda_q + L_d^{'}\frac{di_d}{dt} + M_d^{'}\frac{di_q}{dt} + \omega\frac{\partial \lambda_d}{\partial \theta} \tag{3.7}$$

$$v_q^{'} = r_s i_q + \omega_{re}\lambda_d + L_q^{'}\frac{di_q}{dt} + M_q^{'}\frac{di_d}{dt} + \omega\frac{\partial \lambda_q^{'}}{\partial \theta} \tag{3.8}$$

A block diagram of these equations of the PM-assisted RSM is shown in Fig. 3.3. In steady state, assuming stator losses are negligible and that flux variation with position is zero, the *d* and *q*-axis voltages are predominantly given by the speed voltages as shown in equations 3.9 and 3.10

$$V_d = -\omega_{re}\lambda_q + \omega_{re}\lambda_{pm} \tag{3.9}$$

$$V_q = \omega\lambda_d \tag{3.10}$$

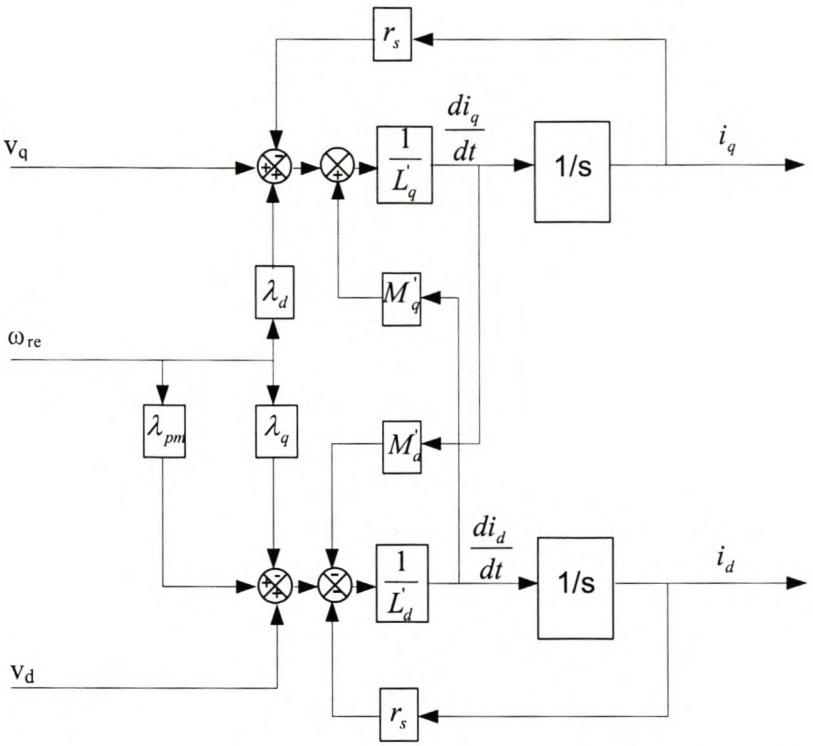

Figure 3.3. Block diagram of the mathematical model of the PM-assisted RSM

The peak phase voltage amplitude is given by

$$V_s = \sqrt{v_d^2 + v_q^2} \tag{3.11}$$

The *d*-axis voltage according to eqn. (3.9) is reduced by the addition of the permanent magnets on the nett *q*-axis since the *q*-axis flux linkage (λ_q) is reduced. The result, thus, is a reduced peak phase voltage according eqn.(3.11). This is an advantage from an inverter point of view, since it was reported [7] that at high speeds the RSM requires relatively high supply voltages to produce torque values comparable to the induction machine of the same rating.

Disregarding the effect of flux variation with rotor position, voltage equations (3.7) and (3.8) above are visualised in the steady state by the schematic diagrams of Fig.3.4.

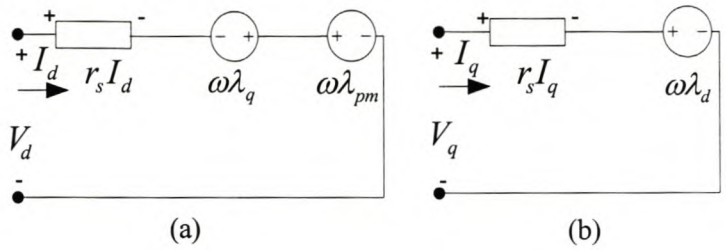

Figure 3.4: Steady state *d*-axis (a) and *q*-axis (b) axis equivalent circuit diagrams of the PM- assisted RSM.

3.1.2 Vector diagram of PM-assisted RSM

The vector diagram of the PM-assisted RSM is shown in Fig. 3.5. Also shown in the figure is the vector diagram of the RSM without permanent magnets for comparison purposes.

The permanent magnet flux component, λ_{pm}, is in the opposite direction to the main stator *q*-axis flux, λ_q, as shown in Fig. 3.5. This results in the reduction of the main stator *q*-axis flux. It can be seen from Fig. 3.5 that the reduced stator flux results in the reduced stator phase voltage V_s. It is clear that also the power factor angle, θ, which is the angle between the phase current and phase voltage, is reduced to, θ', resulting in an improved power factor. It is also important to note that the introduction of the permanent magnets on the *q*-axis has no effect on the *d*-axis flux component.

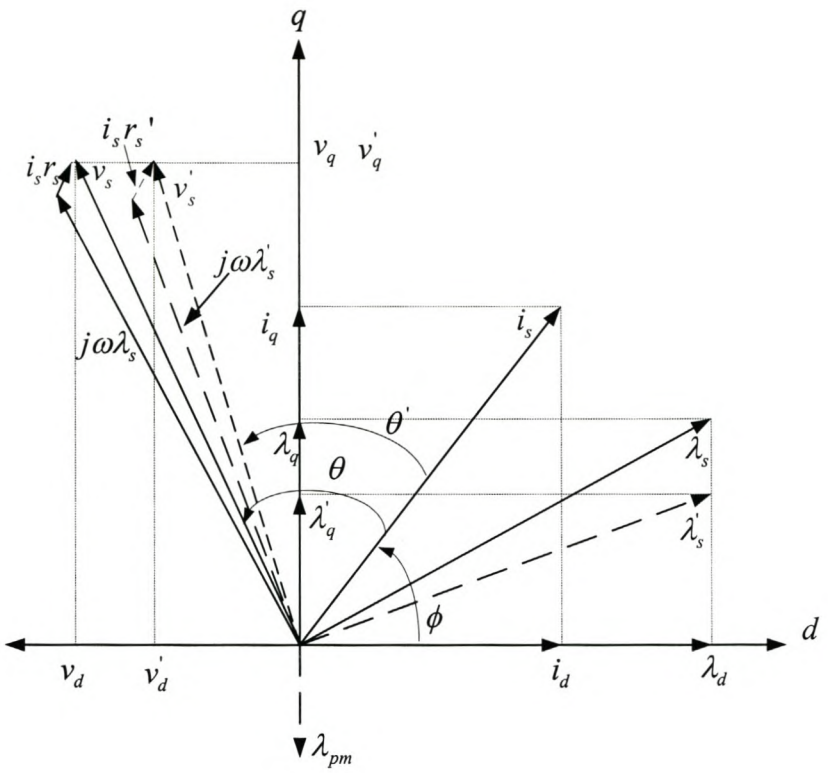

Figure 3.5: Steady state vector diagram of the RSM (solid lines) and PM-assisted RSM (dashed lines and superscript " ' " for symbols).

3.1.3 Torque equations

The torque equation for synchronous machines as derived in all classical text is given by

$$T = \frac{3}{2} p\left(\lambda_d i_q - \lambda_q' i_d\right) \tag{3.12}$$

where p is the number of pole pairs. Since the permanent magnets produce flux opposite the main stator q-axis flux, the total q-axis flux is thus given as

$$\lambda_q' = \lambda_q - \lambda_{pm} \tag{3.13}$$

where L_q is the q axis inductance. The FE analysis calculated results in Fig. 3.6 shows clearly the effect of the PM sheets flux on the q-axis flux, λ'_q. The d-axis flux is given as

$$\lambda_d = L_d i_d \tag{3.14}$$

where L_d is the d-axis inductance. It can be seen from the FE analysis calculated results in Fig. 3.7 that the effect of the PM sheets flux is minimal on the d-axis flux at rated d-axis current. Substituting equations 3.2-3.3 into equation 3.1 gives

$$T = \frac{3}{2} p\left(L_d - L_q\right) i_d i_q + \frac{3}{2} p \lambda_{pm} i_d$$

or (3.15)

$$T = \frac{3}{2} p\left(\lambda_d i_q - \lambda_q i_d + \lambda_{pm} i_d\right)$$

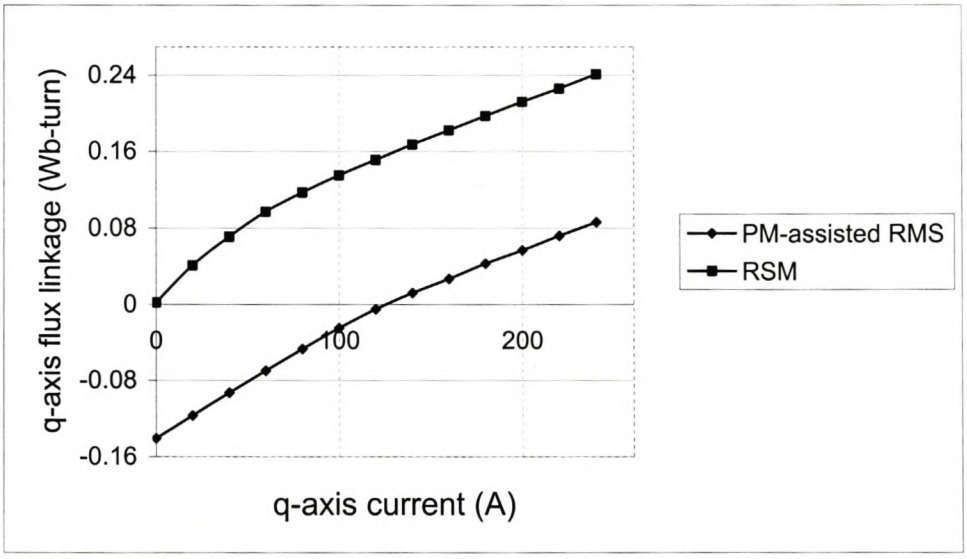

Figure 3.6. FE calculated q-axis flux linkage curves of the RSM and PM-assisted RSM

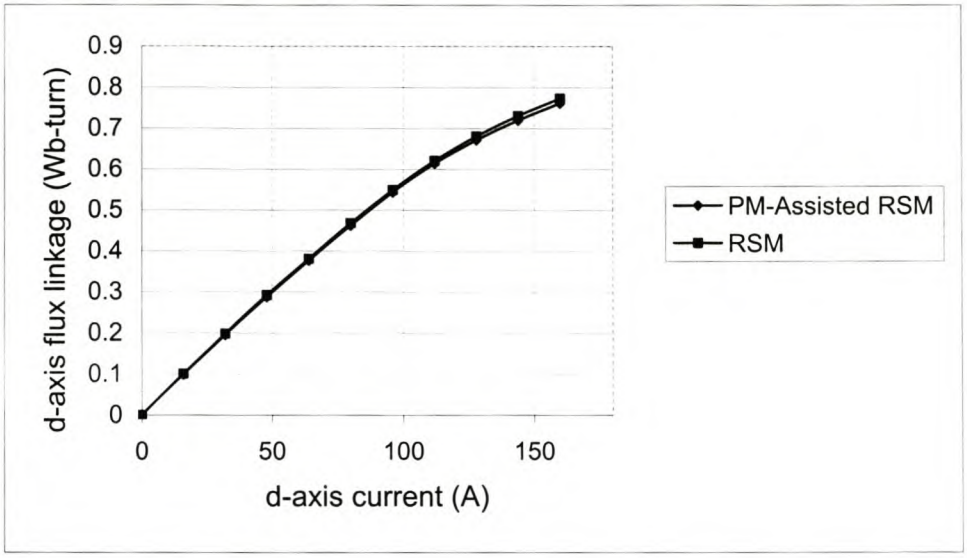

Figure 3.7. FE calculated *d*-axis flux linkage curves of the RSM and PM-assisted RSM

It can be deduced from eqn. (3.15) that the permanent magnets introduce a positive torque component proportional to the *d*-axis current in addition to the reluctance torque. This component is, however, by design, in this case, relatively small compared to the reluctance torque component; an important fact that keeps the machine under investigation a reluctance machine rather than a permanent magnet machine.

The presence of the permanent magnets on the *q*-axis does not affect the *d*-axis inductance much, that is if the PM flux is relatively small and the machine is under full saturation on the *d*-axis. Therefore the inductance difference, $L_d - L_q$, increases due to a decrease in the *q*-axis inductance, which results in an increase in reluctance torque according to eqn. (3.15). This is however only true in the constant torque region as in the flux-weakening region the *d*-axis flux is reduced to allow for high speeds operation. It then follows that it would be logical to optimally design the PM-assisted rotor in the flux weakening region, in fact at the maximum required speed to get best torque performance for the whole operating speed range.

Equation 3.15 above can also be written as [20]

$$T = \frac{3}{2} p (L_d + \frac{\lambda_{pm}}{i_q} - L_q) i_d i_q \tag{3.16}$$

or

$$T = \frac{3}{4} p (L_d + \frac{\lambda_{pm}}{i_q} - L_q) I_s^2 \sin(2\phi) \tag{3.17}$$

where ϕ is the current angle and I_s the phase current. According to eqn. (3.17) above, the maximum torque is attained at a current angle, ϕ, of 45^0. However, it has been shown [2] that due to non-linearities the maximum torque is attained at higher current angle values, typically 65^0 for the RSM. For the PM-assisted RSM, the maximum torque would be attained at current angles less than for the RSM as will be shown in the following sub-sections.

3.1.4 Power factor equations

The power factor equation of the RSM was given in chapter 2 as

$$P_f = \cos(\tan^{-1}(\frac{\sigma / \nu + \nu}{\sigma - 1})) \tag{3.18}$$

where $\sigma = L_d/L_q$. The power factor of the PM-assisted RSM could be derived from eqn. (3.7) by noting that $L_{qm} = L_q - L_m$, where $L_m = \lambda_{pm}/i_{pm}$. The power factor equation for the PM assisted RSM could then be written as

$$P_{fm} = \cos(\tan^{-1}(\frac{\sigma_m / \nu + \nu}{\sigma_m - 1})) \tag{3.19}$$

where $\sigma_m = L_d/(L_q - L_m)$. Equation (3.19) shows that the power factor of the PM assisted RSM is also dependent on the inductance ratio like for the RSM. In fact it is more sensitive to the q-axis inductance difference, $L_q - L_m$.

3.1.5 Analysis of the effect of PMs on the 110 kW performance parameters

This section analyses the effect of the interior PM sheets on the torque and voltage performance parameters, of the 6-pole 110 kW PM-assisted RSM. A cross sectional diagram of the 110 kW PM-assisted RSM is shown in Fig. 3.8. The PMs are slotted along the parabolic flux barriers with magnetic polarity opposite the main q-axis stator flux. The torque and voltage analysis for this machine is similar to the 2-pole torque model and voltage analysis described in sections 3.1.1-3.1.3. The flux plot of the RSM with PM sheets is shown in Figs. 3.9 to Fig. 3.11 and the typical B-H curves for the NdFeB magnets is shown in Fig. 3.12. A two-dimensional finite element analysis simulation of the six-pole 110 kW RSM without and with magnets of different magnetic intensity strength was done to analyse the torque and voltage versus current angle response. The magnet thicknesses were fixed at 3mm. The results are shown in Figs. 3.13 and 3.14.

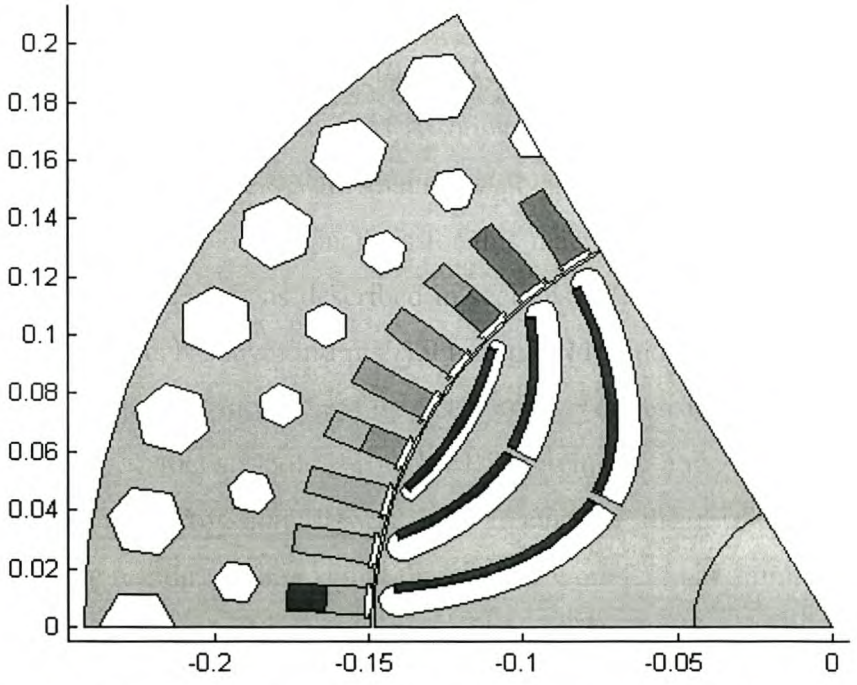

Figure 3.8. Cross-section of RSM with un-optimised PM sheets

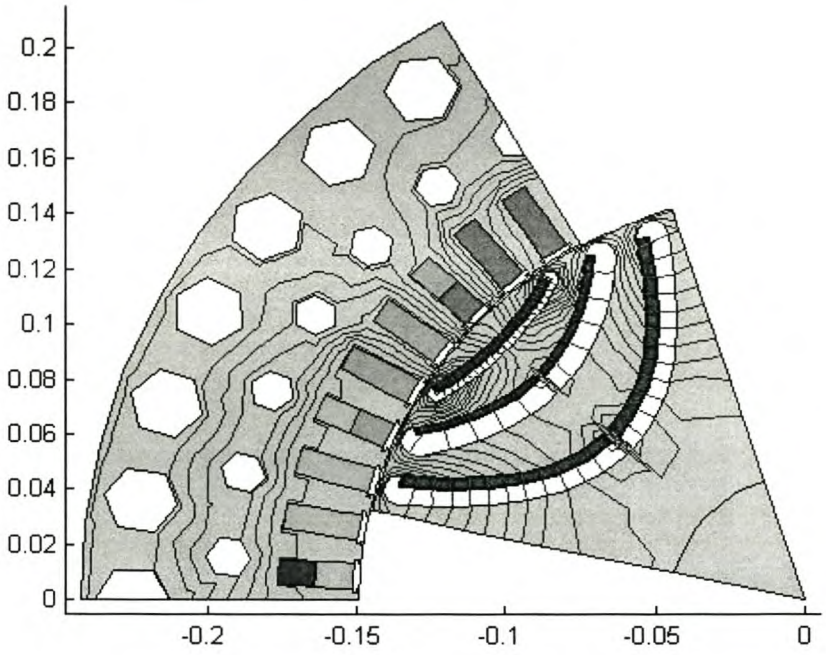

Figure 3.9. Flux plot with only PM's active

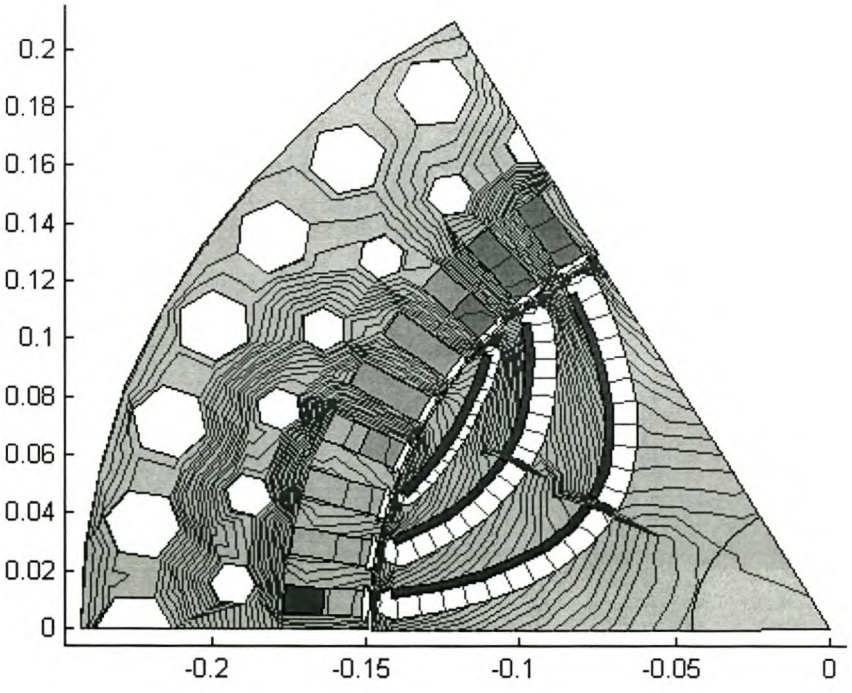

Figure 3.10. Flux plot with only currents active

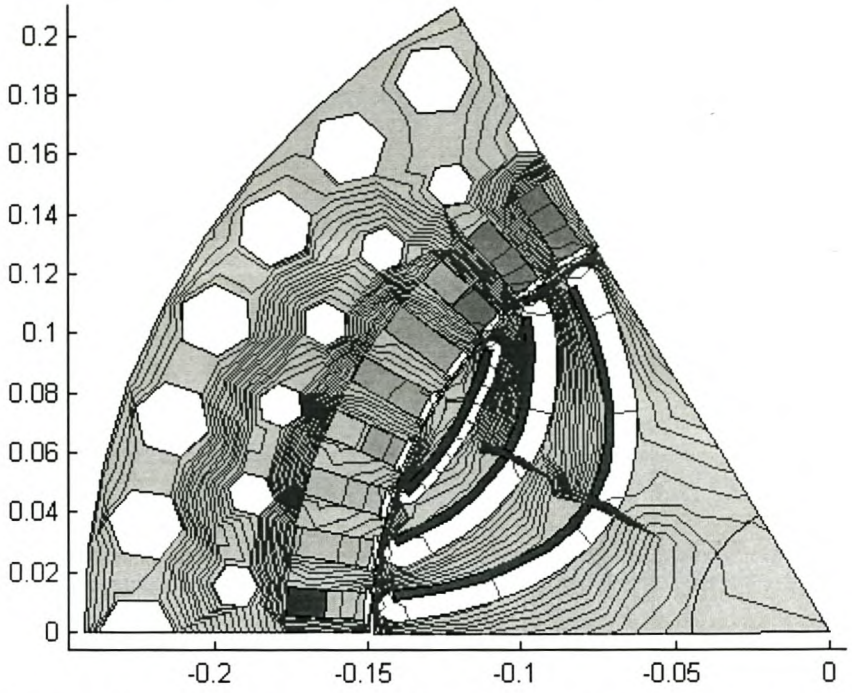

Figure 3.11. Flux plot with both currents and magnets active

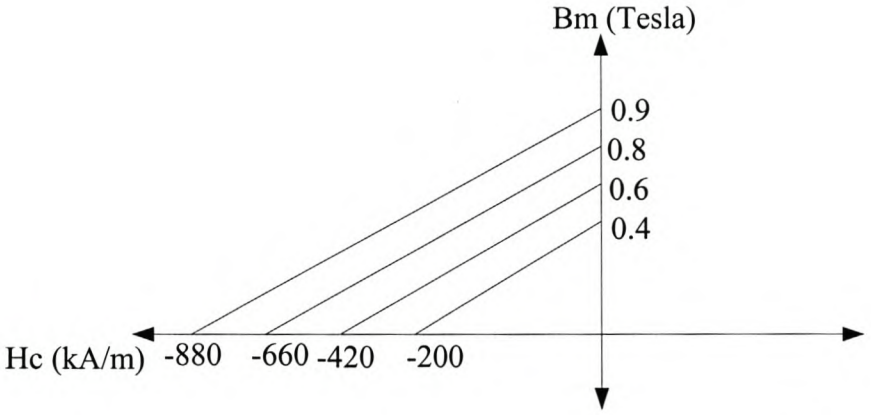

Figure 3.12. Typical NdFeB epoxy bonded PM *B-H* curves

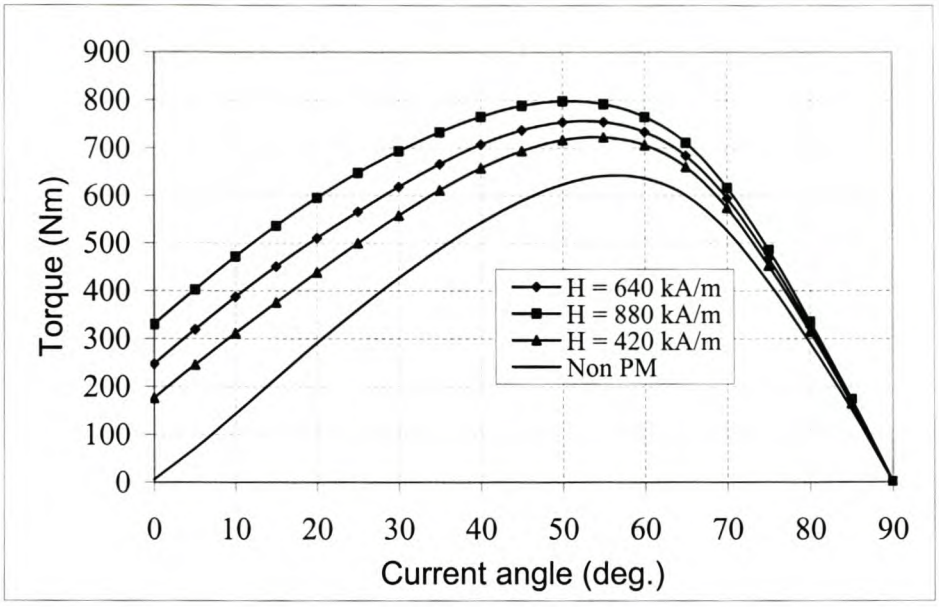

Figure 3.13. Torque versus current angle curves at 200 A and 1500 rpm

From Fig. 3.13, it is clear that the PMs greatly improve the torque capability of the machine, more visibly at current angles below 80^0. However, as the current angle is advanced towards 90^0, corresponding to relatively very high speeds in the flux-weakening region, the *d*-axis current reduces while the *q*-axis current increases. Thus, the rotor iron comes out of saturation on the *d*-axis and the contribution of the PMs is reduced due to increased stator *q*-axis flux. The aim is then to insert just enough PM sheets with the corresponding amount of flux to counteract the stator *q*-axis flux. It can further be deduced from Fig. 3.13 that the PMs tend to reduce (shifts the torque curve to the left) at the rated maximum-torque current-angle. The shifting of the torque curve to the left is a desired effect since it means for maximum speed operation, the current angle is advanced to angles much less than 90^0 resulting in high torque performance at higher speeds.

The effect of the PMs on the supply voltage of the RSM at a speed of 3800 rpm is shown in Fig. 3.14. The RSM is normally operated at current angles between 60 and

83^0 depending on the speed range required. It is clear from Fig. 3.14 that the induced voltage tends to decrease in proportion to the strength of the added magnets.

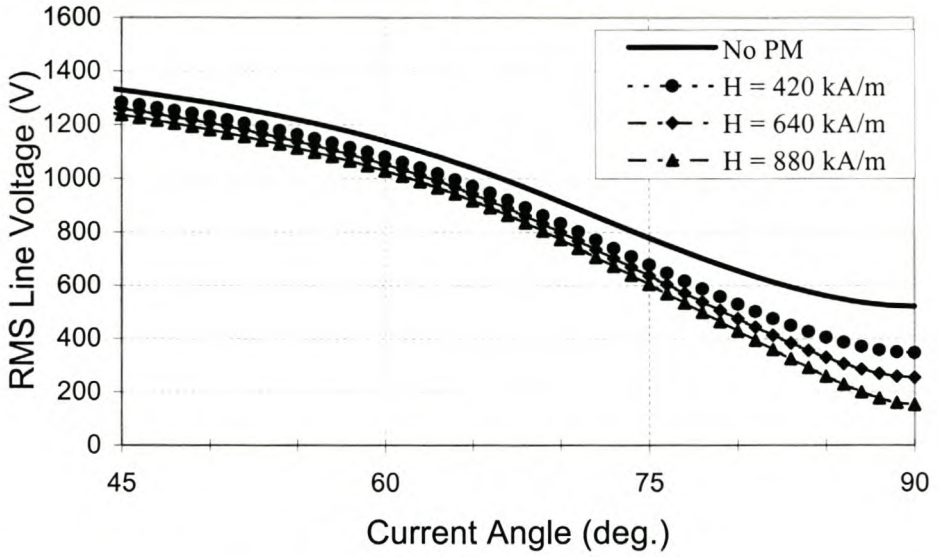

Figure 3.14. Line voltage versus current angle for different magnet strengths at 3800 rpm and 187 A RMS

It can be concluded from the results of Figs. 3.13 and 3.14 that an optimum amount of PM flux could be added on the rotor to achieve the desired torque and voltage performance parameters of the RSM at the maximum speed of 3800 rpm. It is also clear from these results that PMs with low field intensity of 420 kA/m can achieve the minimum desired performance parameters, at a relatively cheaper cost. The author therefore, chose to use these magnets for the research. The other important advantage that led to this choice is that weaker magnets could be distributed along the rotor flux barriers to achieve a sinusoidal flux distribution.

The next section describes the optimal design of the PM-assisted RSM using finite element analysis (see chapter 2) and the optimisation algorithm.

3.2 Design optimisation of the PM-assisted RSM

This section describes the design optimisation of the PM-assisted RSM using Powell's method. The aim of the optimisation procedure is to minimise the PM volume used in the flux barriers subject to minimum voltage and torque constraints. The objective function and constraints are directly calculated using finite element during the optimisation process.

3.2.1 Optimisation algorithms [3, 15]

Vast amount of work [15] has been published on the design optimisation of electrical machines, in particular the reluctance synchronous machines. It is generally understood that both the optimisation problem and the constraint functions in electrical machines design may be non-linear. The choice of the optimisation algorithm depends on the nature of the optimisation problem and other constraints such as time. In this thesis Powell's method, due to its less computational time [10], is used and is explained in the next section.

3.2.2 Powell's method [3]

Powell's method uses an iterative search procedure. Each iteration of the procedure maximises (minimises) the objective function along n linearly independent directions, where n is the number of variables to be optimised. The initial sets of n vector directions are the co-ordinate directions. After each iteration, a new direction is defined which is used to form the vector directions for the next iteration. After n iterations, sets of n mutually conjugate vector directions are obtained so that the maximum (minimum) of a quadratic function is found. A flow chart of Powell's method is shown in Fig. 3.15.

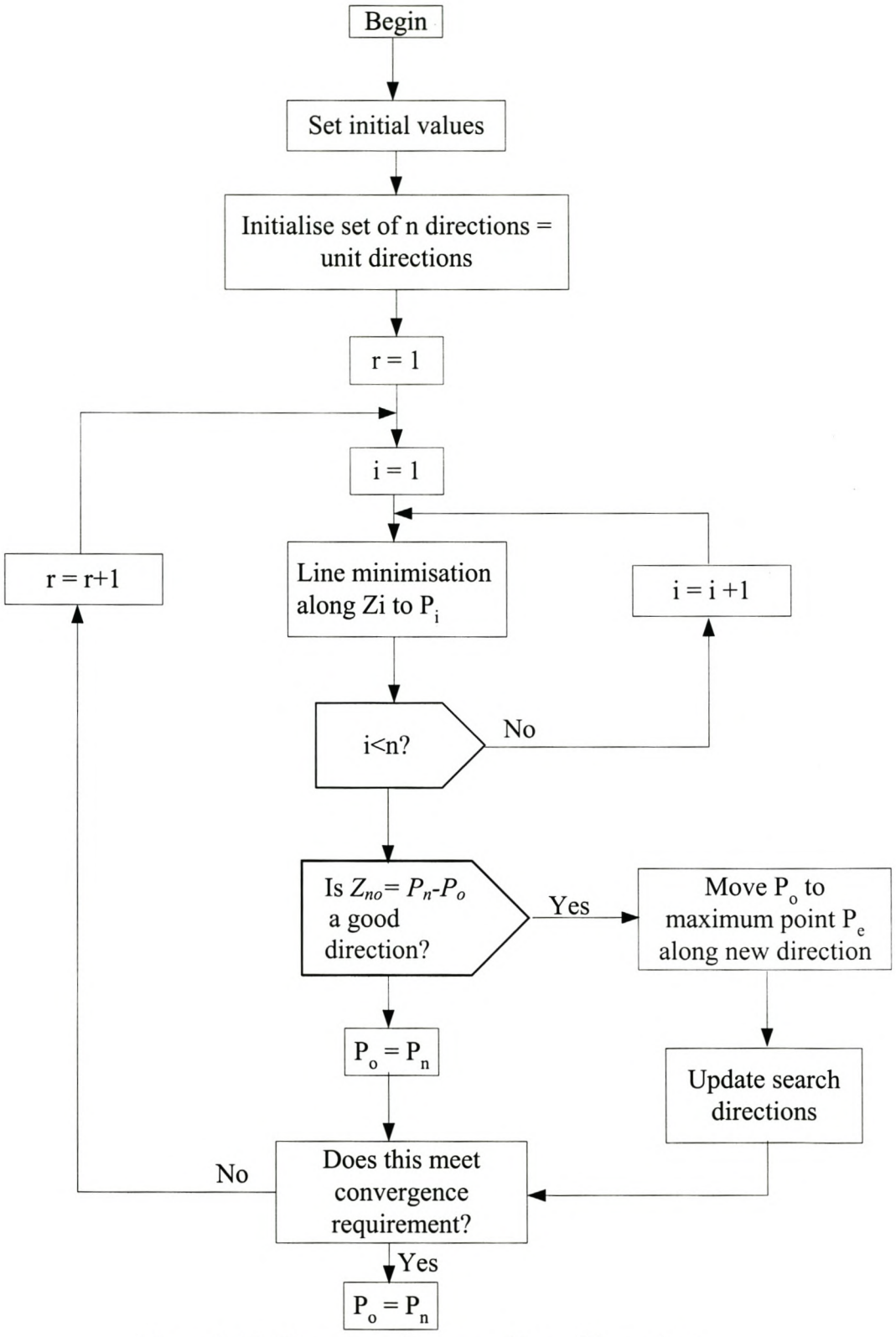

Figure 3.15. Flow chart diagram of Powell's method

The method of Powell uses the line minimisation procedure to minimise the function value in n vector directions as shown in Fig. 3.15. A new direction is then defined after n line minimisations. This procedure, however, may choose linearly dependent directions, which may cause the process to terminate before an optimum is reached. To avoid this, tests are performed after each iteration by defining an extra vector point P further along the proposed new direction. If the function values of these vector points $f_o = F(P_0)$, $f_n = F(P_n)$, $f_e = F(P_e)$ satisfy either

$$f_e \leq f_0 \text{ and/or}$$

$$(f_0 - 2f_n + f_e)(f_0 - f_n - \Delta f)^2 \leq \frac{1}{2}\Delta f(f_0 - f_e)^2 \tag{3.20}$$

where $\Delta f = \max_i(f_i - f_{i-1})$ is the greatest increase of the function value along one of the directions of the iteration, then the old directions are kept for the next iteration with the starting vector point moved to P_n. Otherwise, the new direction L_{no} is incorporated for the next iteration and the next starting point is changed to P_e. The other important step is to discard the direction corresponding to the largest increase of Δf, which is essential to avoid linear dependence in the optimisation process.

The optimisation procedure is terminated when the following criterion is met

$$|f_n - f_o| \leq \xi \frac{|f_n| + |f_o|}{2} \tag{3.21}$$

where ξ is the fractional tolerance of the function value f_0 and f_n are the start and final function value of one iteration, respectively.

3.2.3 Constrained optimisation

Constrained optimisation can be defined as a minimisation (maximisation) subject to constraints in the space of possible solutions. In this thesis the penalty function is used together with Powell's method. The objective function is modified by adding

terms or functions that penalise any increased constraint violation. This can be explained by the following equation:

$$F(\mathbf{X},\mathbf{w}) = f(\mathbf{X}) + \sum_{i=1}^{n} w_i c_i(\mathbf{X}), \tag{3.22}$$

where $f(\mathbf{X})$ is the objective function (magnet volume in this case), n is the number of penalty functions, $c_i(\mathbf{X})$ is the i-th penalty function and $\mathbf{w}_i$ is simply a weight that determines the extent the function is penalising the objective function. Our optimisation program can only *maximise* an objective function. We, thus, implemented the above equation as follows; using two quadratic penalty functions to ensure minimum required torque and maximum allowed supply voltage:

$$Y = F(\mathbf{X},\mathbf{w}) = \frac{1}{Vol_{mag}} - w_1(v_o - v_s)^2 - w_2(T_o - T_{out})^2 \tag{3.23}$$

$$w_1 = \begin{cases} 0 & T_{out} \geq T_o \\ 40 & T_{out} < T_o \end{cases} \tag{3.24}$$

$$w_2 = \begin{cases} 0 & v_s \leq v_o \\ 40 & v_s > v_o \end{cases}, \tag{3.25}$$

where Vol_{mag} is the magnet volume, v_s and T_{out} are respectively the calculated phase voltage and torque of the machine, and $v_o = 553$ V and $T_o = 360$ Nm are the rated induction machine voltage and torque at maximum speed of 3800 rpm (see Table A1 in appendix A). However during optimisation, the voltage and torque values are set slightly lower ($vo = 550\ V$) or higher ($To = 362\ Nm$) to ensure that the optimisation settles to the nearest acceptable values. Thus the constrained optimisation problem is solved by an unconstrained optimisation routine. The difficulty with this procedure is that the weighting functions are found by trial and error. In this case the weighting functions are equal because the importance of meeting the minimum voltage and torque constraints is the same.

3.2.4 Variables to be optimised

A rotor cross-sectional diagram of the 110 kW PM-assisted RSM is shown in Fig. 3.8. Thin sheets (three) of PM material are added to the inner side of the flux barriers of the reluctance rotor as shown in the figure. The thicknesses of these magnet sheets are the variables to be optimised.

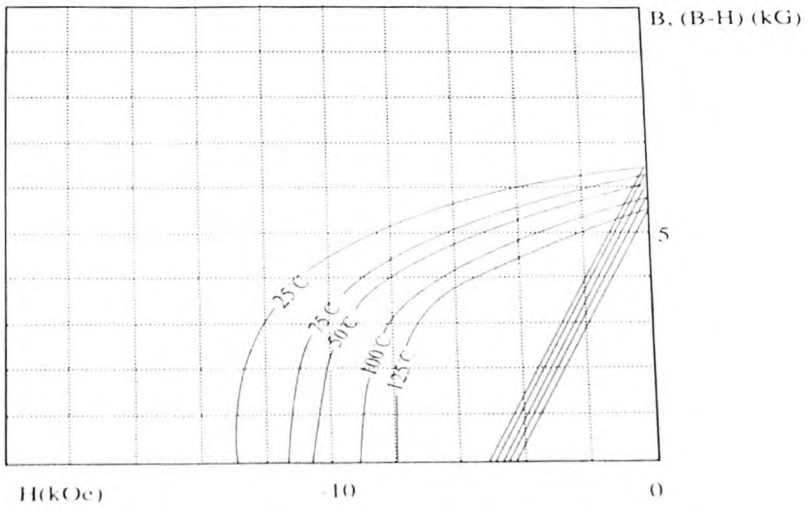

Figure 3.16 Demagnetisation curves of the epoxy bonded NdFeB magnets

The representation of the magnets in the finite element analysis is described in Chapter 2. The magnet material used is a new type of epoxy bonded NdFeB magnet. Typical demagnetisation curves of NdFeB magnets are shown in Fig. 3.16 above. It is clear that the magnetic intensity of these types of magnets is not as strong as the normal hard and brittle magnets, but this is due to the magnet powder that is epoxy bonded. The advantages of the epoxy-bonded magnets are that (i) they are not brittle, (ii) can easily be shaped as required and (iii) are protected against corrosion. The demagnetisation curves of these types of magnets as a function of temperature are also shown in Fig. 3.16. As the rotor of the RSM is basically running cool, as there are very little rotor losses, the temperature of the magnets is expected not to rise above 100°C since the stator winding temperature rise to 100^0C.

3.2.5 Design criteria and optimisation

In the optimisation process, the FE analysis is performed at a fixed rotor position. The mechanical losses were estimated at 7 kW and kept constant in the calculations. The basic structure of the optimisation program is shown in Fig. 3.17.

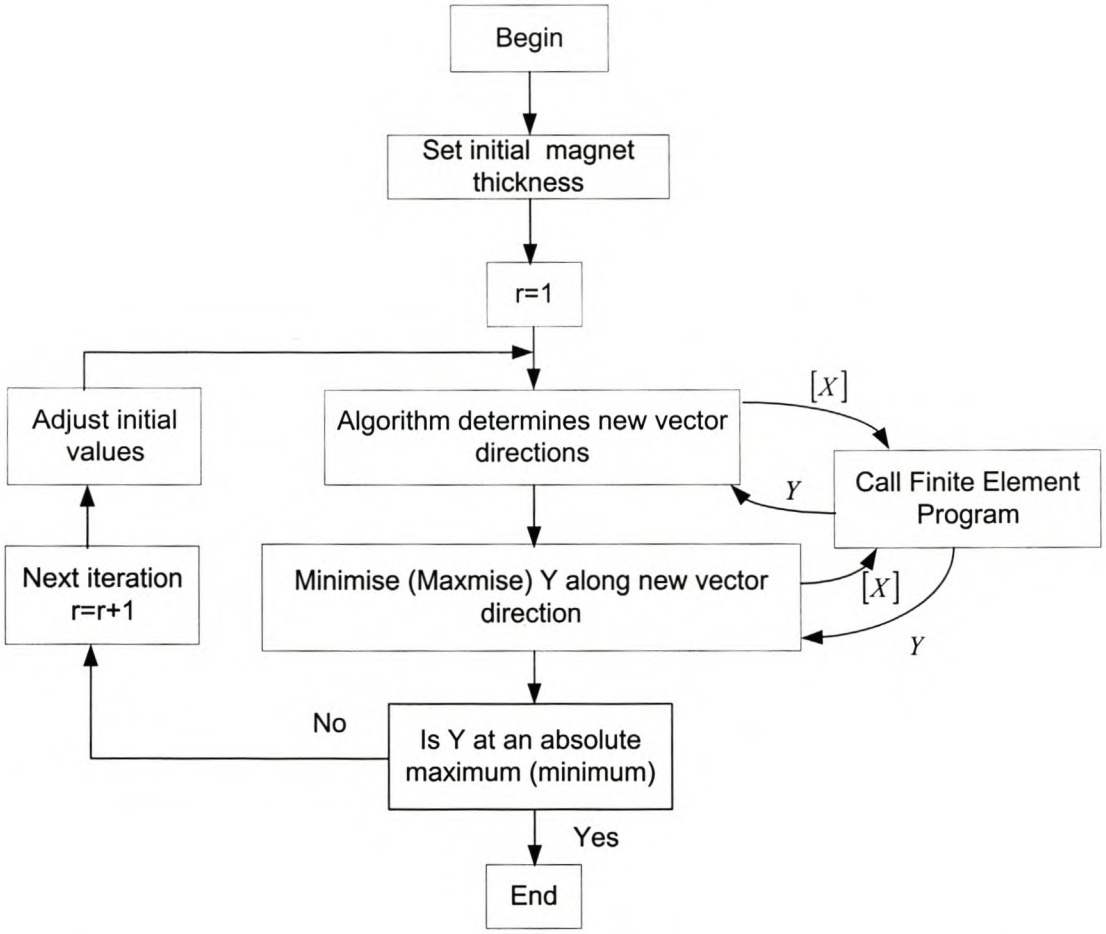

Figure 3.17. Optimisation procedure using the finite element solution directly

Powell's method requires an initial value for each of the variables. If this is too far from the real optimum, then the optimisation may end up being trapped in a local optimum in the vicinity of the initial value, which will lead to the necessity of testing with different sets of starting values to verify the optimum point. In the present

optimisation, a few different sets of starting points were used and the results were found to be sufficiently close to one another.

During the optimisation process, the mesh of the FE changes as the optimisation progresses. Occasionally some of the elements may become badly shaped or ill conditioned, resulting in poor accuracy or even no solution. It is therefore necessary to check that the model dimensions are reasonable before the FE mesh is constructed.

To minimise the magnet volume the thickness of the three magnet sheets of the reluctance rotor of Fig. 3.8 must be optimised. Hence, the variable [**X**]=[*x1 x2 x3*] in Fig. 3.17 as input represents the thickness of the magnet sheets, while Y, as output, represents the magnet volume that must be minimised subject to torque and voltage constraints.

3.2.6 Optimisation results

Implementing the optimisation procedure as described above, the results found for the optimum magnet sheet thicknesses are given in Table 3.1. The type and magnetic strength of the magnet material used in the design optimisation are also given in Table 3.1. A cross-section of the RSM with the optimised PM reluctance rotor is shown in Fig. 3.8 (see Appendix B for drawings). The thicknesses of barriers 2 and 3 were slightly overstated from 2.27 to 3.07 mm and from 3.07 to 3.63 mm respectively, when sent to the manufacturer to ensure a positive tolerance on the practical performance parameters.

Table 3.1: Final optimised magnet thickness

Optimised magnet thickness (mm)		
Inner barrier (1)	Middle barrier (2)	Outer barrier (3)
4.05	2.27	3.07
Material type: Epoxy bonded rare earth permanent magnet **Hc** = 420 kA/m; **Br** = 0.6 Tesla; Density = 6 g/cm^3		

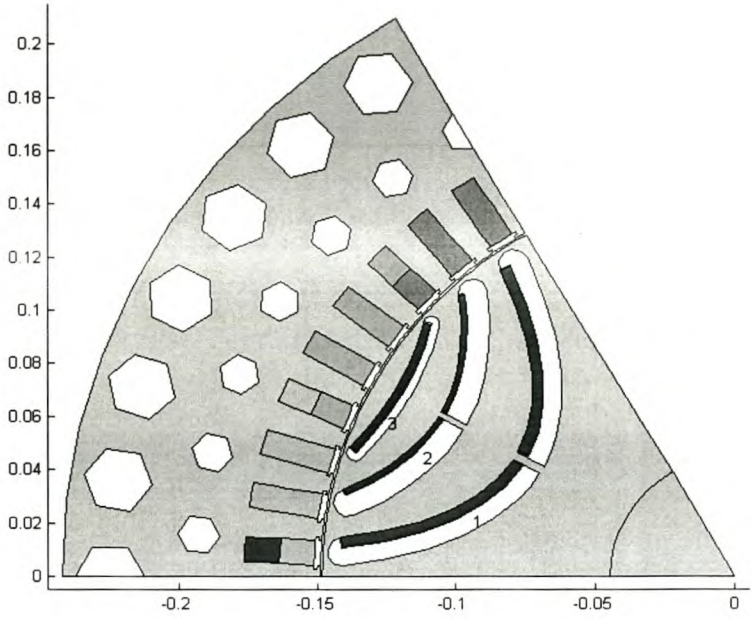

Figure 3.18. Cross section of PM-assisted RSM

3.3 Mechanical strength analysis

With the addition of magnet material as shown in Fig. 3.18, the mechanical strength of the small iron ribs and webs must be checked again at high speeds. Note that the mass-density of the epoxy magnet material is less than that of steel. Mechanical strength finite element analysis has been conducted on the rotor at a speed of 3800 rpm. The result of this analysis is shown in Fig. 3.19. The maximum deflection is found to be 71 μm on the outside of the rotor and the maximum stress of 194 MPa on the inner iron web. The maximun yield strength of the iron is 325 Mpa. Using linear analysis, the maximum stress exerted on the rotor web at an overspeed of 4500 rpm is calculated to be 266 MPa. This gives a safety factor of (325/266 = 1.22). This safety factor can be increased by increasing the width of the inner web from 3 to 4 mm. The maximum stress on the web is a function of the area and therefore with the increased web width it decreases to F/(A x 4/3) = 266 x (3/4) = 199.5 MPa. Therefore the safety factor becomes 325/199.5 = 1.63. The increased web width will have a negligible

effect on the performance parameters since it is always saturated by the flux of the PM sheets.

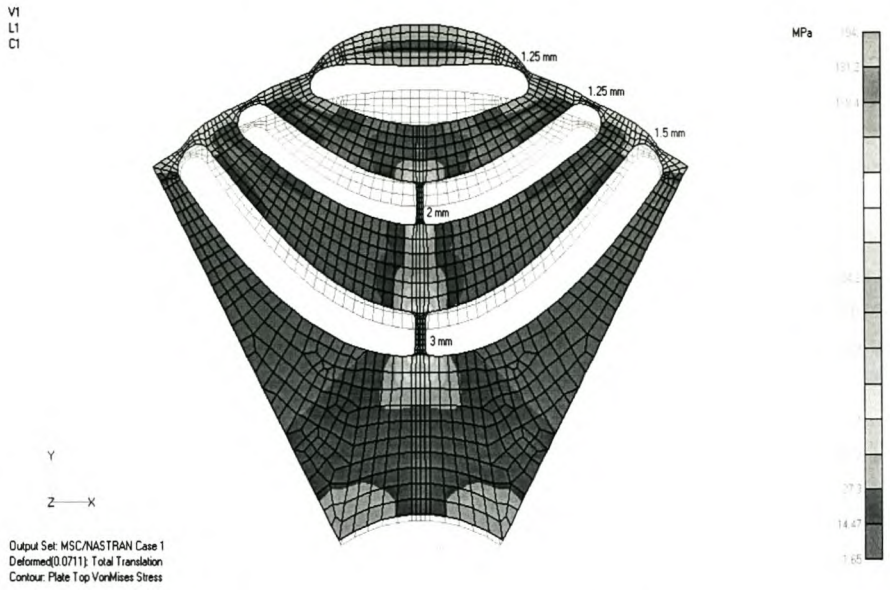

Figure 3.19. Finite element mechanical strength analysis of the PM reluctance rotor

3.3.1 Mechanical model

The mechanical equation of the PM-assisted RSM drive is similar to that of the RSM drive discussed in Chapter 2 and is given by

$$T_{em} = J_{eq}\frac{d\omega_{rm}}{dt} + \beta_{eq}\omega_{rm} + T_L \tag{3.26}$$

and

$$J_{eq} = J_m + J_L \text{ and } \beta_{eq} = \beta_m + \beta_L, \tag{3.27}$$

where J_m and J_L are the inertias of the machine and the load respectively. β_m and β_L are the friction coefficients of the machine and the load respectively. T_{em} is the generated torque of the PM-assisted RSM and T_L the load torque. This is illustrated in Fig. 3.20.

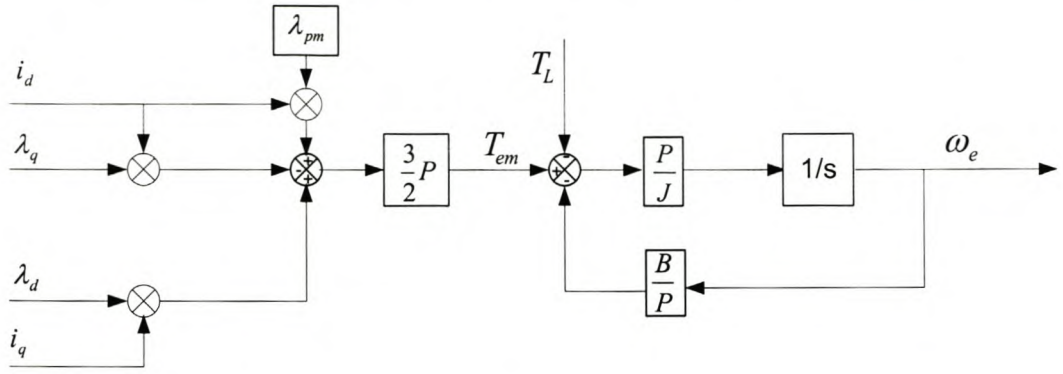

Figure 3.20. Block diagram of the generated torque of the PM-assisted RSM and the mechanical system

The rotor position is derived from the rotor speed using the relation

$$\theta = \int_0^t \omega\xi \, d\xi + \theta(0) \tag{3.28}$$

3.4 Theoretical comparison of IM, RSM and PM assisted RSM

This section compares the performance parameters of the 110 kW IM, RSM and PM-assisted RSM with the same IM stator frame and windings. The performance parameters are the output torque and power factor. A discussion on the rotor losses is also presented.

With the same stator frame and windings, the stator losses for all the machines under consideration will be the same for any selected nominal operating point. However, the IM must sustain rotor slip frequency losses to produce torque. In contrast, the rotors of the RSM and PM-assisted RSM do not exhibit any significant losses.

3.1.1 Torque comparison

The torque equations of the RSM and IM are

$$T_{RSM} = \frac{3}{2} L_d p\left(1 - L_q / L_d\right) i_d i_q \tag{3.29}$$

$$T_{IM} = \frac{3}{2} p\left(\frac{L_{\text{Im}}}{L_r + L_{\text{Im}}}\right) L_{\text{Im}} i_{ds} i_{qs} \tag{3.30}$$

and

$$T_{PM-RSM} = \frac{3}{2} p\left(\lambda_d i_q - \lambda_q i_d + \lambda_{pm} i_d\right) \text{ or } T = \frac{3}{2} p\left(\lambda_d i_q - \lambda_q i_d + L_m\right) \tag{3.31}$$

The torque ratio of the RSM to the IM is

$$\frac{T_{RSM}}{T_{IM}} = \frac{3/2 p i_d i_q L_d (1 - L_q / L_d)}{3/2 p i_{ds} i_{qs} L_m (L_{\text{Im}} / (L_r + L_{\text{Im}})} \tag{3.32}$$

By assuming that the currents and the d-axis inductances, L_d and L_q, for the RSM and IM are the same, eqn. 3.32 can be simplified as

$$\frac{T_{RSM}}{T_{IM}} = \frac{(1 - L_q / L_d)}{L_m / (L_r + L_{\text{Im}})} \tag{3.33}$$

With $L_r << L_{Im}$ it follows that the torque ratio is dependent on the RSMs inductance ratio, i.e. $T_{RSM}/T_{IM} \rightarrow 1$ *if* $L_q/L_d \rightarrow 0$. The torque ratio of the PM assisted RSM to the IM is

$$\frac{T_{PMRSM}}{T_{IM}} = \frac{3/2 p i_d i_q L_d (1 - L_q / L_d + L_m)}{3/2 p i_{ds} i_{qs} L_m (L_{\text{Im}} / (L_r + L_{\text{Im}})} \tag{3.34}$$

Again by assuming that the stator currents and the d-axis inductances are the same, the torque ratio equation can be expressed as

$$\frac{T_{PMRSM}}{T_{IM}} = \frac{(1 - L_q / L_d + L_m / L_d)}{(L_{\text{Im}} / (L_r + L_{\text{Im}})} \tag{3.35}$$

or

$$\frac{T_{PMRSM}}{T_{IM}} = \frac{(1+\frac{L_q - L_m}{L_d})}{(L_{\mathrm{Im}}/(L_r + L_{\mathrm{Im}})} \tag{3.36}$$

For the PM-assisted RSM and IM, the torque ratio is dependent on both the inductance difference $(L_q - L_m)$ and the inductance ratio $(L_q - L_m)/L_d$. It is clear from eqn. 3.36 that with $L_r << L_{IM}$ and $L_m > 0$, the torque ratio T_{PMRSM}/T_{IM} rapidly approaches unity as compared to the RSM in eqn. 3.33. It is also clear from eqn. 3.36 that the PM inductance, L_m, must always be lower than or equals to the q-axis inductance, L_q, otherwise the torque performance of the PM-assisted RSM will be drastically reduced.

3.5 IM rotor losses consideration

It is generally argued that the RSM, when designed correctly, does not exhibit any significant rotor losses. However, on the other hand the IM must sustain frequency slip losses in order to produce any torque.

If it is assumed that the IM stator losses are equal to the rotor losses, then based on the above reasoning, the ratio of copper losses for the RSM and IM operating at a nominal point is

$$\frac{P_{RSM}}{P_{IM}} = 0.5 \tag{3.37}$$

If the losses of the RSM are to be made equal to the IM losses, and considering that losses are proportional to the square of the current, the RSM current would have to be raised by a factor of $\sqrt{2}$. Thus in general, the RSM stator current could be raised by the factor

$$\sqrt{\frac{P_{IM\ copper\ losses}}{P_{IM\ copper\ losses} - P_{RSM\ copper\ losses}}} \tag{3.38}$$

to match the IM copper losses. Since the d-axis current should remain constant due to saturation, this corresponds to raising the q-axis current and effectively the torque of the RSM and PM-assisted RSM.

3.6 Conclusions

It was theoretically shown in section 3.4 that the torque performance of the RSM compared to the IM can be greatly improved by adding slight amount of PM flux on the q-axis of the rotor. In section 3.5 it was shown that the torque performance of the RSM compared to the IM could also be improved by carefully considering the losses of the machines in the design process.

It can be concluded that the RSM can produce torque relatively comparable to the IM if the losses are taken into account in the design process. A very slight amount of PM sheets can then be added if necessary just to match the RSM and IM torques.

Chapter 4

4. Digital Control of the RSM

This chapter focuses on the feedback control of the RSM and PM-assisted RSM in the low and high-speed regions. The control is done in the reference frame fixed to the rotor. The *dq* mathematical models (see chapters 2 and 3) are used to describe the decoupled control of the RSM. It also describes the design of the *dq* PI current controllers and the speed controller using Matlab and their implementation onto the DSP control.

4.1 Control of the RSM and PM-assisted RSM

The torque of a RSM is given by

$$T = K_1(\Delta L) I_d I_q \tag{4.1}$$

or

$$T = K_2(\Delta L) I_s^2 \sin(2\phi) \tag{4.2}$$

and that of a PM assisted RSM as

$$T = K_2 (\Delta L + \frac{\lambda_{pm}}{i_q}) I_s^2 \sin (2\phi) \tag{4.3}$$

or

$$T = K_1(\Delta L + \frac{\lambda_{pm}}{i_q}) i_d i_q \tag{4.4}$$

where $K_1 = \frac{3}{2}P$, $K_2 = \frac{3}{4}P$ are torque constants and $\Delta L = L_d - L_q$ is the inductance difference. The inductance difference is not a constant but varies with the *d* and *q*-axis currents.

The *d*–axis current is responsible for producing the stator magnetising flux while the *q*-axis current is for producing the torque. The magnitude of the torque is controlled by regulating the magnitude of the *q*-axis current while the flux is controlled by regulating the *d*-axis current.

It then follows that for the RSM to have better efficiency and maximum torque per ampere both the flux producing (*d*-axis) and torque producing (*q*-axis) currents must be effectively controlled independently. This type of control is referred to as vector control since the flux and torque producing current components are controlled independently. This is equivalent to controlling the RSM like a separately excited dc machine.

The complete closed loop control block diagram of the RSM and PM-assisted RSM is shown in Fig. 4.1 below where ω^*, i_d^*, i_q^*, λ_{pm} are respectively the speed, the *d*- and *q*-axis current references and the flux linkage due to the permanent magnets. The permanent magnet flux linkage, λ_{pm}, term is not present in the RSM. The flux and torque produced by the RSM is controlled by assigning non zero *d* and *q*-axis reference currents.

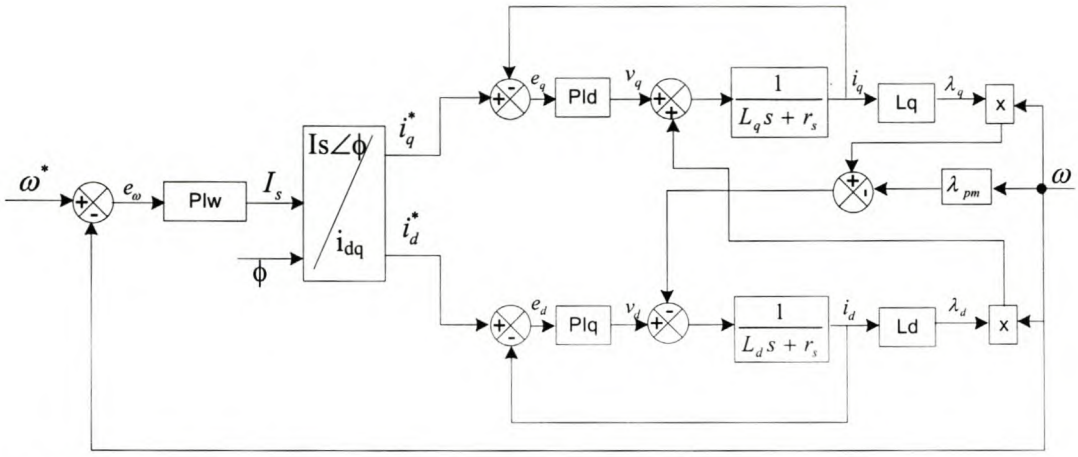

Figure 4.1: Control block diagram of the RSM and PM-assisted RSM

The speed and current controllers (*PIw, PId, PIq*) are proportional integral controllers which attempts to minimise the speed (e_w) and current (e_d *and* e_q) errors at all times, thereby ensuring that speed (ω), *d*-axis (i_d) and q-axis (i_q) current track their reference points ω^*, i_d^*, and i_q^* respectively.

The current regulation is performed in the rotor reference frame as the *d* a *q*-axis currents are dc quantities at steady state thereby justifying the use of linear *PI* controllers. Closed loop control of the RSM is achieved by incorporating an outer speed control loop as shown in Fig. 4.1. The outer control speed loop serves to regulate the speed of the motor against the effect of the load torque disturbance.

4.2 Current control method

There are two methods of controlling the reference *dq* currents in the machine. The first one is the conventional method where the *d*-axis current is kept constant (constant flux) in the constant torque region and reduced as speed increases in the flux-weakening region. The second method is known as constant current angle control. With this method the magnitude of the current vector is used to control the

torque and the flux in the machine. A complete analysis on the performance of this type of controllers was done [21] and it was found that the advantage of using the constant current angle control method is the improved efficient use of energy. This is because with this control method optimum *d*- and *q*-axis currents flow corresponding to the load applied.

In this thesis the constant current angle control method is used as will be discussed in the next sections.

4.3 Decoupling of the *d* and *q*-axis circuits

It is clear from Fig. 4.1 that the design of the current controllers would be complex since the *d* and *q*-axis currents of the RSM model are interconnected by the speed dependent terms. This phenomena is often called the cross coupling between the *d*- and *q*-axis circuits. The cross coupling terms introduce non-linearities in the RSM motor model since they are speed dependent terms.

The overall RSM model can be simplified if the cross coupling between the *d* and *q*-axis is eliminated. The decoupling is normally done by adding or subtracting the speed dependent terms in the control algorithm. This is shown in equations 4.5 and 4.6. With the decoupled model, the *d* and *q*-axis PI controllers are designed independently since each has to respond to the stator current and inductance respectively.

$$\left(v_d + \omega_{re}\lambda_q - M'_d \frac{di_q}{dt}\right) = \left(r_s i_d + L'_d \frac{di_d}{dt}\right) \tag{4.5}$$

$$\left(v_q - \omega_{re}\lambda_d - M'_q \frac{di_d}{dt}\right) = \left(r_s i_q + L'_q \frac{di_q}{dt}\right) \tag{4.6}$$

The RSM with the decoupled *d* and *q*-axis models is shown in Fig. 4.2 below. Considering the *q*-axis model (Fig. 4.2a), it is clear that the speed voltage term is added in the control algorithm and added inside the machine model. With this decoupling in the *q*-axis of the RSM, the resulting approximate motor model resembles a linear first order system with the time constant ($\tau = \frac{L_q}{r_s}$). Similar arguments prevail for the *d*-axis model of the RSM shown in Fig. 4.2b.

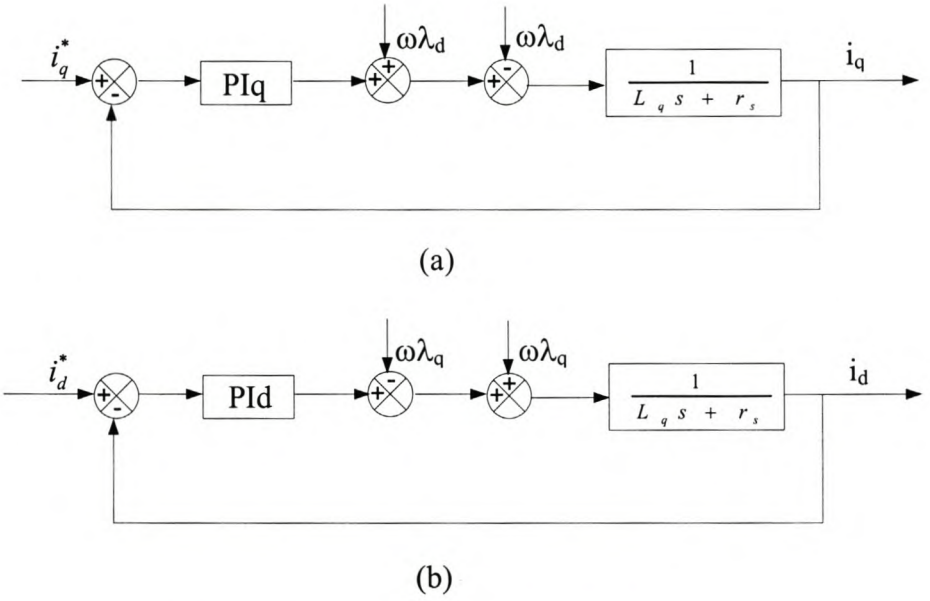

Figure 4.2: Decoupling of speed voltages [21]

4.4 Design of the current controllers [21]

The general closed loop control block diagram of the RSM is shown in Fig. 4.3 below. Where K_{inv} is the transfer function of the inverter, K_s the DSP conversion factor and Zoh the zero order hold. These parameters will be described later in the thesis.

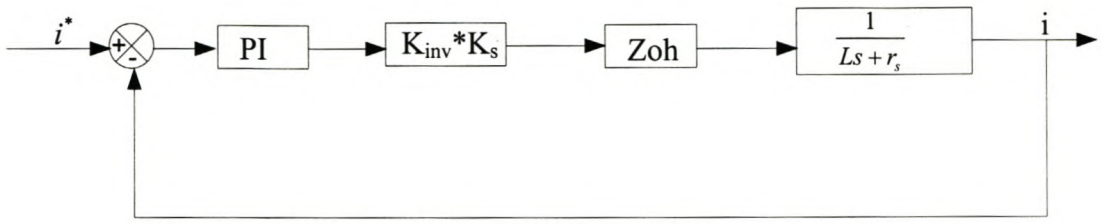

Figure 4.3: Current control block diagram [21]

The PI controller in the analog domain is given in equation 4.7 below as

$$D(s) = K_p + \frac{K_i}{s} \tag{4.7}$$

where K_p and K_i are the proportional and integral coefficients. The equivalent discrete time system is obtained using the backward difference method such that

$$D(z) = \frac{(K_p + TK_i)z - K_p}{z - 1} \tag{4.8}$$

T is the sampling period. The transfer function of the zero order hold (ZOH) and the system are given below in equations 4.9 and 4.10 respectively as

$$G_{zoh}(s) = \frac{1}{s}\left(1 - e^{-sT}\right) \tag{4.9}$$

$$G(s) = \frac{1}{r_s(1 + s\tau)} \tag{4.10}$$

where L' is the phase inductance and $\tau = \frac{L'}{r_s}$ is the time constant of the system. The discrete time combined transfer function ($G(s) = G_{zoh}(s)*G(s)$) of the system and the ZOH is given by

$$G(z) = \frac{1 - e^{-\frac{r_s T}{L'}}}{r_s\left(z - e^{-\frac{r_s T}{L'}}\right)} \tag{4.11}$$

The closed loop transfer function is then given as

$$G_{cl}(z) = \frac{\frac{K_{inv}K_s}{r_s}\left[1-e^{-\frac{r_sT}{L'}}\right]\left[\left(K_p+TK_i\right)z-K_p\right]}{z^2+\left[\left(-1-e^{-\frac{r_sT}{L'}}\right)+\frac{K_{inv}K_s}{r_s}\left(K_p+TK_i\right)\left(1-e^{-\frac{r_sT}{L'}}\right)\right]z+\left[e^{-\frac{r_sT}{L'}}-\frac{K_pK_{inv}K_s}{r_s}\left(1-e^{-\frac{r_sT}{L'}}\right)\right]}$$

There are two unknown variables (K_p and K_i) in this equation, which are calculated by means of equating coefficients of the closed loop system with the general second order system given by

$$s^2+2\zeta\omega_n s+\omega_n^2=0 \tag{4.12}$$

The equivalent z-transform is given by

$$z^2-ze^{-\omega_n\zeta T}\left(e^{\zeta-\sqrt{\zeta^2-1}}-e^{\zeta+\sqrt{\zeta^2-1}}\right)+e^{-\omega_nT\left(2\zeta-\sqrt{\zeta^2-1}+\sqrt{\zeta^2-1}\right)}=0 \tag{4.13}$$

where ω_n, ζ are the natural frequency of the system and the damping factor respectively. These are specified in the design phase of the controller, e.g. the system must be overdamped ($\zeta > 1$) with a settling time of less than 1 ms. The natural frequency is then calculated from

$$\omega_n = \frac{4}{T\zeta} \tag{4.14}$$

The calculated values of K_p and K_i are then substituted into equation 4.8 to give the controller k(z). The root-locus design is then implemented in matlab after the controller and the transfer function has been calculated.

4.1.1 Design of PI controllers in Matlab

In matlab, the transfer function $g(z)=\frac{x}{(z-p)}$ is entered on the command window as $P = tf(x,[1 \quad -p],T)$, where T is the sampling period. Then to enter the control

parameters, on the command window, type rltool, then an empty root locus diagram will appear. Select file on the root-locus diagram, then import model (P), then enter the control parameters and select step on the root-locus window. The complete root-locus diagram with step response will be displayed. The control parameters are then adjusted till the desired response is attained.

4.1.2 Transfer function of the inverter (K_{inv})

The inverter used is a three-phase inverter with a switching frequency of 2.5 kHz. The inverter will be discussed in detail in chapter 5. However, in the design of the PI controllers, the inverter is represented as a transfer function (K_{inv}) as shown in Fig. 4.3. This sub-section discusses how the transfer function of the inverter is determined.

If the effects of the time delay and switching frequency of the inverter are ignored, then the transfer function of the inverter can be simplified to a constant value, K_{inv}, as shown in Fig. 4.4. To obtain the value of the transfer function (K_{inv}), the system is simulated for different values of input voltage as shown in Fig. 4.5. The value of K_{inv} is then calculated as the slope of the graph of Fig. 4.5 to be 0.225. This value of K_{inv} is used in the calculation of the controller parameters, as will be discussed in the next sections.

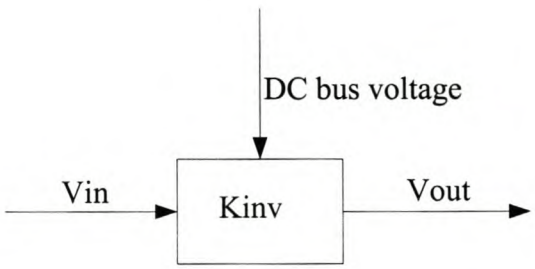

Figure 4.4. Transfer function of the inverter

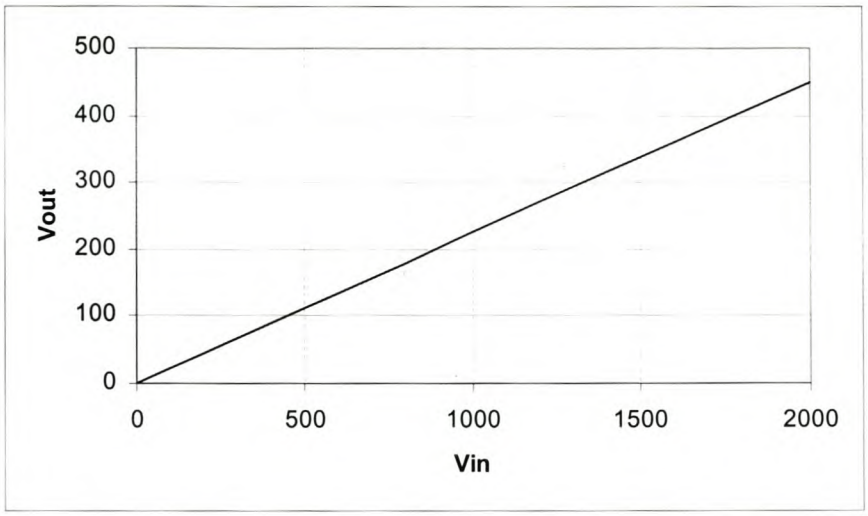

Figure 4.5. Inverter transfer function results

4.1.3 D-axis PI controller

The *d*-axis open loop transfer function of eqn. 4.11 is derived by substituting the parameters r_s = 15 mΩ, T = 400 us, Ks = 1 = 500/512, and K_{inv} = 0.225. The *d*-axis self inductance is obtained from Fig. 4.6 at rated current (200 A rms) and current angle of 60^0 (Id = 141 A and Iq = 245 A) to be 0.3 mH. The *d*-axis transfer function of the system is then calculated to be

$$g(z) = \frac{0.0225}{z - 0.9985} \tag{4.15}$$

The design of the PI controllers for this system is implemented in Matlab as discussed in the previous section. The corresponding controller transfer function is calculated as

$$k(z) = \frac{8(z - 0.999)}{z - 1} \tag{4.16}$$

The PI controller constants are calculated from eqn. 4.16 as *Kp* = 7.992 and *Ki* = 20. The step response of the system with the controller and the corresponding root locus diagram are shown in Figs. 4.7 and 4.8 respectively. It is clear from Fig. 4.7 that the *d*-axis circuit has a settling time of about 8.5 ms and is underdamped. The system will

however, be stable if operated at rated conditions since at any other conditions the inductances will be different and hence the system response to step inputs. This was found to be true in the practical experiments, that at speeds higher than base speeds (where the *d*-axis current is reduced), the control parameters had to be changed corresponding to different operating points. The adjusted speed, *d* and *q*-axis PI controller parameters are also presented in the results section of chapter 6.

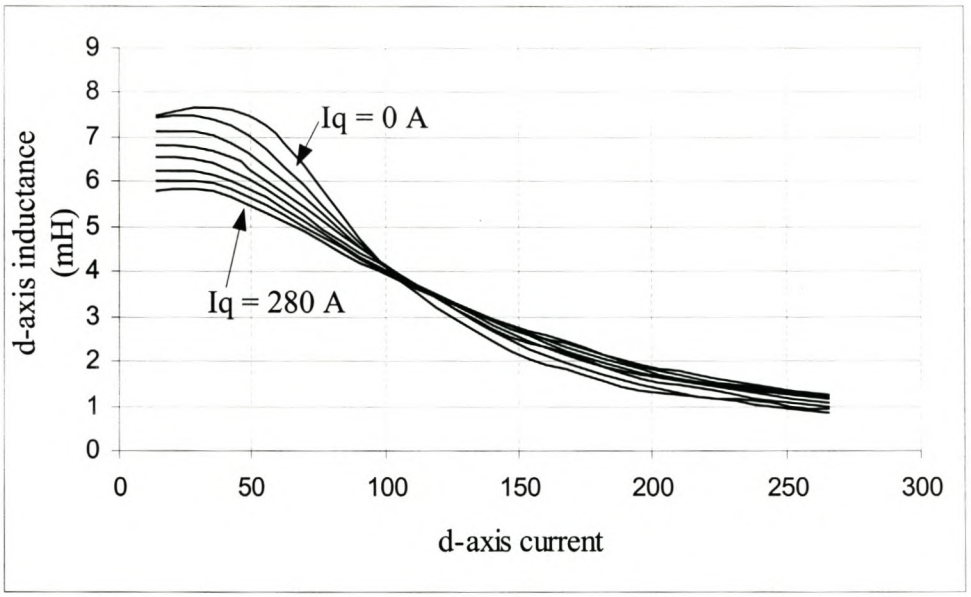

Figure 4.6: *d*-axis inductance curves (RSM)

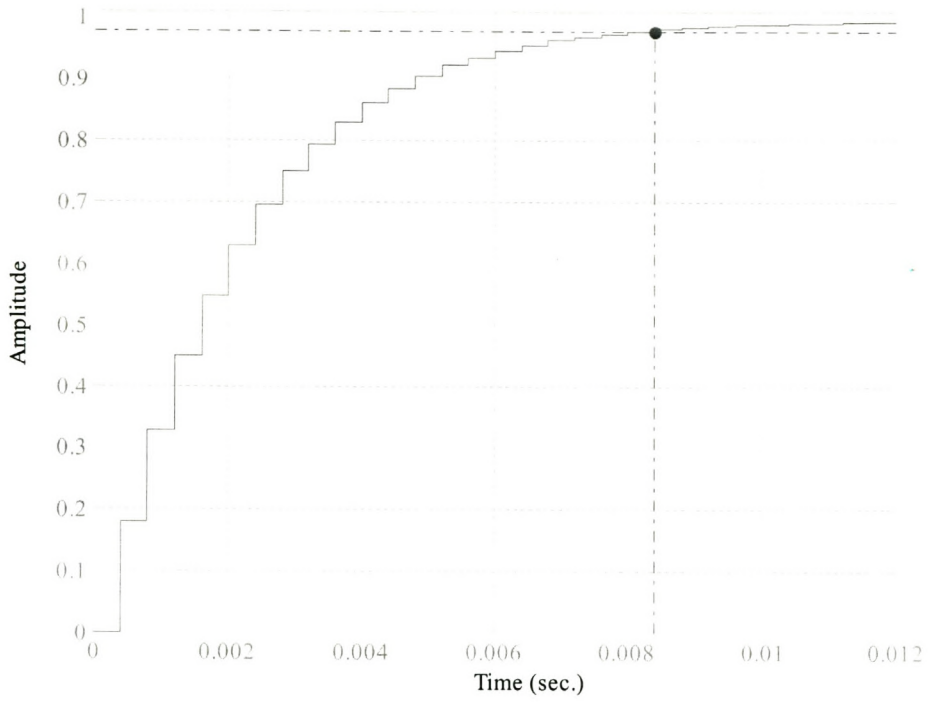

Figure 4.7. *d*-axis step response curve

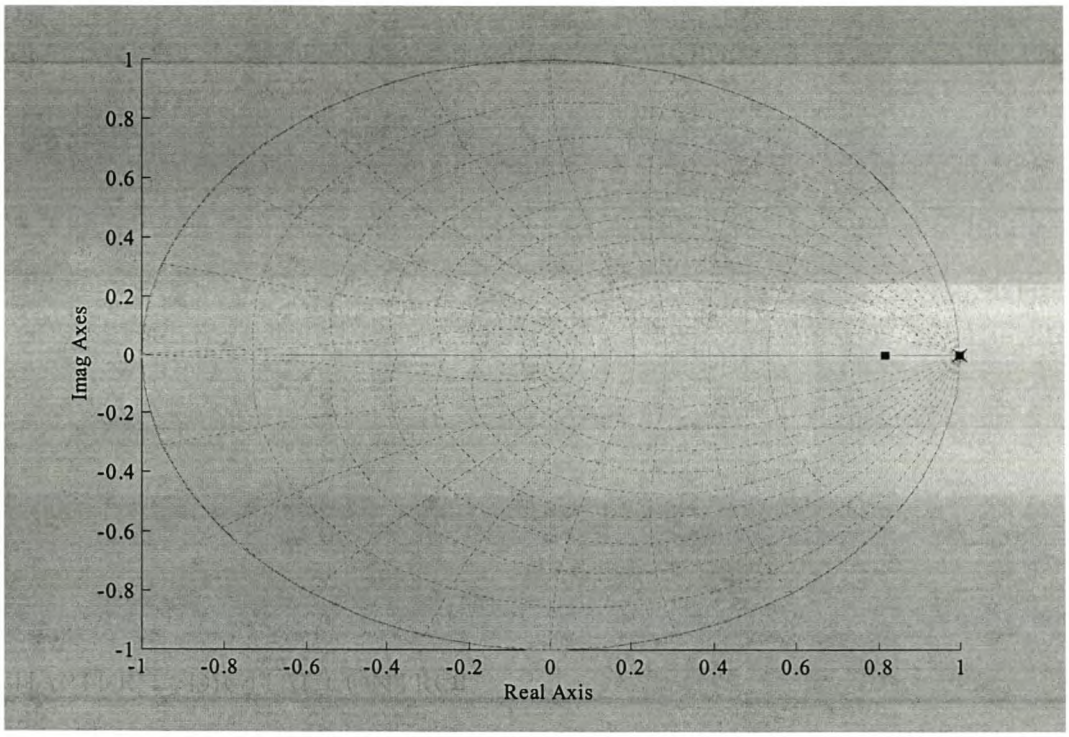

Figure 4.8. *d*-axis root locus diagram

4.1.4 Q axis PI controller

The *q*-axis open loop transfer function of eqn. 4.11 is derived by substituting the parameters r_s = 15 mΩ, T = 400 us, Ks = 1 = 500/512, and Kinv = 0.225. The *q*-axis self inductance is obtained from Fig. 4.9 at rated current (200 A rms) and current angle of 60^0 as 0.7 mH. The *q*-axis transfer function is then calculated to be

$$g(z) = \frac{0.128}{z - 0.9915} \tag{4.15}$$

The design of the PI controllers for this system is implemented in Matlab as discussed in the previous section. The corresponding controller transfer function is calculated as

$$k(z) = \frac{5(z - 0.9999)}{z - 1} \tag{4.16}$$

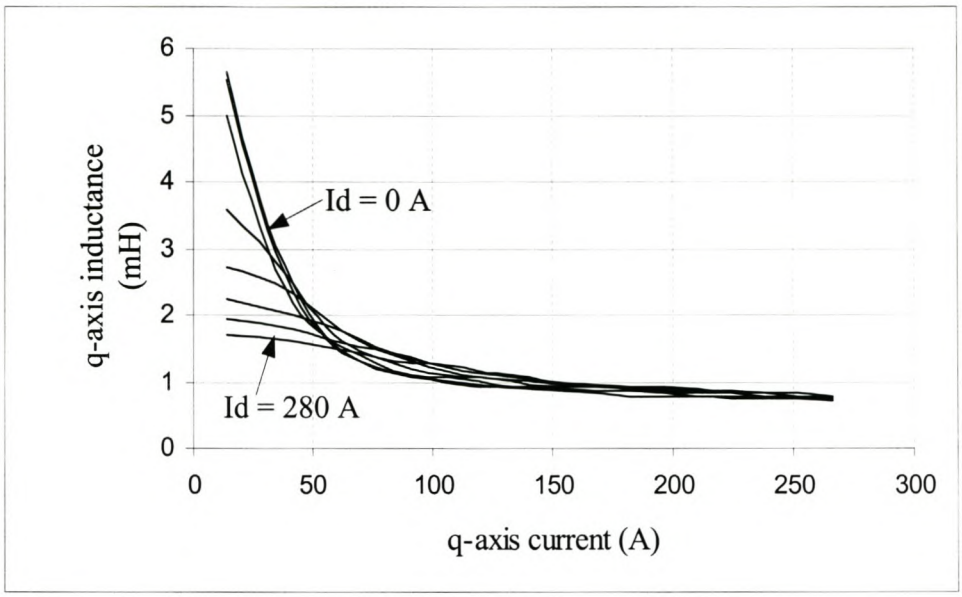

(a)

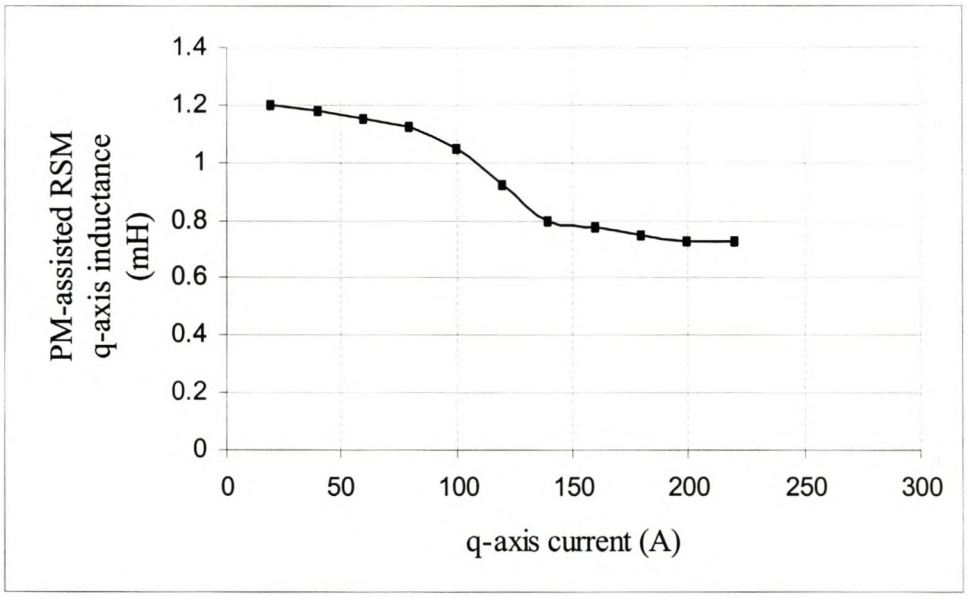

(b)

Figure 4.9. q-axis inductance versus q-axis current (a) and PM-assisted RSM q-axis inductance versus q-axis current at rated d-axis current (b) curves

From eqn. 4.16 the PI controller constants are calculated as $K_p = 4.995$ and $K_i = 1.25$. The step response of the system with the controller and the corresponding root locus

diagram are shown in Figs. 4.10 and 4.11 respectively. It is clear from Fig. 4.10 that the *q*-axis circuit has a settling time of about 2 ms.

The q-axis inductance of the PM-assisted RSM is shown in Fig. 4.9b. It is calculated from the *q*-axis flux linkage (as $L_{pm} = \lambda_{pm}/I_q$) of the PM-assisted RSM presented in Chapter 3. This *q*-axis inductance curve is used to design the *q*-axis PI controller of the PM-assisted RSM. However, it is evident from Fig. 4.9b that at steady state, the q-axis inductance of the PM-assisted RSM is about the same as that of the RSM ($L_{pm} = L_{RSM} \approx 0.7$ mH. So the RSM PI controllers can also be used for the PM-assisted RSM.

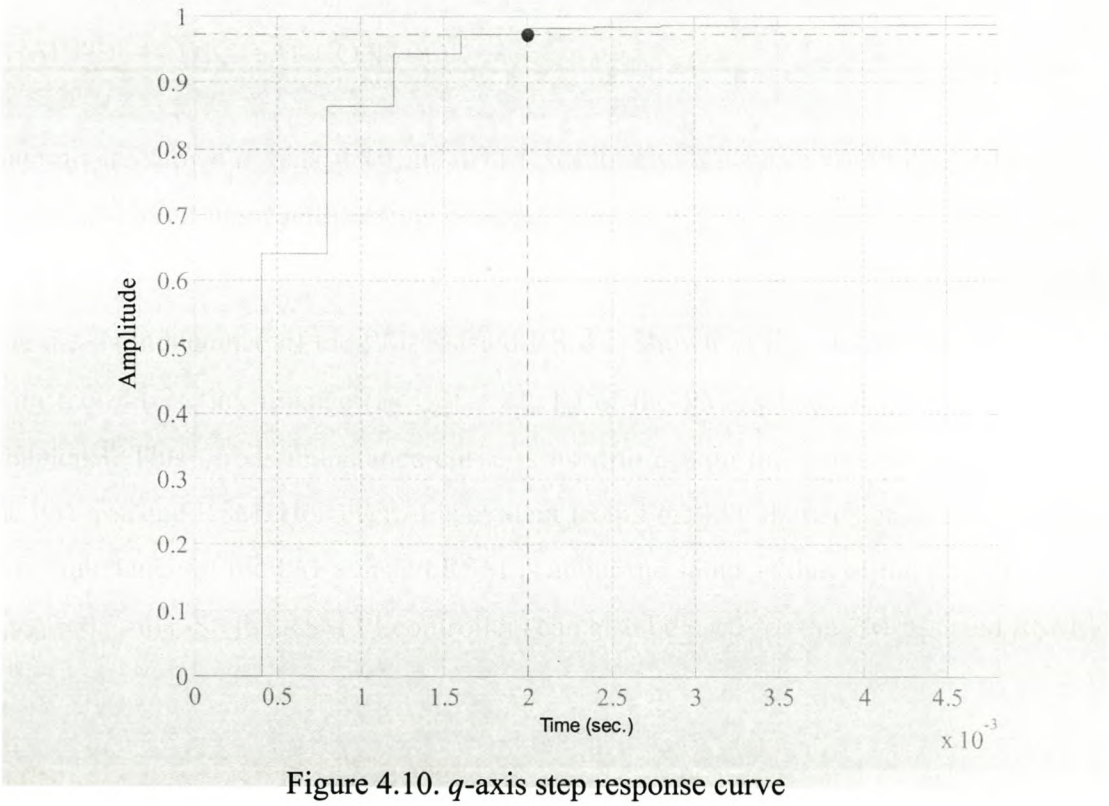

Figure 4.10. *q*-axis step response curve

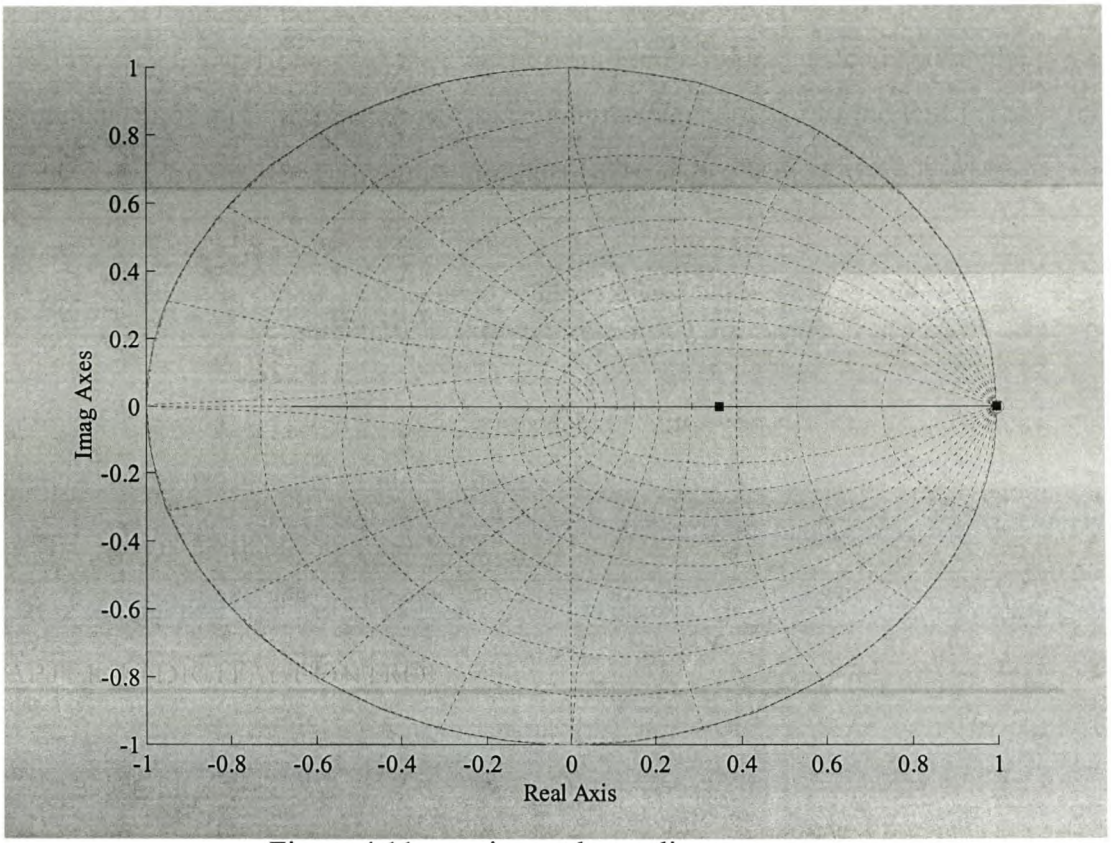

Figure 4.11. q-axis root locus diagram

4.2 Speed Controller

The block diagram of the speed feedback controller is shown in Fig. 4.12. The parameters *Kw*, *PI*, *Gcc* and *Zoh* in Fig. 4.12 are the speed constant, *PI* speed regulator, current transfer function and the zero order hold circuit. The speed constant is equivalent to the current constant (*Ks*) and is a scaling factor for the speed to the DSP. The speed PI regulator and the current transfer function are discussed in this section. The zero order hold is the sample and hold circuit as described in section 4.1.

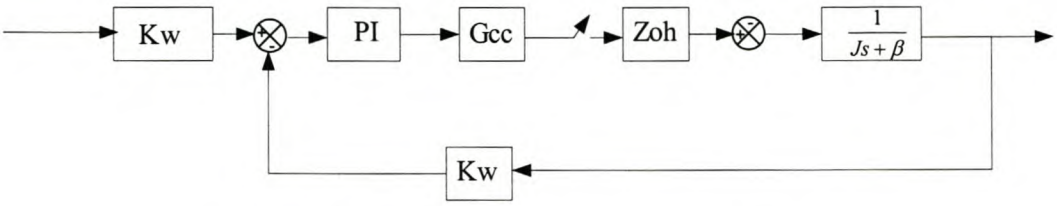

Figure 4.12. Speed closed-loop diagram of the RSM

The transfer function of the current controller is simplified to a first order transfer function as the transition response is close to a first order response. The transfer function of the current controller is

$$G_{cc}(s) = K_{cc}(\frac{1}{\tau_{cc}s+1}) \tag{4.17}$$

where τ_{cc} is the time constant and Kcc is the gain of the transfer function. The time constant depends on both the *d* and *q*-axis current responses. However, the *q*-axis response is faster than the *d*-axis response and therefore the overall current response of the current controller is dependent on the *d*-axis response. The time constant of the current controller can then be chosen equal the *d*-axis response time constant, which is 8.5 ms. The next step is to calculate the gain of the current controller between the reference current and the torque. The torque-current relationship is given by

$$T_{em} = \frac{3}{4}p(L_d - L_q)I_s^2 \sin(2\phi) \tag{4.18}$$

or else

$$\frac{T_{em}}{I_s^2} = \frac{3}{4}p(L_d - L_q)\sin(2\phi) = K_{cc} \tag{4.19}$$

The torque current relationship is then calculated at the rated current angle of 60^0 and different input values of current as shown in Table 4.1. For dynamic speed response, the torque current relationship should be correctly calculated as per current (Tem/Is) rather than per current squared as in equation 4.19.

The performance parameters of the IM, RSM and PM-assisted RSM are shown in Table 3.2. It is clear that at base speed, the performance of the PM-assisted RSM is better than that of the IM.

Table 3.2: Rated and maximum speed specifications of the IM, RSM and PM-RSM

Rated speed = 1500 rpm, f = 75.5 Hz					
Machine	Torque (Nm)	V	A	ϕ	Pf
IM	700	503	205	-	0.66
RSM	665	490	205	59	0.63
PM-RSM	759	482	205	54	0.74
Maximum speed = 3800 rpm, f = 191.7 Hz					
IM	360	553	187	-	0.85
RSM	352	748	187	76	0.60
PM-RSM	338	555	187	78	0.77

The calculated torque results of the Pm-assisted RSM at the maximum speed of 3800 rpm are slightly less than those of the RSM and IM. This is due to the less accurate modelling of the PM sheets in the FE software as discussed in Chapter 2. It will be shown in Chapter 6 that the PM-assisted RSM torque is actually higher than that of the IM and RSM.

Table 4.1: Calculation of the gain (K_{cc}) of constant current angle for the speed controller

Is-ref	Id	Iq	Ld	Lq	3/4P	Sin(2ϕ)	Kcc
282	141	245	0.728	0.239	4.5	0.866	1.905
220	110	190	0.645	0.212	4.5	0.866	1.687
180	90	155	0.574	0.199	4.5	0.866	1.461
120	60	104	0.417	0.167	4.5	0.866	0.974
80	40	70	0.287	143	4.5	0.866	0.561

The gain of the current controller, *Kcc*, is calculated (averaged) from Table 4.1 as 1.3. The transfer function of the current controller can then be simplified as

$$G_{cc}(s) = \frac{1.3}{0.008s + 1} \tag{4.20}$$

However, this time constant is much smaller compared to the speed controller time constant. The transfer function of the current controller is then simplified to Gcc(s) = 1.3. The transfer function of the speed controller with the zero order hold in the z-plane is given by [21] as

$$g(z) = \frac{1 - e^{-\frac{\beta T}{J}}}{\beta(z - e^{-\frac{\beta T}{J}})} \tag{4.21}$$

where J is the moving mass inertia and β the friction constant. The other parameters of the rotor and shaft are given as

- Rotor radius = 0.15 m
- Rotor shaft radius = 0.045 m
- Density of iron (ρ) of rotor = 7.85 g/m3
- Stack length = 0.34 m

Therefore the volume of the rotor excluding the shaft is calculated as $V = pi * (0.15)^2 * 0.34 - pi * (0.045)^2 * 0.34 = 0.02187\, m^3$. In this calculation the flux

barrier openings are neglected, hence the rotor is taken as a solid mass. The mass of the rotor is given by

$$M1 = \rho v = 7.85e^3 * 0.02187 = 171.68kg \tag{4.22}$$

The rotor shaft mass is

$$M2 = 7.85e^3 * (0.045^2 * 0.34 * pi) = 16.979kg \tag{4.23}$$

Therefore the inertia of the rotor is

$$J = \frac{1}{2}[M1(r_{rotor}^2) - M2(r_{shaft}^2)] \tag{4.24}$$

$$= \frac{1}{2}[171.68 * (0.15)^2 - 16.979 * (0.045)^2] = 1.914 \tag{4.25}$$

The work covered in this thesis does not focus on dynamic response but steady state performance. Therefore the speed response is designed to be slow, just to allow for steady state measurements on the machine. The initial requirements on the speed controller are then chosen to have a settling time of 3s and under damped (ζ = 0.95). Therefore the natural frequency is calculated as $\omega_n = \frac{4}{T\zeta} = 1.4 rad/s.$

The closed loop transfer function of the speed controller is given by

$$G_{cl} = \frac{\frac{K_{cc}K_w}{\beta}[1 - e^{-\frac{\beta T}{J}}][(K_p + TK_i)z - K_p]}{z^2 + [(-1 - e^{-\frac{\beta T}{J}}) + \frac{K_{cc}K_w}{\beta}(K_p + TK_i)(1 - e^{-\frac{\beta T}{J}})]z + [e^{-\frac{\beta T}{J}} - \frac{K_p K_{cc}K_w}{\beta}(1 - e^{-\frac{\beta T}{J}})]}$$

This equation is used to find the controller constants *Kp* and *Ki* as described is sub-section 4.3 for the current controllers. From eqn. 4.21, the speed closed loop transfer function is calculated as

$$g(z) = \frac{47.5e^{-6}}{z - 0.9996} \tag{4.26}$$

The design of the PI controller for this system is implemented in Matlab as discussed in the previous section. The corresponding controller transfer function is calculated as

$$k(z) = \frac{5(z - 0.9995)}{z - 1} \tag{4.27}$$

From equation 4.16 the PI controller constants are calculated as $Kp = 5$ and $Ki = 6.25$. The step response of the system with the controller and the corresponding root locus diagram are shown in Fig respectively. It is clear from Fig. 4.13 that speed has a settling time of about 4.5s.

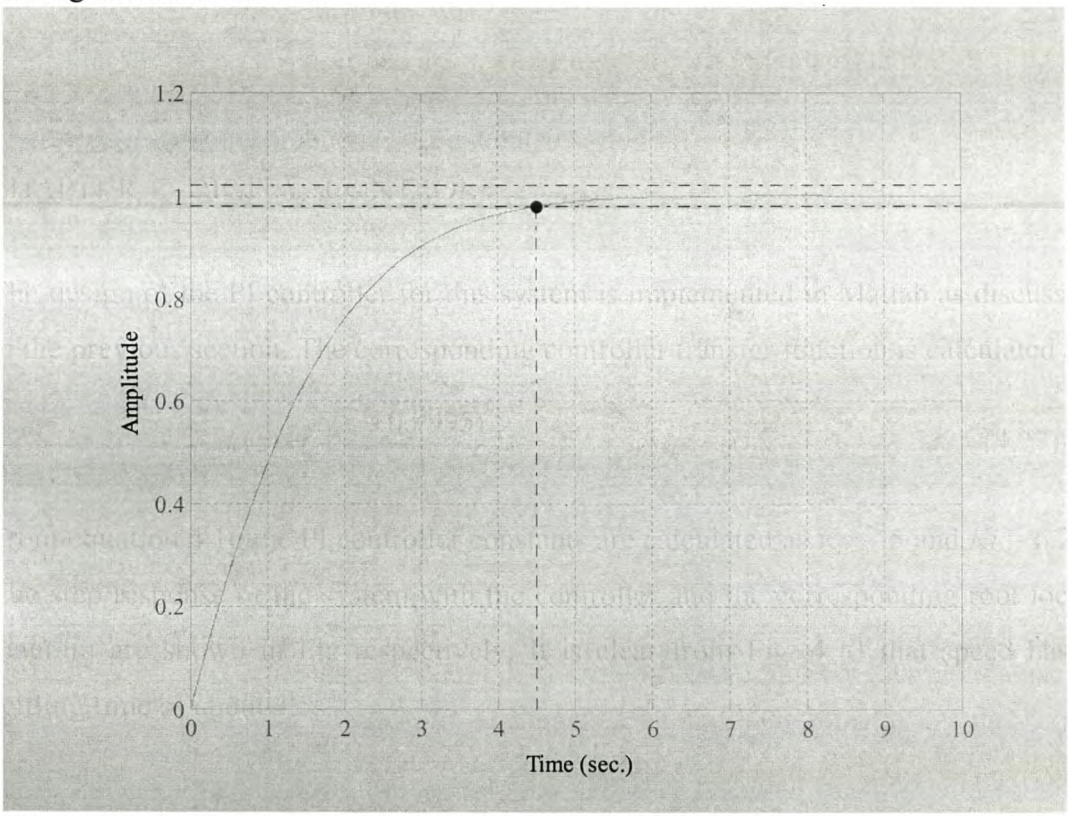

Figure 4.13. Speed step response curve

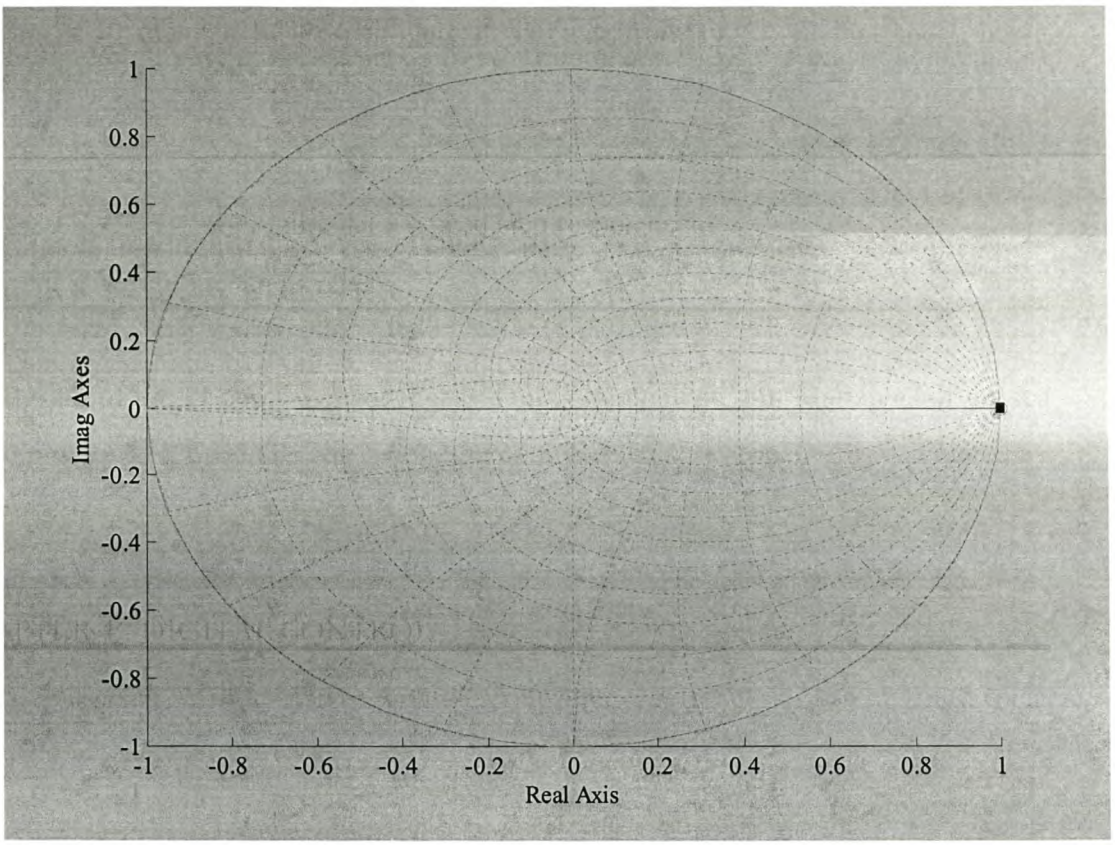

Figure 4.14. Speed root locus diagram

4.3 Implementation of the controllers

The current controllers are implemented in two ways. Firstly by simulating the controllers and the whole drive system and secondly by implementing them in an actual drive system using a fixed-point DSP digital controller. For simulation results, SIMUWIN software, developed by the University of Stellenbosch is used. The SIMUWIN block diagram of the inverter with the current regulators and speed decoupling terms is shown in Fig. 4.15.

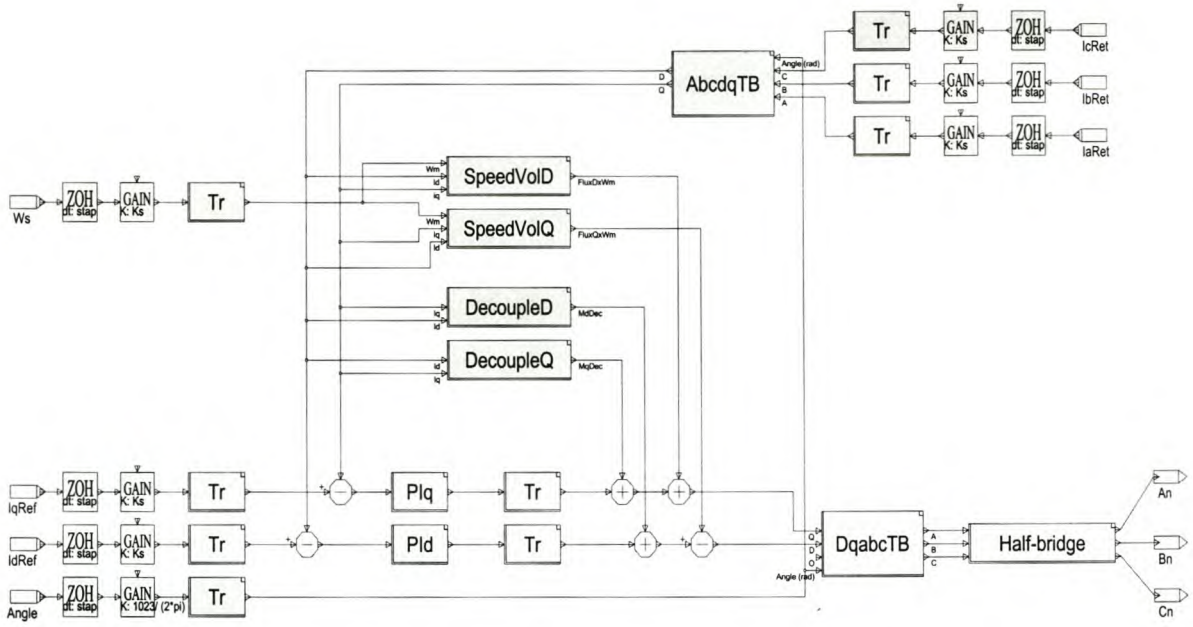

Figure 4.15. Simulation block diagram of the controller

The inputs (*IqRef*, *IdRef*, *Angle* and *Ws*) are the reference currents, electrical angle and the speed of the machine. These inputs are scaled as discussed earlier in section 4.1. The inputs (*IaRet*, *IbRet* and *IcRet*) are the actual measured currents of the machine and these are also scaled. The currents are in the abc-reference frame and are therefore transformed to the *dq0*-reference frame by means of Park's transformation. These measured *dq*-currents are then subtracted from the *dq*-reference currents and the error values are given to the two PI controllers implemented in the *PIq* and *PId*-blocks as discussed earlier in the section. In the middle of the diagram (Fig. 4.15), the speed-voltages and cross magnetisation terms are calculated and decoupled from the system at the outputs of the *PI* controllers. The speed-voltages are calculated using two look-up tables (*d* & *q*-axis flux linkages) that were generated from the finite-element results given in Chapter 2. The curves chosen to generate the look-up tables for each of the *dq*-currents are chosen at the rated current of the opposite *dq*-current. The cross magnetisation blocks also consist of two look-up tables determining *M'd* and *M'q*, which are then multiplied by the derivative of the *dq*-currents.

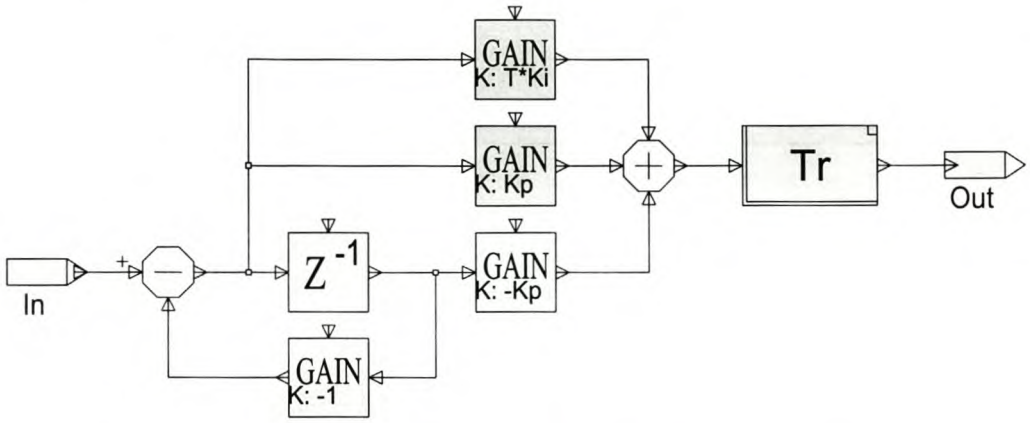

Figure 4.16. Simulation block diagram of digital PI controller

Fig. 4.16 shows the simulation block diagram of the digital *PI* controllers. This block diagram is realised from eqn. 4.8 where *Kp* is the proportional constant, *Ki* the integral constant and z^{-1} the unit delay at the sampling rate. The block '*Tr*' in Fig. 4.16 is the truncation block. This block is necessary to convert the floating point *PI* controller output to integer values to be used inside the DSP. This is necessary because only the PI calculations in the DSP are done in floating point but the rest of the calculations are done in fixed point.

It was shown by [6] that at high speeds the current controllers tend to saturate in part of the cycle due to the finite voltage capability of the inverter. These effects have to be considered in the simulations and practical system. However, in the simulations, the instantaneous *dq*-voltages must be known. The *dq*-voltages are directly determined by the current controllers of the system. The current controller, and thus at every instant of a power switch opening or closing, must be simulated to predict the changes in the *dq* voltages and currents accurately. The desired *dq* currents are determined by the speed controller (phasor current Is) and are compared with the actual returned *dq* currents. The errors are used by the PI controllers to directly determine the *dq* voltages of which are transformed using Park's transformation to obtain the *A- B -C* voltages.

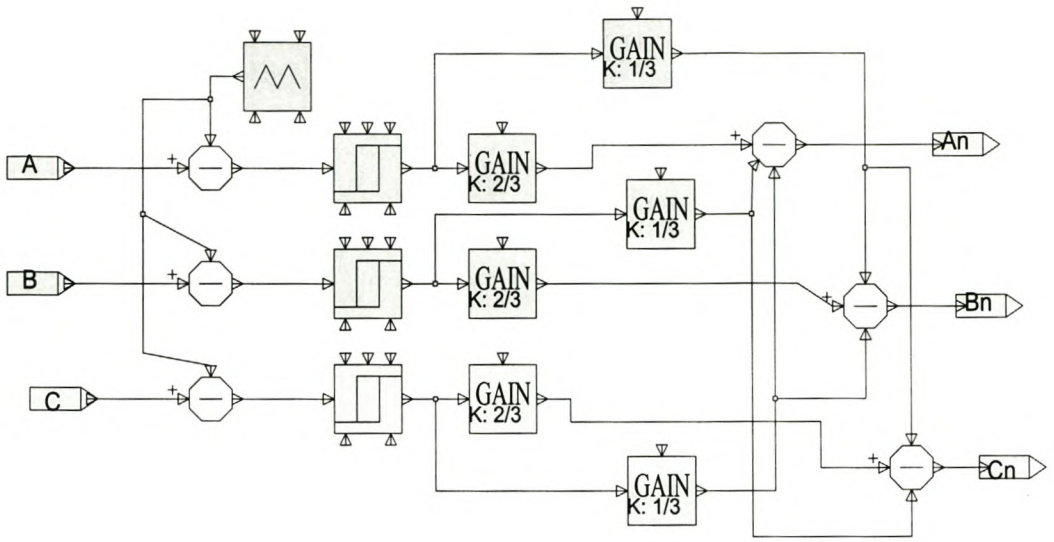

Figure 4.17. Simulation block diagram of the half-bridge inverter

These voltages are used to obtain the instantaneous line-neutral phase voltages by means of the well-known equations:

$$V_{an} = \frac{1}{3}(2V_{ao} - V_{bo} - V_{co}) \tag{4.27}$$

$$V_{bn} = \frac{1}{3}(2V_{bo} - V_{ao} - V_{co}) \tag{4.28}$$

$$V_{cn} = \frac{1}{3}(2V_{co} - V_{bo} - V_{ao}) \tag{4.29}$$

These instantaneous phase voltages are then transformed using Park' transformation to obtain the actual *dq*-voltages. From here the real *dq* currents response of the system can be predicted. Finally the *dq*-currents are transformed backwards to obtain the real *abc* currents.

4.4 Practical implementation of the controllers

The controllers are also implemented in an actual RSM drive system using a fixed-point DSP controller. The hardware of the controller is described in detail in Chapter 5. The controller measures the 3-phase currents of the machine and converts these to digital values to be used by the processor. The rotor position is measured digitally using a resolver and then read by the processor. The rest of the code is implemented in software running in the DSP processor.

4.4.1 Synchronised control loops with DSP

It is important to measure in a switching cycle, the average or fundamental value of the currents. This is done by:

- Synchronising the program control loop (and the sampling of the currents) with the triangular wave of the PWM generator
- Sampling the currents at an instant when no power switching is taking place to avoid any noise measurements.

In this case, the instant when no power switching is taking place is the instant when the triangular wave is at a minimum or maximum as shown in Fig. 4.18.

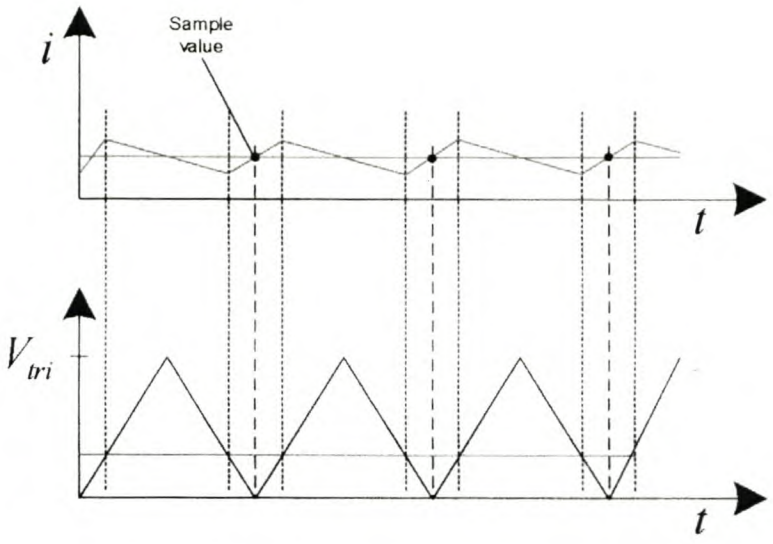

Figure 4.18. Illustration of the sampling of current with PWM switching [21]

4.4.2 Programming the DSP

The DSP program is written in ANSI C-code. As with the simulation implementation discussed in the previous section, the separate parts of the controller are described and also how these are programmed into the source program. The flow chart diagram of the DSP controller code is shown in Fig. 4.19. The main part of the program is the infinite for loop in which all the tasks are done in one sampling period. This loop-time is the sampling time for the controller and starts on the lowest value of the triangular wave used for the PWM generation. The sampling rate is equal to the switching frequency of the PWM generator (400 μs in this case). The first task of the control program is the reading of the measured values starting with the three phase currents, the rotor position and then the current reference command. This part includes the scaling of the measured values, which is necessary because of the method of measurement and the type of analog-to-digital conversion that is used and also to prevent any overflow in the DSP. The currents are measured with a hall effect "LEM"

module together with an analog circuit, before being converted to a digital value within the DSP.

The ADC can only read positive values because the input to the ADC is between 0 and 5 V. The voltage, representing the current measurement, is offset by 2.5 V before being inputted to the ADC. Inside the DSP the zero level is thus at the halve way value of the 10-bit ADC, which is at 512. The second part is to scale this value back to a zero reference level, as well as to a 16-bit value because the DSP uses a 16-bit data bus. Following this is the reading of the rotor position. This is done using a resolver together with its digital circuitry. This gives the DSP a 10 bit accurate mechanical angle, and from that the electrical angle is derived. Thus the angle from 0 to 2π is equal to 0 to 1023 in the DSP as shown in Fig. 4.20.

The position value is read in from the resolver in the first part of the program and saved into MrotorAngle. The resolver is 12-bit accurate and is converted to a 16-bit value for the DSP calculations. A fixed angle is added to the mechanical rotor angle to line up the zero position of the rotor to the correct position of the stator. This angle is called an 'offset angle'. The last part of the code is the calculation of the electrical angle, ErotorAngle.

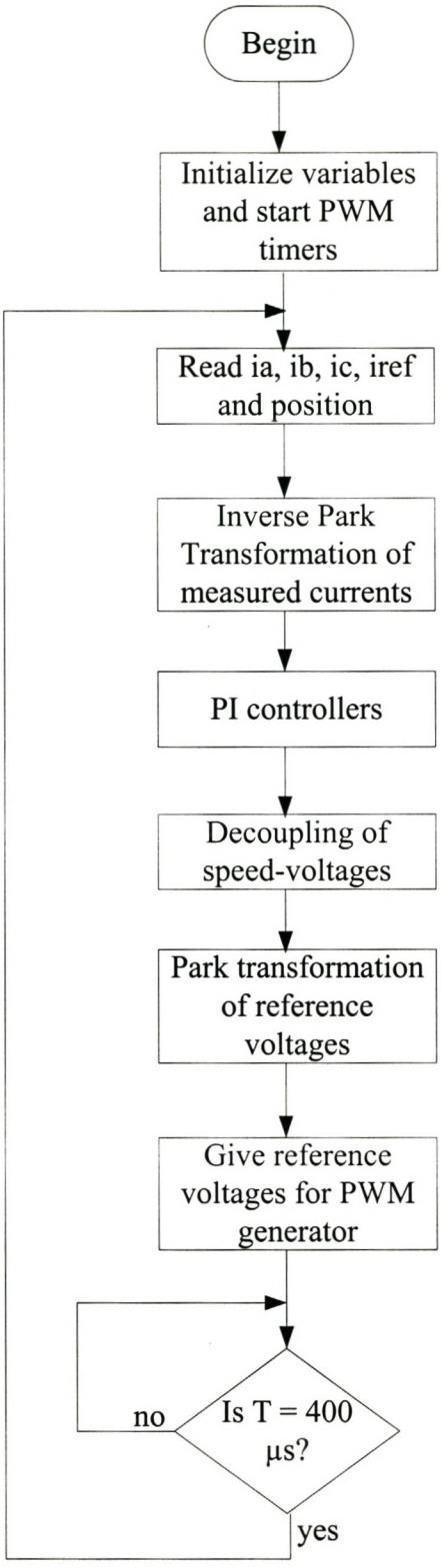

Figure 4.19. Flow chart of the DSP control program

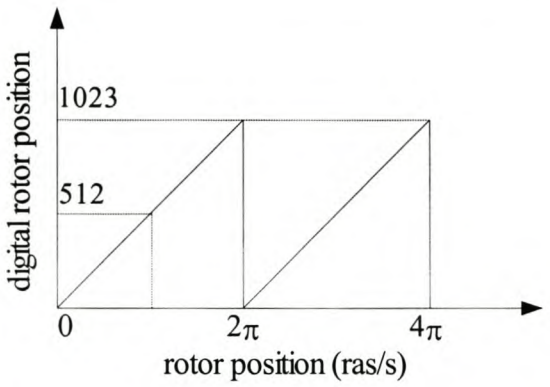

Figure 4.20. Rotor position from 10-bit accurate resolver

After the input of all parameters the measured currents are converted to the *dq0*-reference plane. As mentioned earlier the Park'-transformation is used for this and the inverse of this transformation is used at the end of the program to transform the result of the controllers back to the 3-phase coordinate plane to obtain three reference values for the inverter. For these transformations the angles used are in the 0 – 1023 range.

The transformation and its inverse is done by first scaling down the input values to prevent overflow in the DSP. Then the transformation equations are realized. The sine of the angles is obtained from a sine look-up table that is also loaded together with the control program to the DSP. The sine lookup table is a 10-bit table as shown in Fig 4.21. This DSP also does not have the cosine function, so it is calculated from the loaded sine (lookup table) function using the relation $\cos(\theta) = \sin(\theta + 90^0) = \sin(\theta + 256)$. After the transformation, the values are scaled up to their original scale. This scaling up and down of the values influence the accuracy and the dynamics of the current controller. The reason for the scaling is to prevent overflow within the processor.

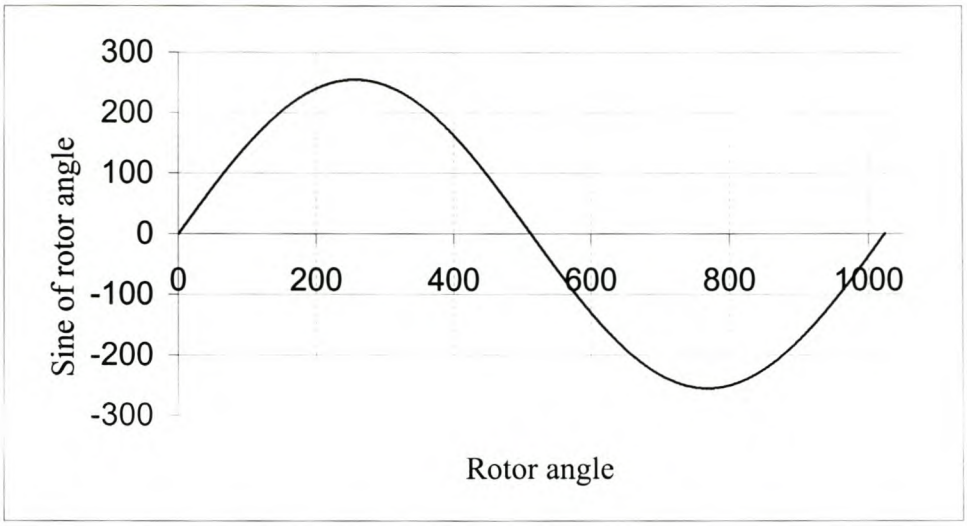

Figure 4.21. DSP sine look-up table

Next is the program code of the PI controllers. This part of the code makes use of floating-point values because of the accuracy of the constants of the controllers. In the DSP, the PI regulators are implemented as follows.

$$g(z) = \frac{(Kp + TKi) - Kp}{z - 1} = \frac{Kp + TKi - Kpz^{-1}}{1 - z^{-1}} \tag{4.30}$$

or else

$$g(z) = g(z)z^{-1} + Kp(1 - z^{-1})g(z) + TKig(z) \tag{4.31}$$

For each controller the error is calculated before the PI transfer function is implemented. The outputs of the transfer functions are saved into two variables to be available for the next loop as previous values. The initial values for these two variables are set at zero.

After the PI controllers, the decoupling of the speed voltages is done. The flux linkages that are used to calculate the speed-voltages are obtained by using look-up tables for the *d* and *q*-axis. Some of the scaling is incorporated in the lookup tables to make them 10 bits and real numbers since the DSP lookup table does not compile

floating-point values. The flux linkages are then multiplied with the electrical speed of the machine to get the speed voltages. The complete DSP control code is given in the appendixes.

Chapter 5

5 Description of the Drive System

This chapter describes the RSM drive system shown in Fig. 5.1 below. The drive is a voltage fed, current controlled system. It consists of a rectifier, an inverter, 110 kW RSM (or PM-assisted RSM), a dynamic brake circuitry, DSP controller, Norma measurement system and the load. The drive is fed from an AC supply which is rectified to give the inverter a constant dc voltage. The inverter with the DSP controller then generates the three-phase supply voltages for the machine.

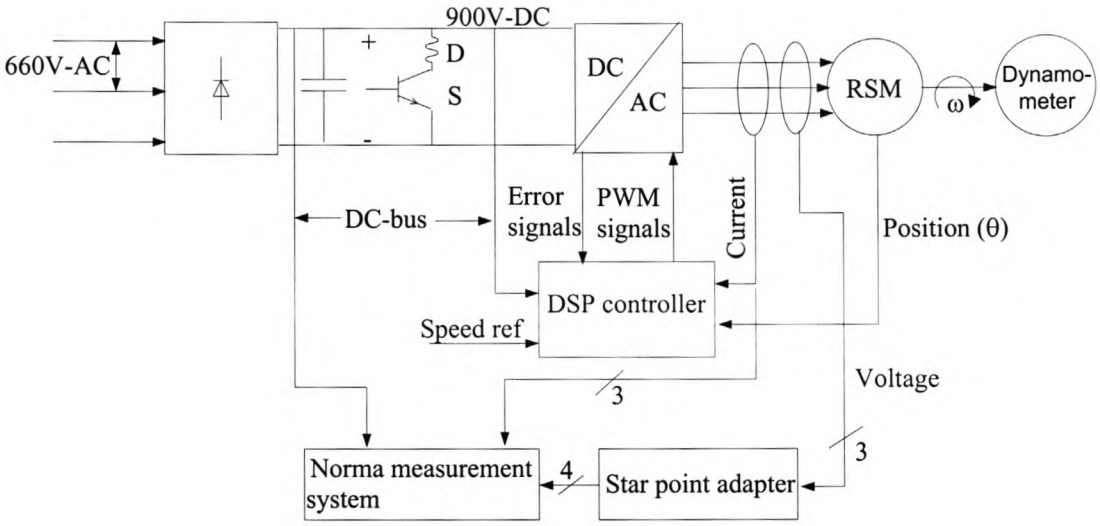

Figure 5.1. RSM Drive System

5.1 Rectifier

The schematic diagram of the supply and rectifier is shown in Fig. 5.2. The supply to the drive system is a 660 V line-to-line AC supply voltage. This supply is able to give

up to 500 A of line current. The rectifier is a normal 3-phase AC-DC thyristor controlled rectifier rated at 630 kVA. It rectifies the AC voltage to 900 V DC. This DC bus voltage is fed to the invertor through an LF filter.

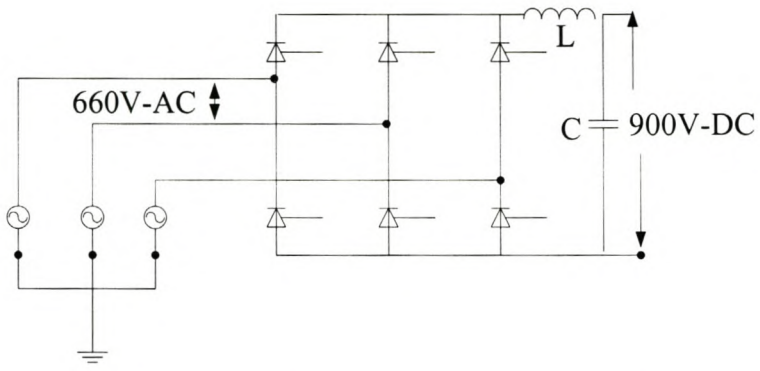

Figure 5.2. Supply and thyristor-controlled rectifier

5.2 Inverter

The inverter used is a 630kVA half-bridge 3-phase IGBT inverter as shown in Fig. 5.3. Each phase winding is connected to one phase arm rated 1000 V and 500 A. The inverter is built in a unit comprising of cooling fans, over current protection circuit and the fibre optic interface boards. The fibre optic interface boards convert the DSP PWM optic signals to analog switching signals for the IGBT switches.

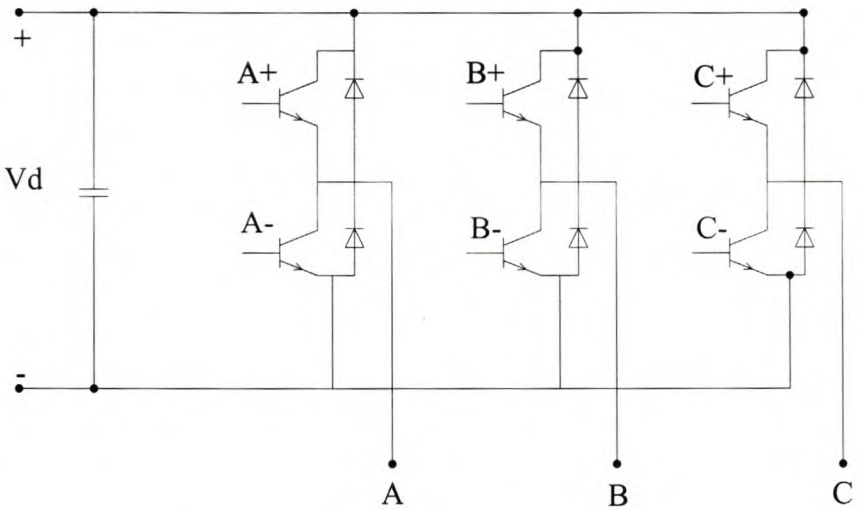

Figure 5.3. Three-phase inverter

5.3 Norma 5000 power analyser measurement system [36]

The Norma 5000 measurement system can be used to measure, amongst others, the 3-phase input power, 3-phase output power, fundamental and RSM phase currents, fundamental and RMS AC phase voltages, DC bus voltage, rectifier DC current, drive efficiency and fundamental and RMS power factor.

The power analyser allows for the analysis of currents from DC to several MHz. Voltage values up to 1000 V and currents up to 10 A can be directly measured accurately by the Norma system without any complementary circuitry. The respective real, reactive and apparent powers can be determined. The intrinsic uncertainty is between 0.1% and 0.3%. The current measuring range can be extended by connecting external shunts in parallel to the supply lines to scale down the Norma system input current to a maximum of 10 A. If necessary, appropriate fuses must be installed to prevent any damage to the system. The Norma system caters for simultaneous measurements of AC voltages and AC currents of up to six channels each.

The three-phase measurement connection diagram of the Norma system with external shunts is shown in Fig. 5.4. The shunts are labelled I_1-I_3 and the broken lines indicate the fuses. L1, L2 and L3 are the three-phase cables to the motor and N the neutral phase. However, in this case the motor is star connected but the star point is not accessible for use as a neutral point.

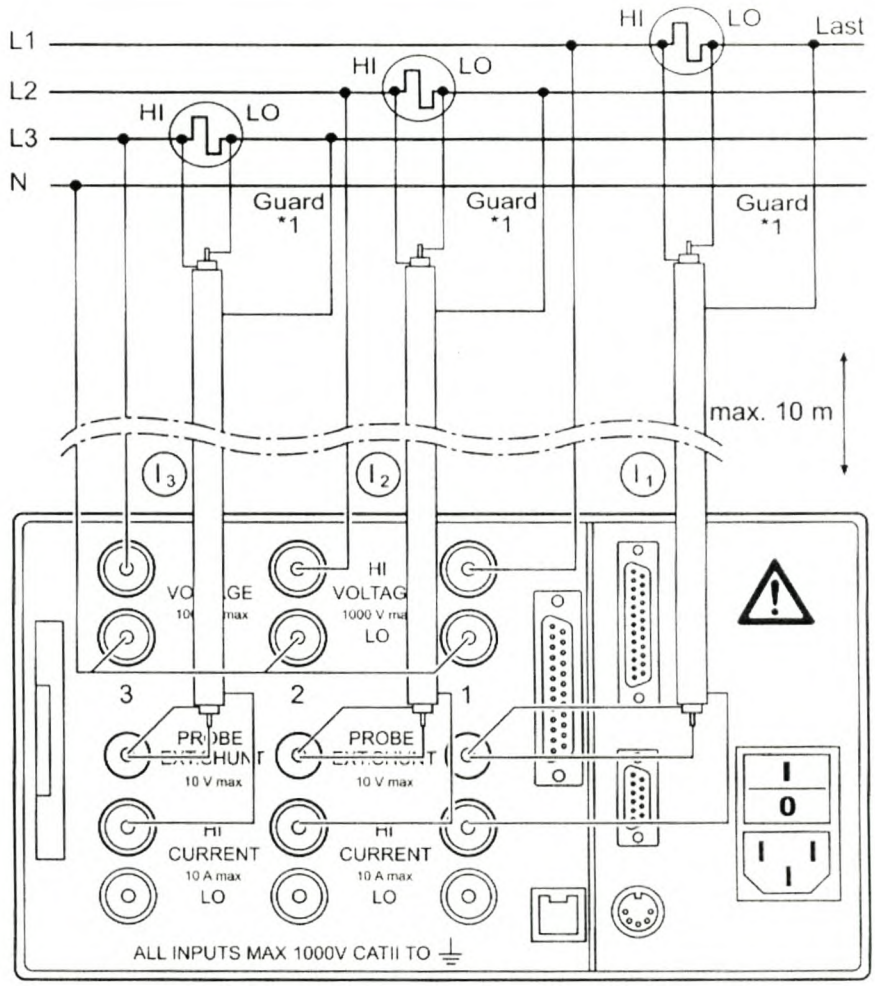

Figure 5.4. Connection diagram of the Norma system back panel with the external shunts

The star point adapter was then acquired to create the neutral point as shown in Fig. 5.1. With the Norma system in place, the complete measurements were done and are presented in chapter 6.

5.4 Electrical machine

The electrical machine is a six-pole 110 kW PM-assisted RSM traction machine. The PM-assisted RSM is designed to match the continuous rating of the IM of 700 Nm output torque for a line voltage of 500 V line and current of 200 A rms. The rotor is normal laminated and unskewed. The rotor was optimally designed using the FE analysis software together with an optimisation algorithm.

5.5 Digital controller

The TMS320F240 DSP is used to control the drive. This DSP is a fixed-point processor. This means that all calculations are done with real numbers. This type of DSP is created specifically for use in the control of variable speed AC motor drives and power electronics. It has built in ADC converters and PWM outputs. This DSP has, amongst others, the following features: 16K flash RAM, 12 compare/PWM signals, dual 10 bit ADC conversion module, serial communications interface modules and serial peripheral interface module.

The DSP consists of four main blocks as shown in Fig. 5.5 below. These are the processor/protection, fibre optic interface, position and voltage and current measurement card with the protection circuitry. All these DSP function blocks are discussed in the following sections.

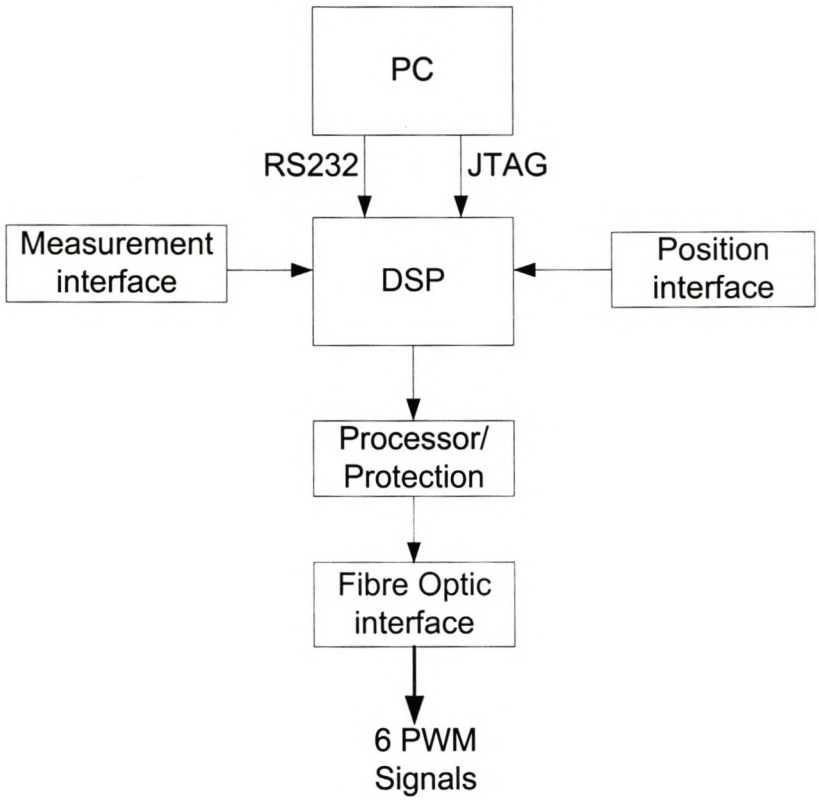

Figure 5.5. Block diagram of the DSP control unit

5.6 Processor/Protection card

The processor block is the main card of the controller. It contains the following modules:

- 20 MHz fixed point DSP
- Electrically programmable logic device (EPLD)
- Four DAC outputs
- RS232 communication port
- JTAG communication port
- All the above modules are described in the following sections.

5.7 Communication interface (JTAG and RS232)

The processor has two communication ports through which it can be programmed. These are the JTAG and the RS232 communication ports. The JTAG port and cable is used to initialise the processor and to load its serial ports loader program directly into the flash RAM of the DSP. This is performed by loading the following files in the flash RAM from the DSP: (i) BCO.bat (ii) BEO.bat and PrSbl.bat. The serial port loader program is required when using the serial communication port. The serial communications port is used to download the control software program to the DSP. When programming the DSP, this port is connected to COM1 serial port of the computer. In addition to the communication ports, there is communication between the user and the DSP. With this communication the user can access all the variables inside the DSP while it is on the running mode. The communication is trough the standard I/O pins and the four analog channels from the DAC's connected to the data bus. These channels are available on the front panel of the DSP controller.

5.8 The Processor circuit

The DSP has 16 analog to digital (ADC) channels connected via the universal bus to the other interface cards of the controller. These channels are divided into two groups. The first eight are connected to the first ADC and the last eight to the second ADC. The control of these ADCs is done through the software program of the DSP. The DSP was configured to produce 6 PWM outputs for the full bridge inverter. Three PWM signals for the top IGBTs and the last three for the bottom IGBTs. All six PWM signals have a dead time of $6.4\mu s$ programmed in the software program. These PWM signals are connected to the inverter through the protection circuit of the EPLD program. The EPLD disables the drive signals in case of a fault.

5.9 Protection circuit

The DSP supplies the EPLD with six PWM signals for the half bridge converter. The EPLD also receives error signals from the measurement and the fibre optic interface cards. These signals are the over-current error, DC bus over-voltage error and the drive error signal from the inverter. The over-voltage and overcurrent protection circuitry is shown in Fig. 5.6. The symbols AF+, AF-, etc. represents the positive and negative over-current signals for phase *a* respectively. The over-voltage signal is obtained separately from the DC bus analog measurement circuitry and the drive error signal from the inverter is transmitted in its own directly to the EPLD. The voltage and current signals are then combined using the AND gate as shown in the figure.

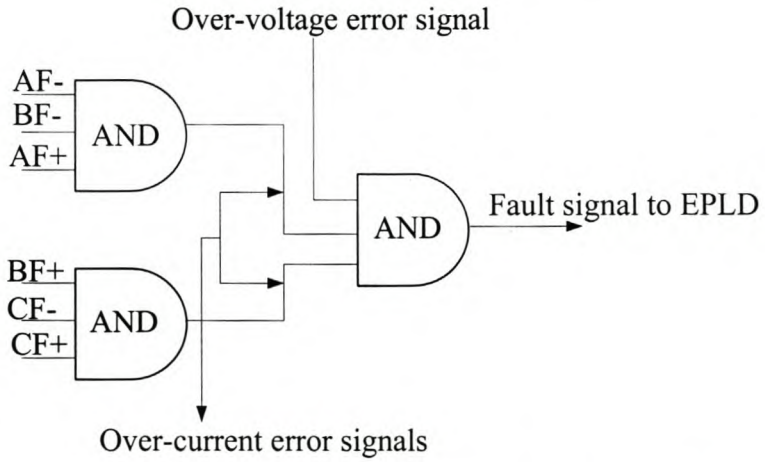

Figure 5.6. DSP analog protection circuit diagram for DC over-voltage and rms phase over-currents

The over-voltage and over-current protection circuit is implemented within the DSP measurement card using the CD74HC11E chip. The state of the AND gate input and output pins is normally high. A single change in the input pins will trigger the EPLD fault signal. The EPLD disables all the drive signals to the inverter on any of the error signals received.

5.10 Position measurement

The position is digitally measured by a brushless resolver and transmitted to the DSP via a serial cable. The resolver has its own control circuitry that can be selected to give 10, 12, 14 or 16 bit resolution. A 10-bit accurate resolution was selected for this application.

5.11 Current measurement

The DSP circuitry has five current measurements. The first three current measurements have fault detection. This protection looks at the measured current waveform and gives an error signal to the EPLD when the current increases beyond the maximum or minimum safety limits that are set by adjusting the voltage levels via potentiometers. The currents are measured using 500A RMS LEM current transducers (see appendix F). It has a conversion ratio of 1:5000. Therefore when 500A RMS flows in the primary circuit, the secondary current is 100mA. This current is then converted to a voltage signal by a termination resistor. The converted voltage signal is transmitted via a cable to be read by the DSP as shown in Fig. 5.7. This voltage signal is then compared to a reference precalculated voltage signal through a comparator. The output of the comparator will be high if the measured signal exceeds the reference signal, initiating the protection through the EPLD as explained in section 5.9.

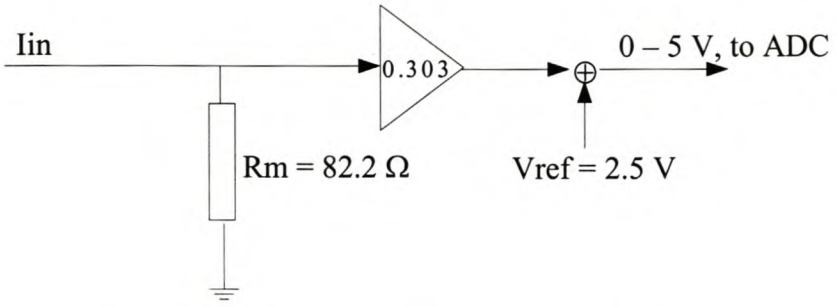

Figure 5.7. DSP current measurement circuit

Thus when 100 mA flows in the secondary of the transducer, the voltage drop across the termination resistor will be ±8.22 V. This voltage is then amplified with a gain of 0.303 to get the required 0 – 5 V range for the ADC.

5.12 DC bus voltage measurement

The DC bus voltage measurement is done on the same principle as the current measurements described in section 5.11. The difference is that with the voltage measurement, there is no termination resistor but there is high voltage sensor capable of handling voltages up to 1000 V. The voltage sensor consists of a resistive voltage divider circuit as shown in Fig. 5.8. The voltage divider attenuates the high voltage to a voltage within the DSP 15 V range. The voltage on the output of the voltage divider circuit is then fed to the ADC and a comparator. The comparator compares the reference signal to the measured signal, if the measured signal is higher than the reference, an error signal is sent to the EPLD, which then shuts down the system.

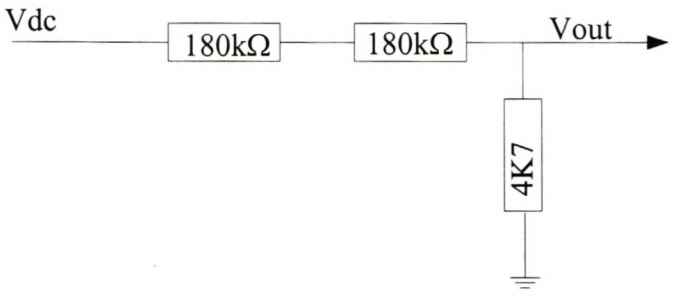

Figure 5.8. DSP DC bus Voltage measurement circuit

5.13 Fibre optic interface card

The fibre optic card is an interface between the DSP controller and the inverter. It converts the digital electric drive signals to optic signals. These optic signals are then transmitted to the inverter via fibre optic cables. On the inverter side, there is a fibre receiver optic card, which converts the optic signals back to electric drive signals for the IGBTs. There are also three optic error signals from the inverter to the DSP fibre optic card. These signals are combined through an AND gate to form one drive error signal to the EPLD.

Chapter 6

6. Experimental results and machine comparison

This Chapter presents experimental results obtained from the practical work done on the 110 kW RSM and PM-assisted RSM described in Chapters 2 and 3 respectively. It was mentioned in Chapter 1 that the primary objective of this work was to improve the performance of the RSM specifically in the flux-weakening region. Therefore most of the experimental work presented in this chapter was devoted into the analysis of the performance parameters of the RSM and the PM-assisted RSM in the flux-weakening region.

The fixed point DSP processor using constant current angle control and the water-brake Dynamometers described in Chapter 5, were used for the control of the speed and currents of the machine and for the load respectively. The experimental results presented in this chapter were measured using the Norma 5000 measurement system also described in Chapter 5. Both the RSM and PM-assisted RSM were tested under the same operating conditions, i.e. the same current, speed and DC supply voltage. The prime performance parameters are the output torque, supply voltage, current angle, power factor and the drive efficiency. Finite element calculated results are also included in this chapter to compare the calculated results with the practical results.

The machines were tested at derated values due to the difficulties experienced with the DSP controller. The whole system became unstable once the phase voltage exceeded 220 V and the DSP protection signals were enabled (see Chapter 5) as a result of over-current/over-voltage or inverter error signals. As a result, the experimental results presented in this Chapter are based on the base speed of 1200 rpm (which correspond to 220 V), maximum test speed of 2800 rpm and a maximum

phase voltage of 220 V. This is different from the original results presented in Fig. 1.3 [7] of Chapter 1 and the optimisation results presented in Chapter 3. The optimisation and the results of Fig. 1.3 are based on the base speed of 1500 rpm, maximum speed of 3800 rpm and the maximum phase voltage of 318 V. The induction machine, PM-assisted RSM and RSM drives were all tested to get their optimum output performance parameters under the derated conditions. See appendix C for IM data. It is also important to note that due to the instability of the controller, the measured machine speeds indicated are the average speeds to the nearest ± 1% unless indicated otherwise.

6.1 RSM torque and voltage versus current relationship

The main purpose of the experimental work covered in this section is to verify that the Finite element calculated results corresponds with the practical measurements. The first experimental results presented are the torque versus supply current relationship at a fixed current angle of 55^0 as shown in Fig. 6.1. Tfe is the finite element calculated torque and Tprac is the measured torque. In the practical measurements, the current angle is manually fixed in the DSP control code before it is programmed into the DSP processor. It is clear from Fig. 6.1 that the torque versus current of the RSM has a linear relationship. It is important to note that there is no particular reason why the current angle was chosen to be 55^0; infact tests done at other current angles showed similar characteristic of the torque versus current. The most important finding is that the experimental and calculated torque results are within 5% of each other.

The fundamental phase and line voltage measurements versus current at a current angle of 55^0 and a speed of 800 rpm were also done. The results of phase voltage versus current are shown in Fig. 6.1 where Vfe is the finite element calculated voltage and Vprac is the measured voltage. At measured 198 A, it is clear that the calculated phase voltage is much lower than the fundamental phase voltage of 220 V at base

speed (1200 rpm). This is due to the fact that the measurements were done at a speed of 800 rpm. It is also important to note that the calculated and measured voltages are in the vicinity of each other (8%) and that the practical voltage is generally higher than the calculated voltage. The reason for the low calculated voltage can be attributed, amongst other things, to the less accurate BH-curve in the FE program.

These initial experimental results of the torque and voltage versus current of the RSM with current angle as a parameter shows a general positive correlation with the calculated results. The positive correlation between the experimental and calculated results does not just validate the machine design using the FE analysis, but also the validity of the control strategy applied. Lastly, the actual current waveform at a speed of 834 rpm and at rated rms current of the RSM drive is shown in Fig. 6.2.

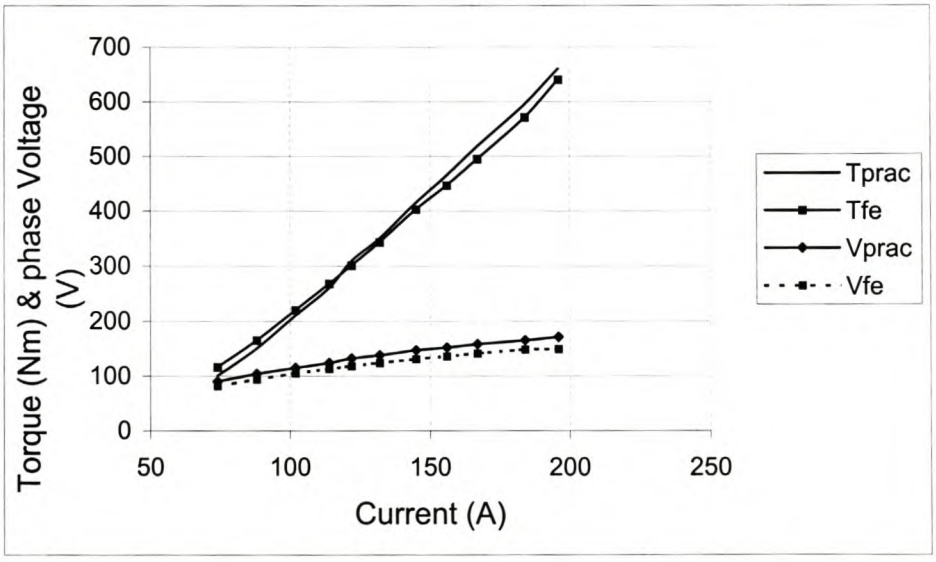

Figure 6.1. Calculated and measured torque and voltage versus current of the RSM drive at a current angle of 55^0 and speed of 800 rpm.

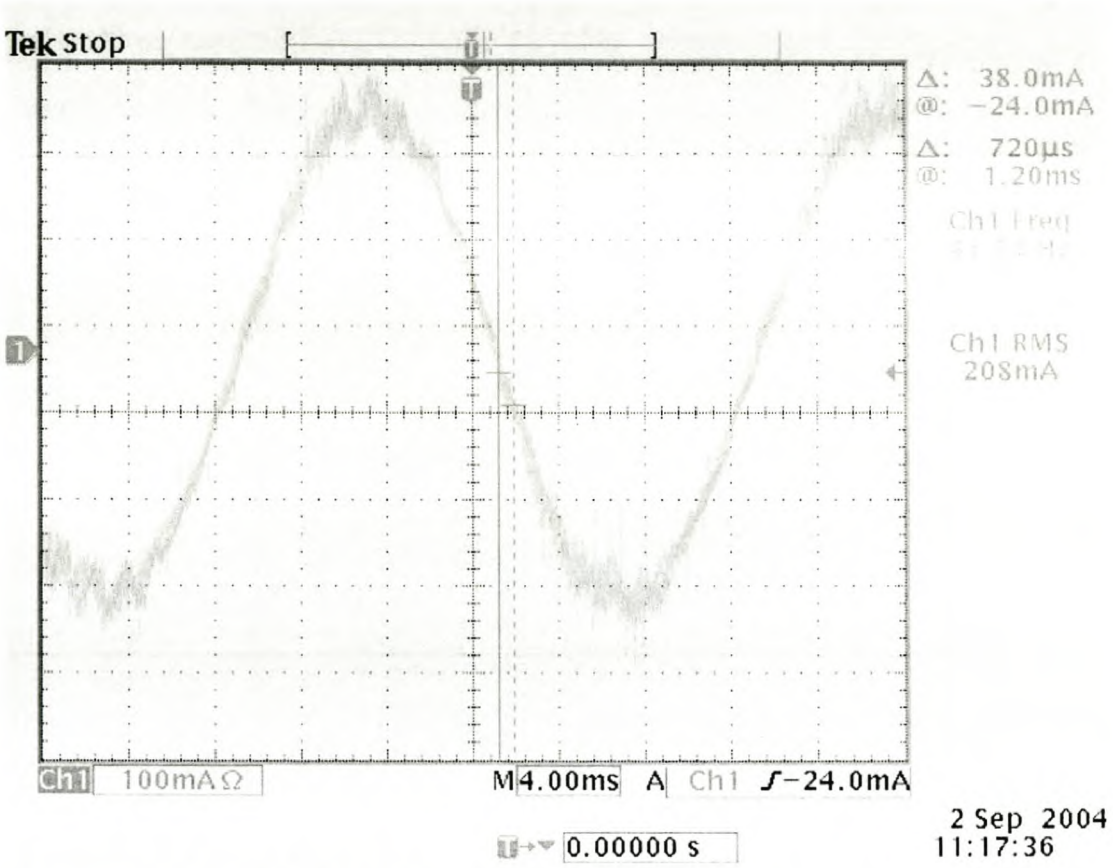

Figure 6.2. Captured rated (200 A rms) phase current signal of the RSM drive at a speed of 834 rpm

6.2 Determining the optimal current angle in the constant-torque region

It was mentioned in Chapter 1 that the RSM's performance is determined by its maximum output torque per ampere. It was also mentioned in Chapter 4 that maximum torque per ampere of the RSM is attained by controlling the RSM at an optimum current angle at each speed. Therefore this section and 6.3 deal with determining the optimum current angle of the RSM in the constant torque and in the flux-weakening regions respectively.

Tests were done at different current angles to determine the optimal current angle of the RSM in the so-called constant torque region at a speed of 800 rpm. At each current angle the machine was speeded up to 800 rpm and the load was increased till rated current of 200 A flows. The corresponding torque exerted by the Dynamometers was then noted. The results are shown in Fig. 6.3 where Tfe is the finite element calculated torque and Tprac is the measured torque. It is clear that the torque curve attains its peak value at a current angle of 60^0. This angle is then used as the optimum current angle in the constant torque region. It is important to note that the measured optimum current angle tends to correspond with the finite element calculated optimum current angle as shown in Fig. 6.3.

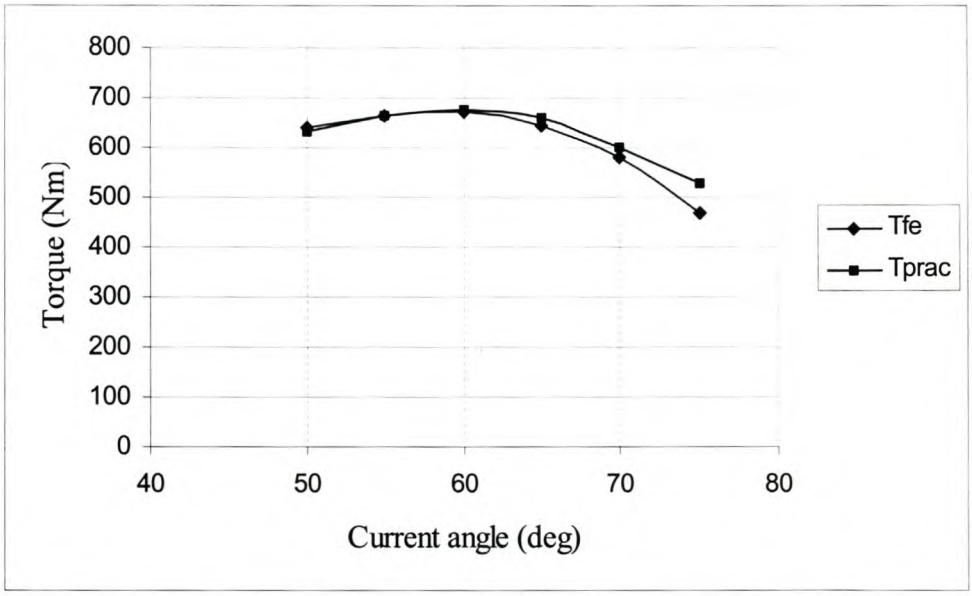

Figure 6.3. RSM calculated and measured torque versus current angle at a speed of 800 rpm

The fundamental phase voltage of the RSM at each current angle and rated current was measured using the Norma system. The results are plotted in Fig. 6.4 where Vfe is the finite element calculated phase voltage and Vprac is the measured phase voltage. It is clear that both the measured and calculated voltage decrease as the current angle is increased. This result also agrees with the Finite element calculated

results presented in Chapter 2. The calculated voltage is generally lower than the measured voltage.

The power factor of the RSM was also measured as a function of the current angle as shown in Fig. 6.5. In Fig. 6.5, Pffe is the finite element calculated power factor and Pfprac is the measured power factor. The power factor is defined as the ratio of the real power (P) supplied to the motor to the apparent power (S) or else

$$Pf = \frac{P}{S} \tag{6.1}$$

It is clear that the measured maximum power factor of the RSM is found to be 0.68 at a current angle of 70^0 and the maximum calculated power factor is attained to be 0.71 at a current angle of 69^0. This discrepancy may also be due to the less than accurate BH-curve in the finite element program as stated on page 103.

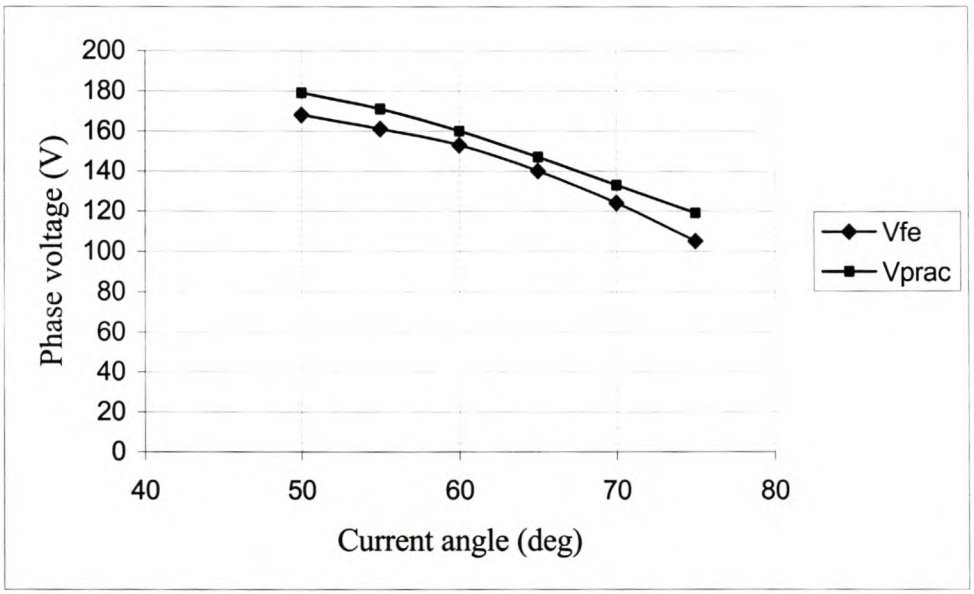

Figure 6.4. RSM calculated and measured phase voltage versus current angle at rated current and a speed of 800 rpm.

The measured optimal current angle of the RSM in the constant torque region is 60^0 as shown in Fig. 6.3. In principle, as shown by other researchers before [6, 23], this current angle is an optimum for all speeds in the constant torque region.

The complete measurements of the RSM in the constant torque region at optimum current angle and at speeds of 800 and 1200 rpm were done and are presented in Table 6.1. In the table, Iho1, Vho1 and Pf1 are the fundamental phase current, phase voltage and power factor. The other performance parameters are the rms three-phase voltage (Vrms), machine input power (Pm), inverter DC input power (Pdc), DC current (Idc), DC voltage (Vdc) and the output torque (T). It is clear from Table 6.1 that the DC voltage is less than the required 900 V supply voltage at both speeds of 800 rpm and 1200 rpm. In particular at 800 rpm the voltage is lower than that at 1200 rpm. The reason for this could be attributed to the fact that the measurements were done at different times with possible different three-phase supply voltages to the rectifier.

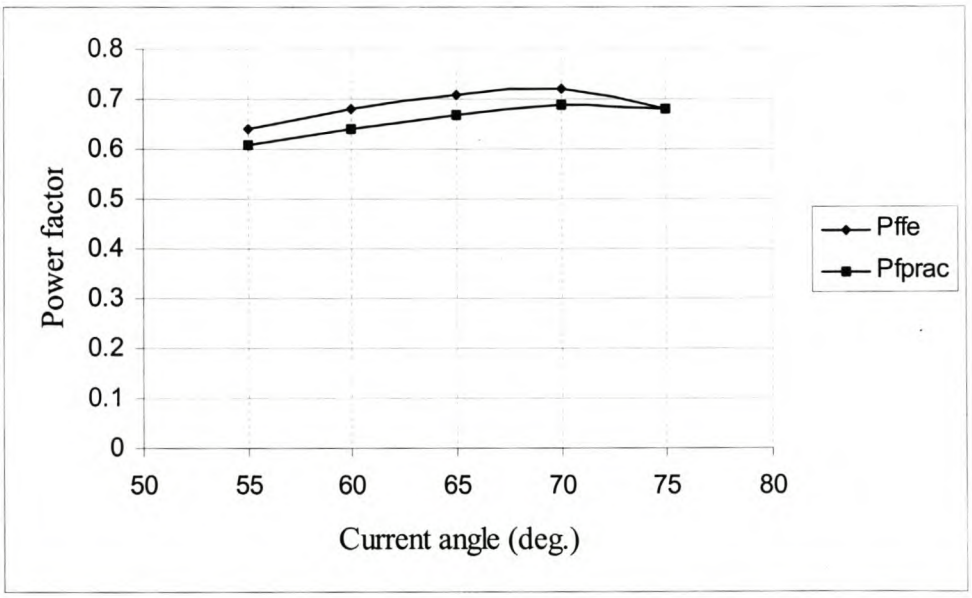

Figure 6.5. RSM calculated and measured power factor versus current angle at rated current and speed of 800 rpm

Table 6.1. Measured RSM results below base speed at the indicated average speeds (within ± 1% error)

ϕ Angle	Irms (A)	Iho1 (A)	Vrms 3-phase	Vho1 3-phase	Vho1 Phase	Pm kW	Pdc kW	Idc (A)	Pf1	Pf	Vdc (V)	T (Nm)
Speed = 800 rpm (± 1%)												
60	200	199	482	281	162	65	68	83.2	0.64	0.37	852	684
Speed = 1200 rpm (± 1%)												
60	197	196	538	382	221	87	89	105	0.67	0.46	862	681

6.3 Flux weakening operating speed region

The results presented in sections 6.1 and 6.2 were based on fixed speed measurements in the constant torque region. In particular the optimum current angle determined in section 6.2 is applicable only for speeds up to base speed. In the flux-weakening region the current angle has to be advanced as the speed is increased, this advancement of the current angle corresponds to reducing the *d*-axis flux of the machine as explained in Chapter 3. However, at each operating point (of speed) in the flux-weakening region, an optimal current angle must be determined as in the case of the constant torque region presented in section 6.2. In the flux-weakening region the optimum current angle at each chosen operating speed is determined as follows:

- The operating speed is selected
- Three current angles are chosen, ideally to include the anticipated optimum current angle
- The machine is loaded at the selected speed and at each current angle. The output torque exerted by the Dynamometers is noted.

There are two constraints not to be violated in taking the measurements and that is the maximum allowed voltage and the rated current. The importance of these constraints can be explained as follows: lets take an operating speed of 1350 rpm in Fig. 6.6, the current angles are 70^0, 71^0 and 73^0. At this speed of 1350 rpm the machine could be

loaded up to rated current at all three current angles, because there is no limitation in supply voltage, or else neither the voltage or currents constraints have been violated. However, it is clear from Table 6.2 that at a current angle of 71^0, the voltage limit is almost reached and the current cannot be increased any further. But at a current angle of 73^0 and at the same speed of 1350 rpm and rated current of 200 A, the voltage is less than the maximum voltage of 220 V. If at this current angle of 73^0 the current was increased more than the rated current till rated voltage was reached, this would make inconsistency in the determination of the optimal current angle since at this point in speed the machine would be overrated.

From this discussion it is clear that at low current angles at a certain point in speed, the constraint is the supply voltage and at high current angles at the same speed the constraint is the current.

The complete measurements in the flux-weakening region were then done as described in this section to determine the optimum current angle at each operating point of speed and these results are presented in Table 6.2 and plotted in Fig. 6.6. At each point of speed, the current angle that gives the highest torque is clearly visible in Fig. 6.6. It is clear that at the speeds of 2400 rpm and 2800 rpm the currents are below rated current, and in particular at the speed of 2800 rpm the current angle is not advanced any further. The current versus current angle characteristic in the flux-weakening region with speed a parameter is independently plotted in Fig. 6.7 to clearly illustrate the current versus current angle relationship with speed a parameter. It can be seen in Fig. 6.7 that the optimum current for maximum torque (see Fig. 6.6) into the machine decreases as the current angle is further advanced towards 90^0. This is one characteristic of the RSM that at some high speeds there is no advantage of increasing either the current or current angle because there is no gain in torque. This characteristic of the RSM is evident at the speed of 2800 rpm. A more complete explanation in this regard is presented in the work of Kamper [6].

Table 6.2. Experimental results of the RSM in the flux-weakening region at the indicated average speeds (within ± 1% error)

ϕ Angle	Irms (A)	Iho1 (A)	Vrms 3-phase	Vho1 3-phase	Vho1 Phase	Pm kW	Pdc kW	Idc (A)	Pf1	Pf	Vdc (V)	T (Nm)
Speed = 1320 rpm (± 1%)												
70	196	195	527	372	215	83	86	104	0.68	0.47	847	580
71	196	195	538	371	218	87	90	107	0.68	0.46	852	584
73	197	196	518	351	201	82	86	102	0.68	0.45	851	549
Speed = 1500 rpm (± 1%)												
73	197	196	548	374	218	86	90	107	0.67	0.46	853	510
74	197	196	545	372	215	86	90	108	0.67	0.46	853	525
76	199	198	527	342	198	77	79	96	0.65	0.42	850	468
Speed = 1680 rpm (± 1%)												
76	188	187	552	378	220	80	84	99	0.65	0.44	859	423
77	197	197	554	380	221	84	87	104	0.64	0.44	856	433
79	198	197	531	351	204	76	79	94	0.62	0.4	857	406
Speed = 1950 rpm (± 1%)												
78	175	174	550	376	218	72	75	89	0.62	0.42	855	312
79	184	183	553	382	221	76	79	95	0.61	0.42	854	330
81	198	197	549	380	218	75	78	94	0.58	0.39	853	325
Speed = 2450 rpm (± 1%)												
80	145	144	544	375	220	52	55	66	0.58	0.39	856	175
82	160	160	538	375	216	56	57	71	0.53	0.36	852	185
84	173	173	536	372	215	54	56	69	0.49	0.33	854	176
Speed = 2800 rpm (± 1%)												
80	121	121	563	374	216	42	45	55	0.54	0.35	862	116
82	137	136	564	379	219	46	48	59	0.51	0.34	861	132
84	149	148	563	379	219	45	47	59	0.46	0.3	863	122

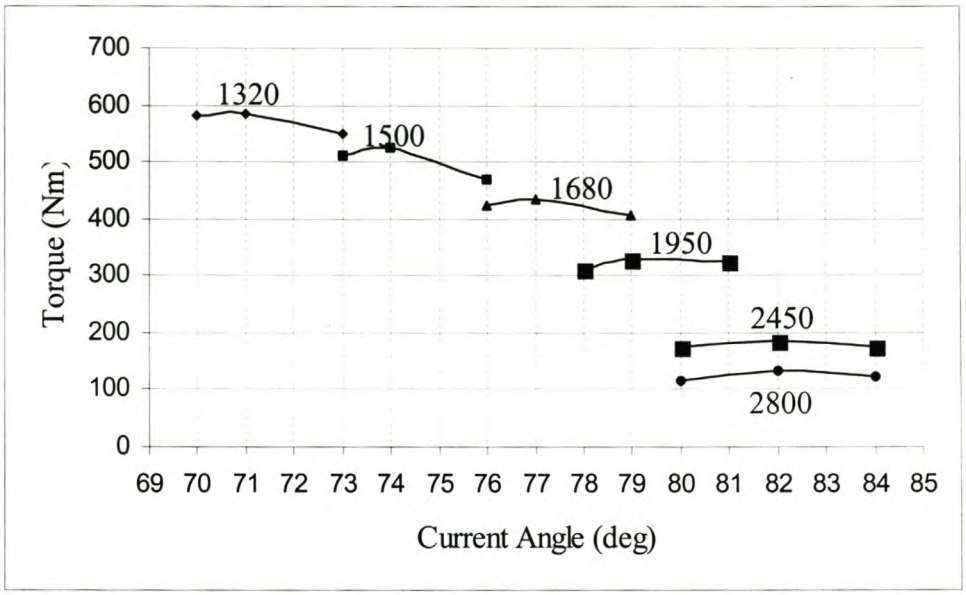

Figure 6.6. Measured torque versus current angle characteristics of the RSM with speed as a parameter and V ≤ 380 V_{L-L} and I ≤ 200 A

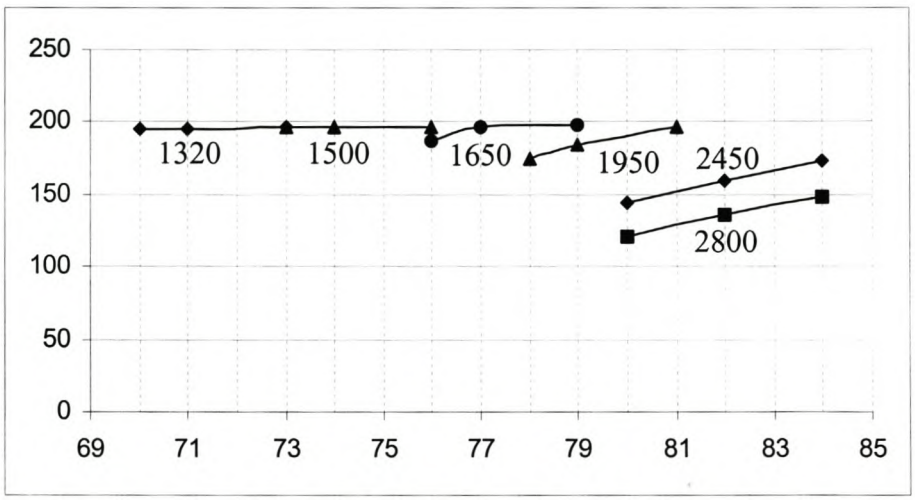

Figure 6.7. Measured current versus current angle characteristics of the RSM with speed a parameter, with V ≤ 380 V_{L-L}

The optimal measured (Tprac) and calculated (Tfe) torque results versus speed are shown in Fig. 6.8. The optimal measured results in Fig. 6.8 are extrapolated from

The optimal measured (Tprac) and calculated (Tfe) torque results versus speed are shown in Fig. 6.8. The optimal measured results in Fig. 6.8 are extrapolated from Table 6.2 and Fig. 6.6. The calculated results are obtained from the FE program using the same operating conditions as the measured results, i.e. the same speed, current and current angle. The calculated torque results are within 5% of the experimental results.

It is evident from Fig. 6.6 that the torque of the RSM vastly deteriorates as the flux-weakening speed region is widened. With the voltage limited to 380 V_{LL}, the torque is reduced from 681 Nm at base speed (1200 rpm) to 132 Nm at 2800 rpm. If more torque is required from the RSM in the flux-weakening region, the voltage must be allowed to increase much more than the maximum allowed voltage of 380 V_{LL}. This is another disadvantage of the RSM that due to the small airgap and significant effect of cross magnetisation in the flux-weakening speed region (see Chapter 1), the induced stator voltage is high. The high-induced stator voltage of the RSM in the flux-weakening speed region calls for a high supply voltage from the inverter to allow for more current to be injected into the machine. This is thus a disadvantage in terms of inverter cost.

The calculated (Vfe) and measured (Vprac) voltage characteristics of the RSM are shown in Fig. 6.8. Again, it is clear that the calculated voltage is generally lower than the measured voltage. Unlike the measured current that reduces with speed to get maximum torque output, the measured voltage is fixed at a maximum phase voltage of 220 V (or 380 V_{LL}).

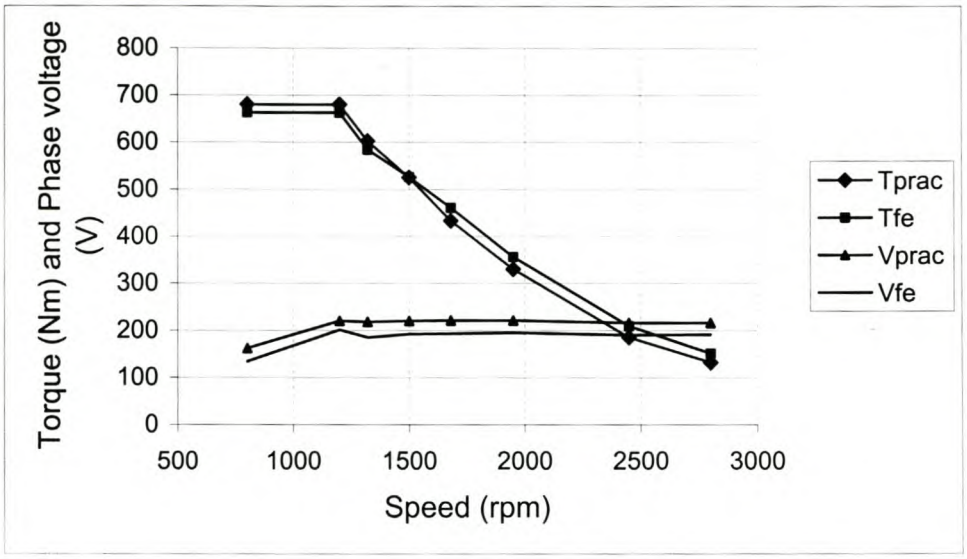

Figure 6.8. Calculated and measured torque and phase voltage versus speed curves

6.4 Performance of PM-assisted RSM

It has been shown in the previous sections that the performance of the RSM vastly deteriorates as the flux-weakening speed region is widened. The poor performance of the RSM in the flux-weakening region generally agrees with initial work presented in [7] (as also described in chapter 1).

As it was mentioned in section 1.5 of Chapter 1, the main objective of the research work is to improve the performance of the RSM, specifically in the flux-weakening speed region. Permanent magnets are added in the rotor of the RSM, as described in Chapter 3, to improve the performance of the machine. The existing reluctance rotor was optimised with PM assistance to give the same output torque as the induction machine subject to a voltage constraint at a maximum speed of 3800 rpm. The FE calculated torque and voltage results of the PM-assisted RSM presented in Chapter 3 are comparable to that of the induction machine. The measured performance results of the PM-assisted RSM are presented in the following sections.

6.5 Induced voltage of the PM-assisted RSM

The PM-assisted RSM was driven by a DC machine at no load and at the base speed of 1200 rpm. The induced phase voltage of the PM-assisted RSM (due to the PM sheets) was captured using the oscilloscope and is shown in Fig. 6.9. Since the neutral of the motor is not accessible, a star-point adapter was used to create the neutral point to enable the phase voltage measurement.

The interesting feature about the PM induced voltage is that it is very much sinusoidal with a high frequency ripple due to the stator slots. However, the important feature about this induced voltage at 1200 rpm is that it is relatively small (40 V rms). This small-induced voltage implies that the magnets strength (and hence PM flux) is also small. The small PM flux implies that the torque generated by the PM sheets is relatively small as compared to the reluctance torque. The small PM torque ensures that the machine is not a PM machine and therefore it does not have the general problem of PM machines of uncontrolled magnetising flux in the flux-weakening region.

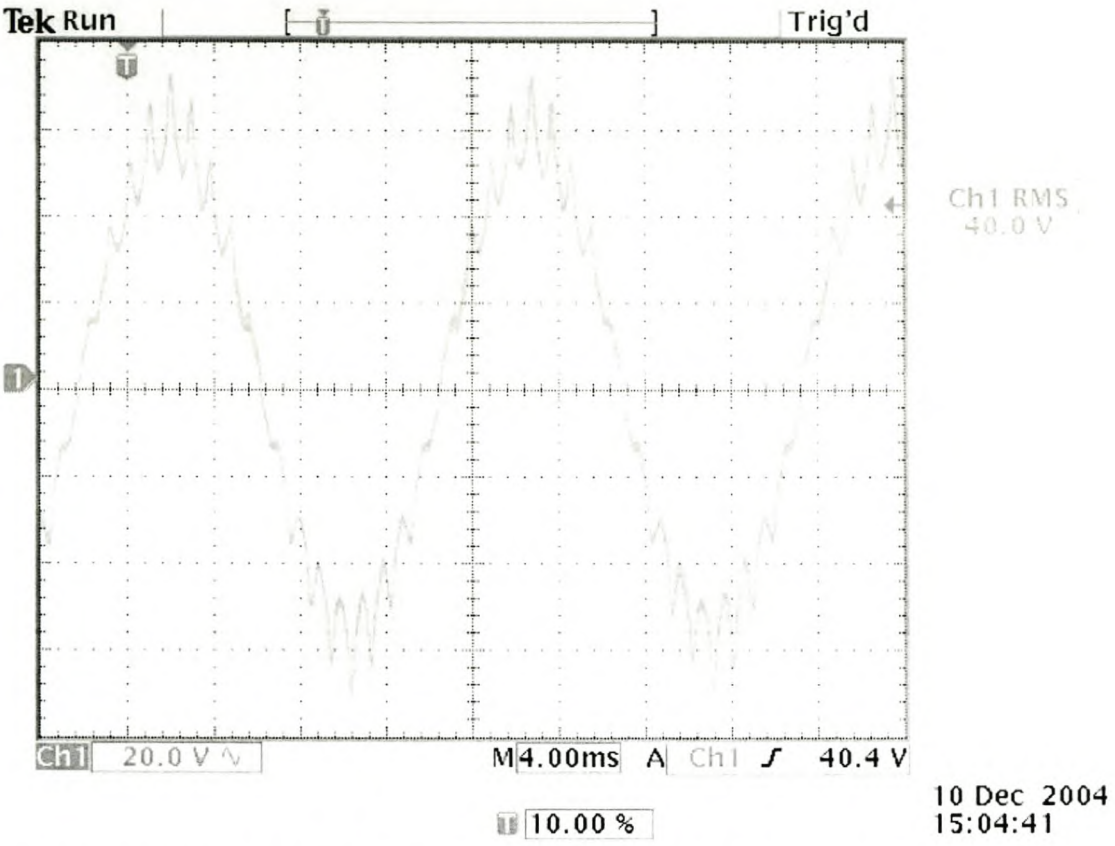

Figure 6.9. Captured induced phase voltage of the PM-assisted RSM at a speed of 1200 rpm (60 Hz)

6.6 Determining the optimal current angle of the PM-assisted RSM in the constant torque region

The conclusion reached in Chapter 3 regarding the optimal current angle of the PM-assisted RSM is that it is generally less than that of the RSM (Fig. 3.11). The optimal current angle of the RSM in the constant torque region was measured to be 60^0 as shown in section 6.2. This section describes the measurement of the optimal current angle of the PM-assisted RSM in the constant torque region.

The optimal current angle of the PM-assisted RSM in the constant torque region was determined in the same way as the RSM, i.e. at the rated current of 200 A and speed of 800 rpm. The current angle was varied from 45-70^0 in steps of 5^0. At each current angle and rated current the load (torque) exerted by the Dynamometers was noted. The measured and calculated torque results versus current angle at the speed of 800 rpm are presented in Fig. 6.10.

The calculated and measured torque results of the PM-assisted RSM in Fig. 6.10 seem to have a large deviation from each other as compared to those of the RSM presented in Fig. 6.3. This could be due to the fact that the actual PM sheet strength is higher than that in the FE program or due to the fact that modelling of non-rectangular PM sheets is not accurate in the FE program. However, these calculated and measured results are within 6% of each other.

It is clear from Fig. 6.10 that the calculated and the measured optimal current angle are 55^0. The optimal measured torque at 55^0 is 821 Nm and the calculated torque at 55^0 is 780 Nm.

The performance measurements of the PM-assisted RSM were all done at the optimal current angle of 55^0 and are presented in Table 6.3. Two torque measurements were done at each speed of 800 and 1100 rpm respectively. The first torque measurement at each speed was at about 700 Nm and 175 A, the second measurement at about 820 Nm and 200 A. The torque measurement at 700 Nm was taken for comparison purposes because the induction machine is rated at 700 Nm at 200 A in the constant torque region. It is clear from Table 6.3 that the PM-assisted RSM produce the rated induction machine torque of 700 Nm at 175 A, thus 25 amps less. At 200 A the torque produced by the PM-assisted RSM is about 15% more than that of the induction machine. The calculated torque results of the PM-assisted RSM in Chapter 3 also

showed that the torque of the PM-assisted RSM is more than that of the induction machine in the constant torque region at rated current.

At base speed of 1200 rpm the PM-assisted RSM was only loaded to a current of 175 A, generating a torque of 696 Nm according to Table 6.3. The machine could not be loaded more as the machine phase voltage was already at a limit of 220 V at a current of 175 A (see Table 6.3).

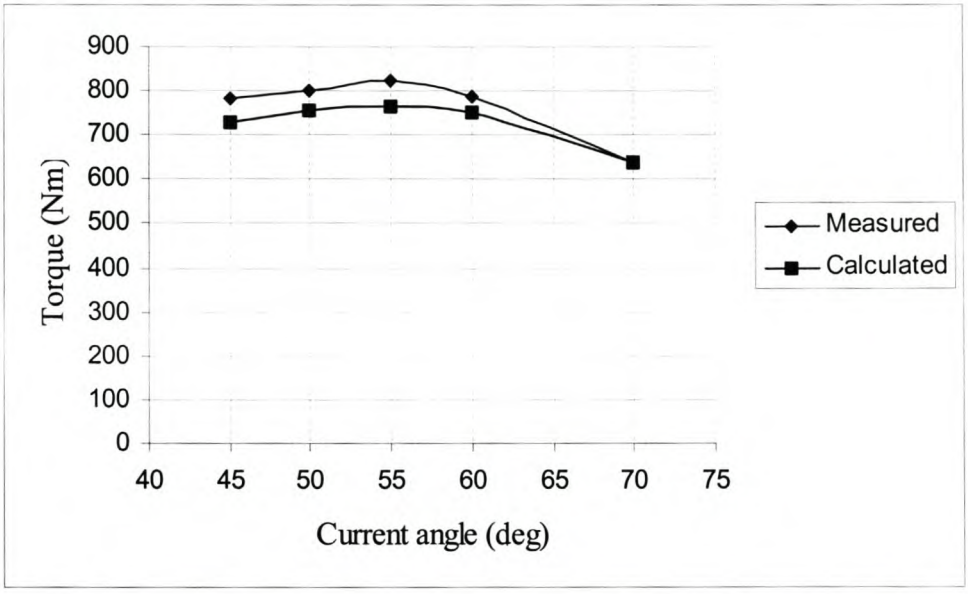

Figure 6.10. Calculated and measured torque versus current angle of the PM-assisted RSM at a speed of 800 rpm and rated current of 200 A.

Table 6.3. Measured results of the PM-assisted RSM in the constant torque region at the indicated average speeds (within ± 1% error)

ϕ Angle	Irms (A)	Iho1 (A)	Vrms 3-phase	Vho1 3-phase	Vho1 Phase	Pm kW	Pdc kW	Idc (A)	Pf1	Pf	Vdc (V)	T (Nm)
Speed = 800 rpm (± 1%)												
55	177	177	457	272	157	63.2	65.8	78	0.75	0.44	861	706
55	200	199	471	283	162	77.5	80	95	0.76	0.46	857	821

Speed = 1100 rpm (± 1%)												
55	175	175	531	372	215	85	88	103	0.74	0.52	854	702
55	201	200	542	384	222	100	103	122	0.75	0.53	850	826
Speed = 1200 rpm (± 1%)												
55	176	175	544	389	223	89	92	109	0.76	0.54	854	696

6.7 Determining the optimal current angle of the PM-assisted RSM in the flux-weakening speed region

The optimal current angle of the PM-assisted RSM in the constant torque region is determined in section 6.6 as 55^0. This optimal current angle of 55^0 of the PM-assisted RSM is valid for all speeds in the constant torque region. However, in the flux-weakening region an optimal current angle must be determined at each operating point of speed. The procedure for determining the optimal current angle at each operating speed is similar to that of the RSM described in section 6.3, and is be described here again for the sake of completeness.

As an initial basis for comparison between the RSM and the PM-assisted RSM, the optimal current angles of the PM-assisted RSM in the flux-weakening region were determined at the same speeds as those of the RSM presented in Table 6.2. At each point of speed, the objective was to get the highest torque per ampere. At each speed, three current angles were selected with the anticipated optimal current angle included. The machine is loaded at each current angle until either the voltage equals the limit of 220 V or the current equals the limit of 200 A. The complete measured results of the PM-assisted RSM in the flux-weakening region are presented in Table 6.4 below. At each point of speed and current angle the prime performance parameters as presented in Table 6.4 are the fundamental phase voltage (Vho1), fundamental current (Iho1), machine input power (Pm) and inverter DC input power (Pdc), fundamental power factor (Pf1) and the output torque (T).

The torque versus current angle relation at each speed in the flux-weakening region with voltage and current as constraints is shown in Fig. 6.11. The current angles that give the maximum torque at each speed are clearly visible from Fig. 6.11. The angles that give maximum torque at each speed are the optimal current angles for that particular point of speed. Consider the speed of 1680 rpm in Table 6.4 and Fig. 6.11 for example; the current angles are 68, 72 and 74 degrees. The torque values are respectively 476 Nm, 574 Nm and 530 Nm. Furthermore at current angles of 68^0 and 74^0, either the voltage or the current is at the limit. But at the current angle of 72^0, either the voltage or the current must be at the limit; in this case the current is at the limit but the torque is more than that at current angles of 68^0 and 74^0. It is evident from Table 6.4 that the optimal current at the speed of 1680 rpm is 72^0 and the corresponding torque is 574 Nm. The rest of the optimal current angles at different speeds and the corresponding torque values are determined in the same manner as that at the speed of 1680 rpm described above. The optimal torque was also calculated using the FE software at each speed and at the optimal current angle and at rated current or voltage.

The complete measured and calculated torque results versus speed are shown in Fig. 6.13. It is clear from Fig. 6.13 that the measured and calculated torque has a strong correlation in the flux-weakening region, more than in the constant torque region. The reason for the strong correlation in the flux-weakening region could be attributed to the fact that the *d*-axis of the machine is less saturated and the calculated results are less sensitive to the BH-curve. However, the calculated and measured torque results are within 5 % of each other over the whole speed region. It is important to note that the optimal torque values presented in Table 6.4 at each speed are obtained at the rated current of 200 A. The fact that the PM–assisted RSM can be loaded to rated current at all speeds in the flux-weakening region without exceeding the voltage limit and with a higher torque as the RSM is an important different characteristic of the PM-assisted RSM as compared to the RSM. It was shown in section 6.4 that there was

no advantage of loading the RSM to rated current at the highest speeds in the flux-weakening region, as the output torque would not increase any further. The current versus current angle relationship of the PM-assisted RSM with speed a parameter is shown in Fig. 6.12. It is clear from Fig. 6.12 that the machine was loaded up to rated current at each optimal current angle at all the speeds. The fundamental power factor, Pf1, of the PM-assisted RSM was also measured at each point of speed. The measured power factor results are also presented in Table 6.4. It is clear that the power factor values are generally above 0.8. The power factor of the PM-assisted RSM was also calculated with the FE program at the same operating conditions as the practical, i.e. at the same speed, current and current angle. The measured and calculated power factors are shown in Fig 6.14. It can be seen in Fig. 6.14 that the measured and calculated results have a positive correlation and are within 5 % of each other.

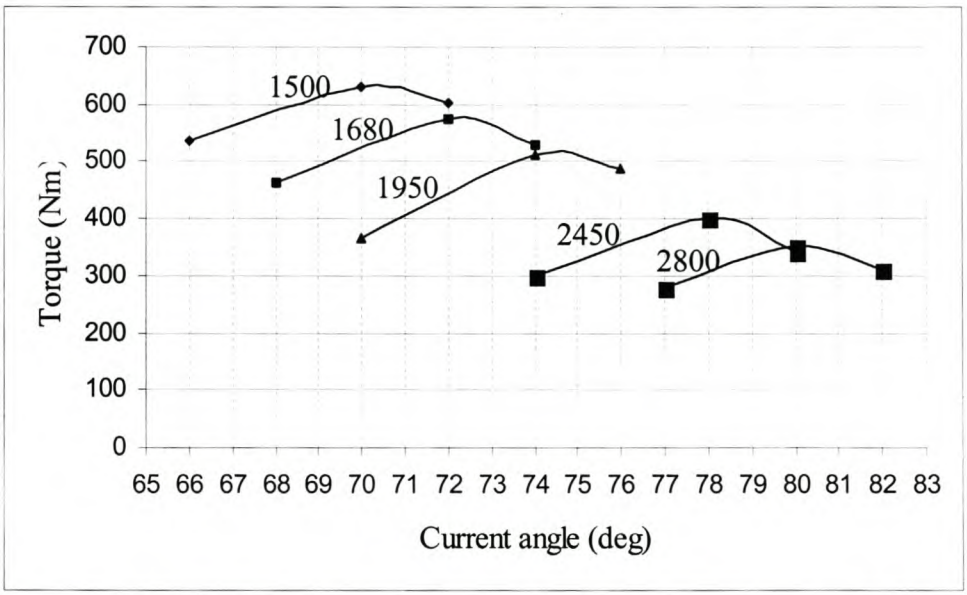

Figure 6.11. Measured torque versus current angle characteristics of the PM-assisted RSM with voltage and current as constrains at different speeds in the flux-weakening speed region

Table 6.4. Experimental results of the PM-assisted RSM in the flux-weakening region at the indicated average speeds (within ± 1% error)

ϕ Angle	Irms (A)	Iho1 (A)	Vrms 3-phase	Vho1 3-phase	Vho1 Phase	Pm kW	Pdc kW	Idc (A)	Pf1	Pf	Vdc (V)	T (Nm)
Speed = 1500 rpm (± 1%)												
66	157	156	544	374	225	89	91.4	108	0.84	0.59	854	535
70	200	199	506	372	194	97.7	99.6	114	0.85	0.56	849	610
72	201	201	492	342	185	96	98.7	117	0.86	0.55	849	603
Speed = 1680 rpm (± 1%)												
68	147	147	553	399	229	86.7	88.9	105	0.856	0.62	853	463
72	199	198	516	353	205	104	107	127.5	0.86	0.58	847	574
74	200	200	499	327	190	98	101.5	120	0.86	0.56	849	530
Speed = 1950 rpm (± 1%)												
70	137	137	549	396	229	81.4	84	99	0.87	0.62	857	365
74	200	200	536	381	220	112	115	136	0.86	0.6	850	512
76	202	201	522	355	208	104	110	130	0.85	0.58	850	486
Speed = 2450 rpm (± 1%)												
74	147	146	552	390	231	83	88	104	0.88	0.63	856	299
78	201	200	536	379	218	112	115	136	0.84	0.58	849	402
80	202	202	518	359	208	100	104	122	0.82	0.54	853	340
Speed = 2800 rpm (± 1%)												
77	130	130	544	360	212	75	77	90	0.9	0.62	858	280
80	201	201	547	382	219	112	115	136	0.82	0.58	852	351
82	204	204	520	357	206	99.8	103	121	0.79	0.53	852	310

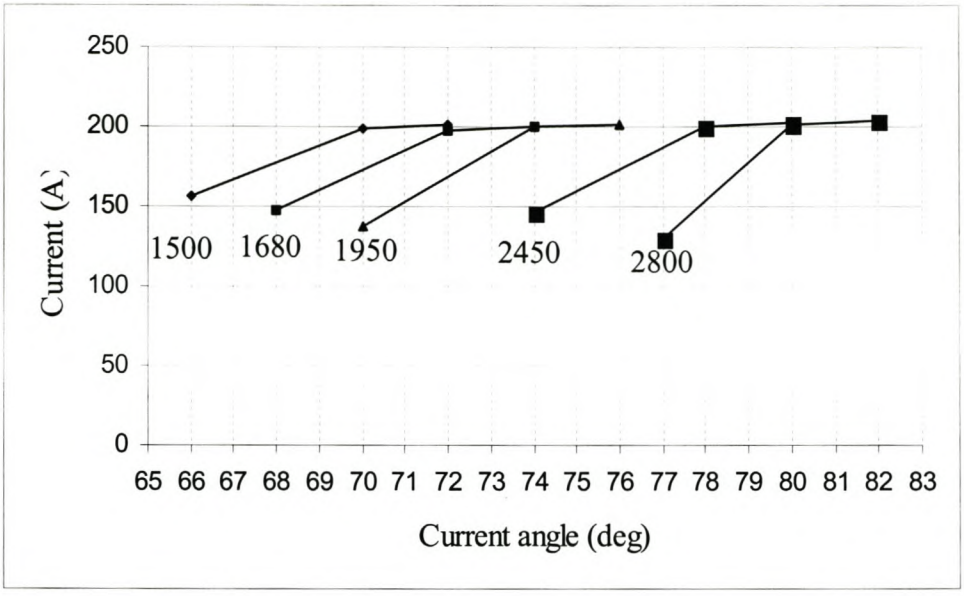

Figure 6.12. Measured current versus current angle characteristics of the PM-assisted RSM at different speeds in the flux-weakening region

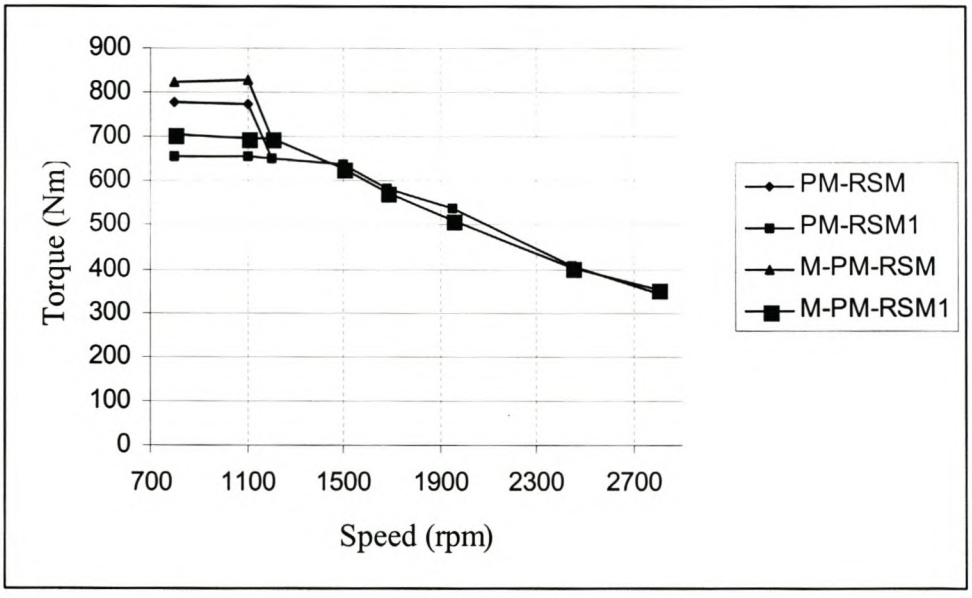

Figure 6.13. Calculated (PM-RSM, PM-RSM1) and measured (M-PM-RSM, M-PM-RSM1) torque of the PM-assisted RSM versus speed

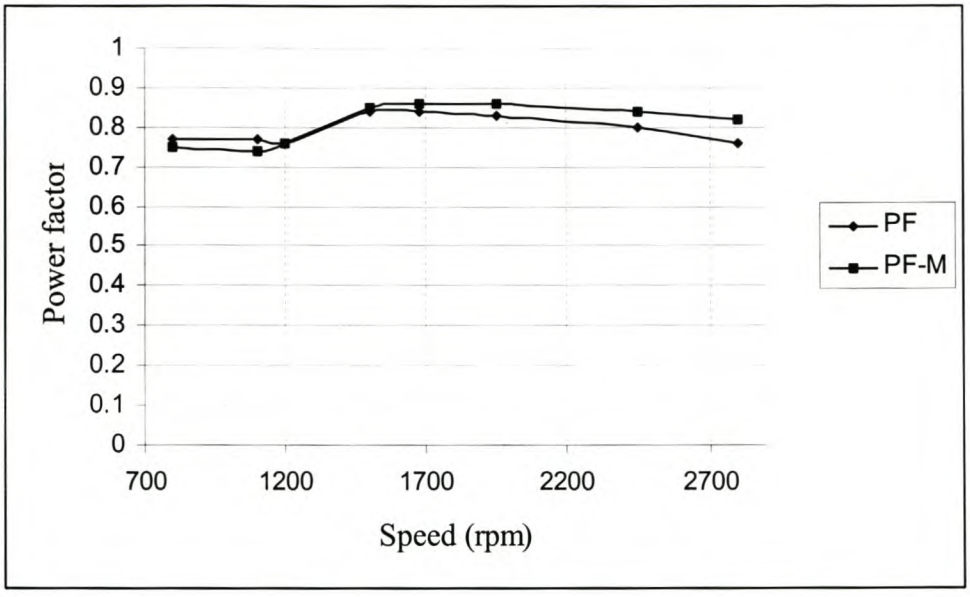

Figure 6.14. Calculated (PF) and measured (PF-M) power factor of the PM-assisted RSM versus speed

6.8 Performance comparison of the PM-assisted RSM, RSM and Induction Machine

The optimal measured and calculated performance parameters of the PM-assisted RSM and the RSM were presented and discussed in sections 6.1-6.8. Great deal of attention was given into determining the optimal current angles for all the operating speeds and hence the optimal performance parameters. It was shown that the measured and calculated results of both the PM-assisted RSM and RSM are respectively within 5% of each other.

The optimal measured performance parameters of the induction machine were acquired from Siemens. The optimal performance parameters of the induction machine at each operating speed were obtained subject to the current ($I \leq 200$ A) and voltage ($V \leq 220$ V) constraints – or else in the same way as the optimal performance parameters of the PM-assisted and RSM were obtained as described in sections 6.1-

6.8. All the induction machine data and performance parameters are listed in Appendix B. The measured torque results of the PM-assisted RSM, RSM and induction machine are presented in Table 6.5 and are also plotted in Fig. 6.15.

It can be seen from Table 6.5 that the measured torque results of the PM-assisted RSM and the induction machine are within 2% of each other at all speeds. This strong correlation in terms of torque of the PM-assisted RSM and the induction machine is clearly visible in Fig. 6.15. The poor torque performance of the RSM in the flux-weakening region cannot be emphasised more. For example, at the maximum speed of 2800 rpm, the torque of the RSM is about 40% less than that of the induction machine and PM-assisted RSM.

In Table 6.5 and Fig. 6.15, PM-RSM1 corresponds to the maximum torque the PM-assisted RSM can produce in the constant torque region and rated current subject to voltage constraints (see section 6.5). The power factor curves of the PM-assisted RSM, induction machine and RSM versus speed are shown in Fig. 6.16. It can be seen that the power factor of the induction machine and the PM-assisted RSM are generally within 2% of each other. The power factor of the RSM is always at the low side compared to the induction machine. Infact, at maximum speed of 2800 rpm the power factor of the RSM is about 0.54 as compared to the power factor of 0.85 of the induction machine and PM-assisted RSM.

The current versus speed curves of the PM-assisted RSM and induction machine for the same output power are shown in Fig. 6.17. It can clearly be seen that the current of the PM-assisted RSM is lower than that of the induction machine in the constant torque region. However, in the flux-weakening region the currents are comparable for both drives. Fig. 6.18 shows the measured efficiency versus speed of the induction machine and the PM-assisted RSM. It is clear from Fig. 6.18 that the efficiency of the PM-assisted RSM is generally higher than that of the induction machine.

The characteristics of the current angle versus speed for the RSM and PM-assisted RSM are shown in Fig. 6.19. The important feature is that the current angle of the PM-assisted RSM is generally lower than that of the RSM. But the current angles for both machines tend to increase sharply as the speed is increased.

Table 6.5. Measured torque results of the induction machine, RSM and PM-assisted RSM

Speed (rpm)	IM (Torque, Nm)	PM-RSM (Torque, Nm)	PM-RSM1 (Torque, Nm)	RSM (Torque, Nm)
800	700	706	821	684
1100	-	702	826	-
1200	700	696	-	681
1500	642	630	-	525
1680	587	574	-	433
1950	514	512	-	330
2450	410	402	-	185
2800	358	351	-	132

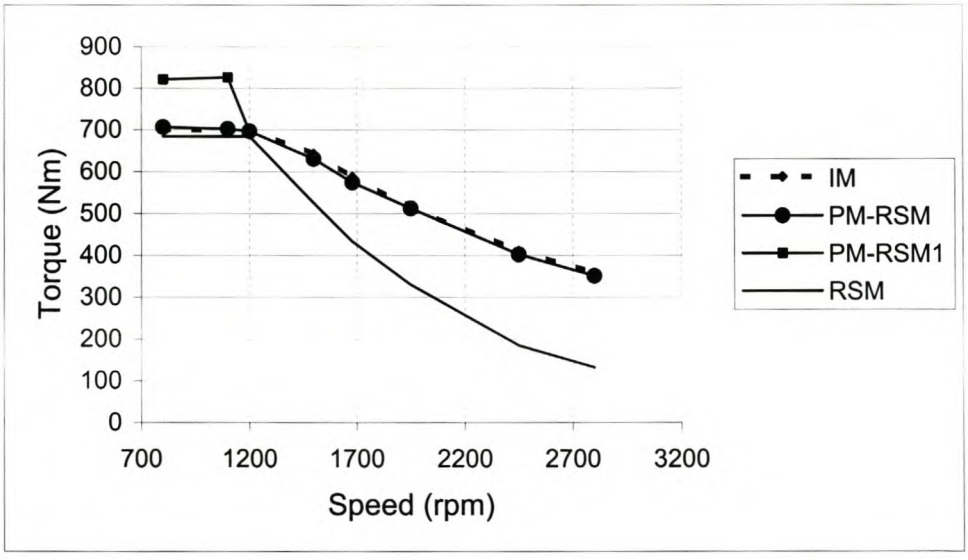

Figure 6.15. Measured torque results versus speed of the induction machine (IM), PM-assisted RSM and RSM

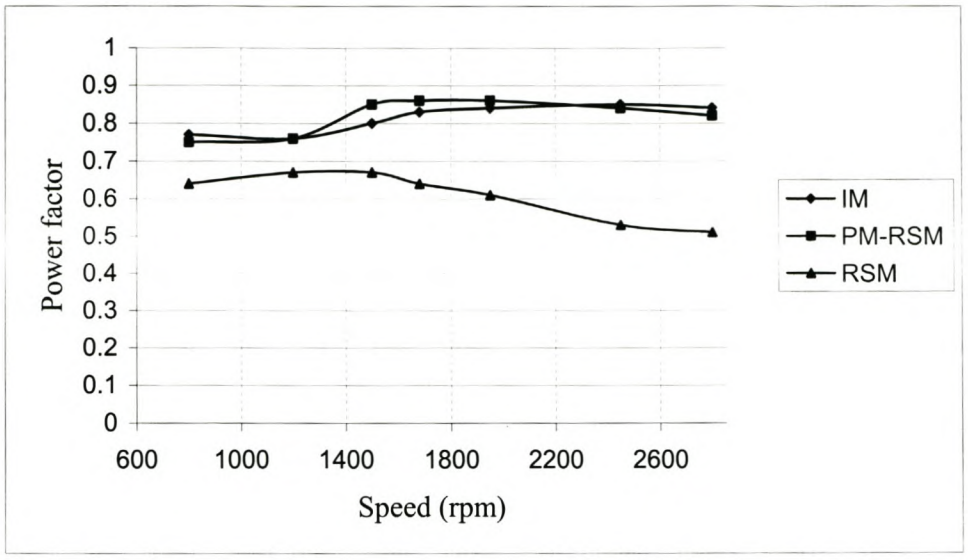

Figure 6.16. Measured fundamental power factor versus speed (frequency) results of the induction machine (IM), PM-assisted RSM (PM-RSM) and RSM

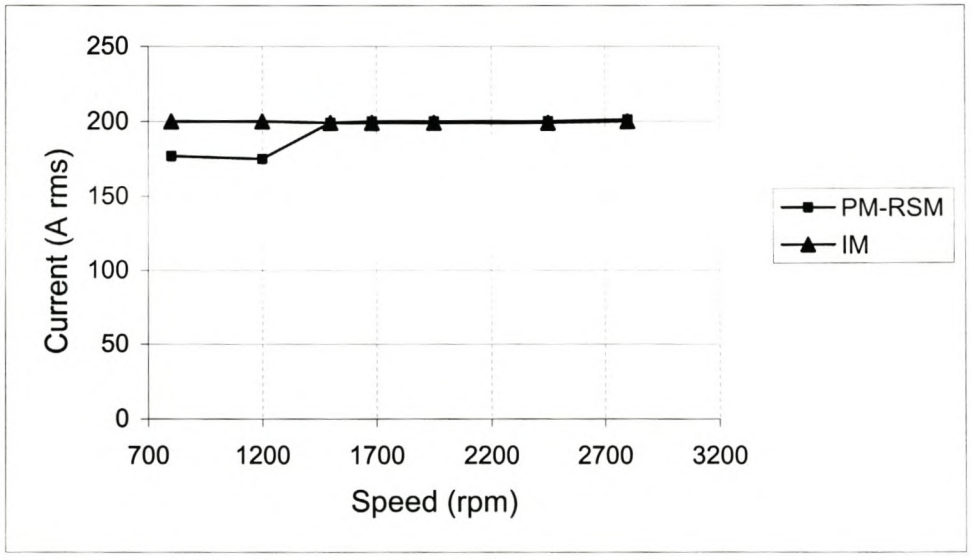

Figure 6.17. Measured fundamental currents versus speed of the Induction machine and PM-assisted RSM

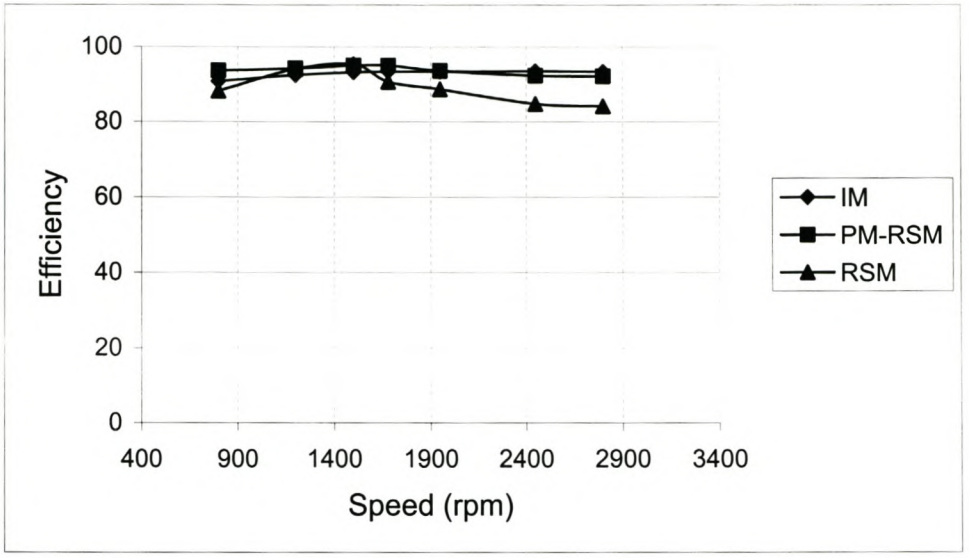

Figure 6.18. Measured efficiency versus speed of the PM-assisted RSM and Induction Machine

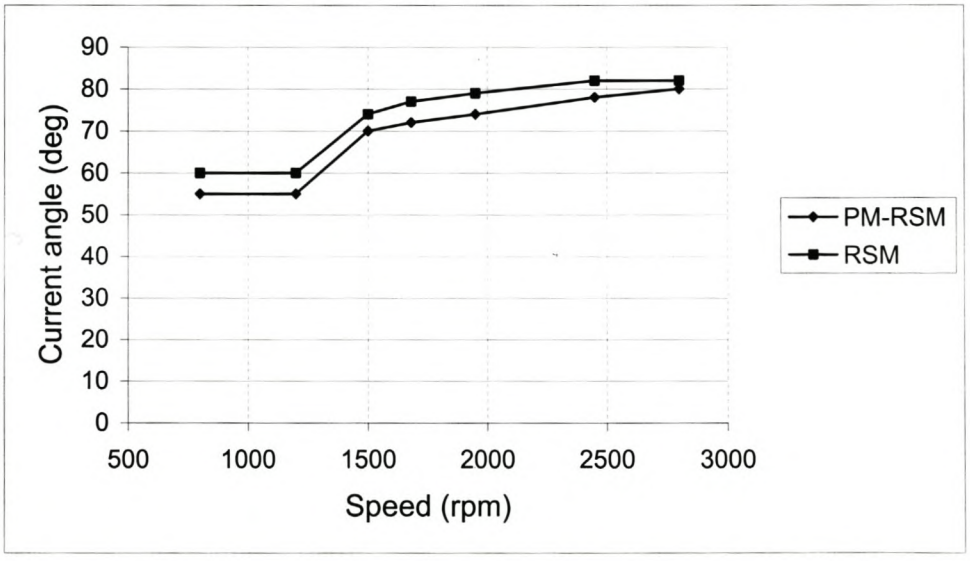

Figure 6.19. Measured current angle versus speed of the PM-assisted RSM and RSM

6.9 Total no-load losses of the PM-assisted RSM

A no-load test on the PM-assisted RSM was done to determine the total no-load losses of the PM-assisted RSM. The test was performed as follows: the PM-assisted RSM was driven by a DC motor at no-load at different speeds. A torque transducer was coupled between the DC motor and the PM-assisted RSM to determine the load exerted by the PM-assisted RSM at each speed. The torque versus speed result of the PM-assisted RSM is presented in Fig. 6.20. It is clear from Fig. 6.20 that the losses of the PM-assisted RSM tend to follow a third order polynomial function. However, the losses of the PM-assisted RSM seem to be generally insignificant, e.g. at the speed of 1200 rpm (from Fig. 6.20 T = 2 Nm) the losses are 1200 rpmx2 Nmx2xpi/60 = 251 W.

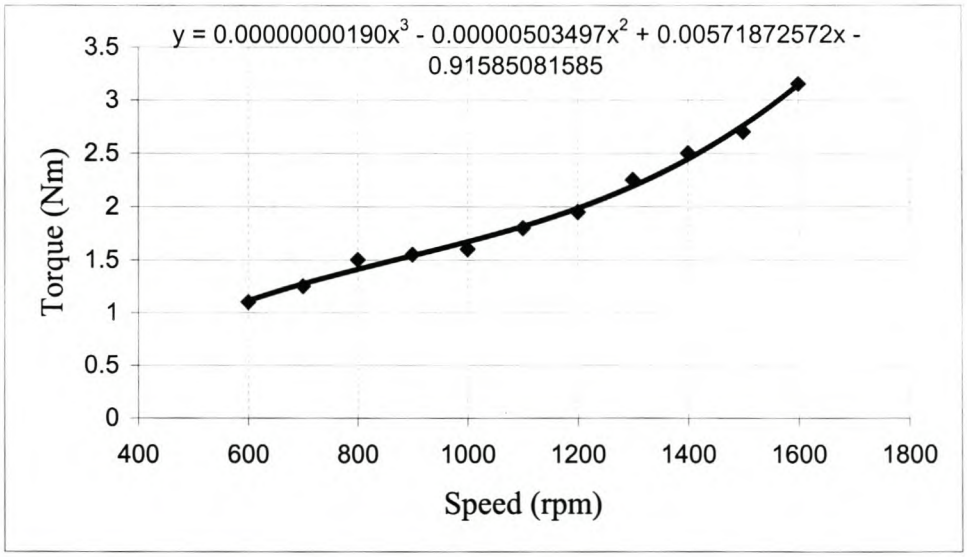

Figure 6.20. No-load losses of the PM-assisted RSM versus speed

6.10 Temperature rise of the RSM and PM-assisted RSM

It was mentioned in Chapter 1 that amongst others, the advantage of the RSM over induction machines is that it runs cool as it does not sustain any rotor losses. However, the stator winding temperature rise of the PM-assisted RSM could be expected to be more than that of the RSM due to the fact that the PM sheets reduce the cooling of the PM-assisted RSM. The heat run tests of the RSM and PM-assisted RSM were done at the speed of 1200 rpm and mechanical load of 570 Nm for three hours. The temperature of the stator windings was measured using an RTD mounted on the stator winding. The temperature rise versus time of both the RSM (average ambient temperature = 27^0) and PM-assisted RSM (average ambient temperature = 29^0) is plotted in Fig. 6.21. It is clear that the temperature rise (difference of actual and ambient) of the PM-assisted RSM is lower than that of the RSM. The reason for the low temperature rise of the PM-assisted RSM is that the required current to produce the torque of 570 Nm is lower than that of the RSM (see also Tables 6.1 and 6.3) and hence the PM-assisted RSM stator losses are less.

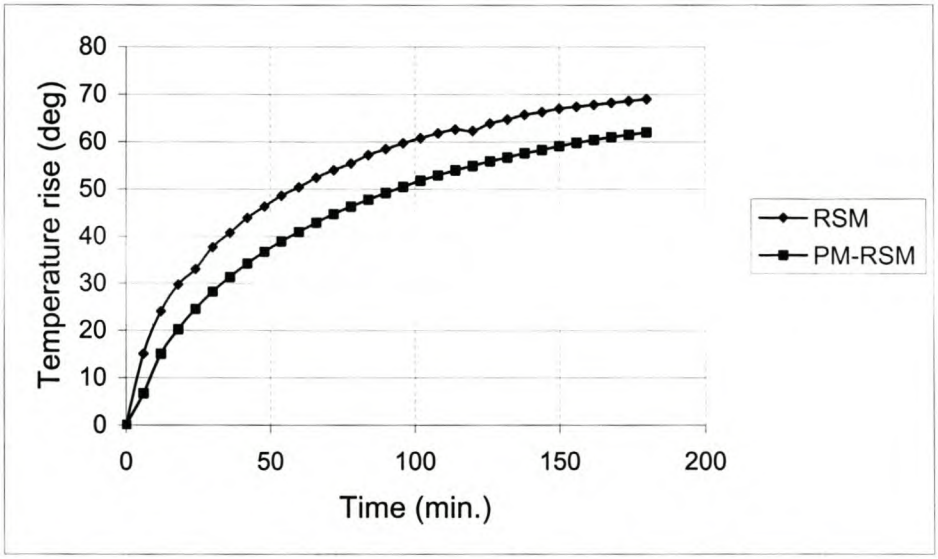

Figure 6.21. Temperature rise of the RSM and PM-assisted RSM at a load of 570 Nm and speed of 1200 rpm

Chapter 7

7 Conclusions and recommendations

The contribution of this thesis can be summarised as the design optimisation and steady state performance evaluation of the 110 kW PM-assisted RSM particularly in the flux-weakening region. The optimum-designed PM-assisted RSM was obtained using the finite element method directly in an optimisation algorithm (*Powell optimisation algorithm*). The PM-assisted RSM was built and tested to verify the finite element calculated results.

The experimental results were obtained using the TMS320F240 fixed point DSP controller under current vector control. The design of the digital speed and current *PI* regulators was implemented using Matlab.

Since the objective of this project was to evaluate the performance of the 110 kW PM-assisted RSM over that of the pure 110 kW reluctance synchronous machine (RSM) and induction machine, the RSM was also tested, and the performance parameters of the induction machine were acquired from Siemens. Each machine was controlled to get its maximum torque under current and voltage constraints and all the result were presented in chapter 6.

7.1 Conclusions

The following conclusions are reached based on the finite element calculated and experimental results of the RSM, PM-assisted RSM and IM drives presented in the thesis.

- With optimum (slight) amount of thin PM sheets added into the flux barriers of the reluctance rotor, the performance (in terms of torque and voltage) of the PM-assisted RSM compares favourably well with that of the IM in the flux-weakening region. In the constant torque speed region, the PM-assisted RSM outperforms the IM in terms of torque and the supply voltage at rated current.
- The finite element calculated and measured induced voltage of the PM-assisted RSM due to the PM sheets (without stator currents) at a speed of 1500 rpm is very low, it is about 10% (55V rms) of the rated voltage. The low induced voltage at high speeds is an important advantage in traction applications because if a locomotive fails and has to be pulled, no high voltages will be induced in the stator windings.
- The power factor of the RSM is improved from 0.63 to 0.76 at rated speed and rated current with the addition of the PM sheets in the flux barriers. The improved power factor of the PM-assisted RSM means that a low rated (and hence cheap) inverter can be used to drive the PM-assisted RSM as compared to the RSM of the same rating.
- It is shown that the torque of the RSM and PM-assisted RSM could further be improved by increasing the supply current by a factor of 1.5 to make the losses of the IM equals those of the RSM and PM-assisted RSM.
- The cost of the parabolic shaped PM sheets relatively increases the cost of the PM-assisted rotor due to the fact that a special mould has to be created to accommodate the rather peculiar shapes of the PM sheets.
- The implementation of non-rectangular magnets in the finite element analysis leads to small calculation errors of the performance parameters of the PM-assisted RSM, since in the calculations the magnets flux distribution is assumed to be of piece-wise rectangular magnets.

7.2 Recommendations

The performance of the PM-assisted RSM in the flux weakening region has been analysed and based on the conclusions reached in section 7.1 the following recommendations are made:

- In future-improvements of the PM-assisted RSM the rotor structure should be changed to a simple structure that can accommodate straight or rectangular magnets. The implementation of rectangular magnet sheets will reduce the average cost of the magnets since no special mould will have to be created as in the case of parabolic shaped magnets. Another advantage of rectangular magnets is that the error in the calculation of the performance parameters will be reduced.
- A complete stator and rotor design optimisation for the PM-assisted RSM should be done to improve on the overall performance of the PM-assisted rotor RSM. This would give a true comparison between the RSM and IM.

BIBLIOGRAPHY

[1] Fratta A. and Vagati A.:" A Reluctance Motor Drive for High Dynamic Performance Applications", IEEE IAS annual meeting, pp 295-302, 1987.

[2] Kamper M.J., Van der Merwe F.S. and Williamson S.:" Direct Finite Element Design Optimisation of the Cageless Reluctance Synchronous Machine", IEE Trans on Energy Conversion, Vol. 11, No. 3, pp 547-553, Sept 1996.

[3] Kamper M.J, "Design Optimisation of Cageless Flux Barrier Rotor Reluctance Synchronous Machine", PhD Dissertation, university of Stellenbosch, 1996.

[4] Kamper M.J, Volschenk A.F: "Effect of Rotor Dimensions and Cross Magnetisation on Ld and Lq Inductances of Reluctance Synchronous Machine with Cageless Flux Barrier rotor", IEE Proc. Electrical Power Applications, vol. 141, no. 4, 1994.

[5] Boldea I and Nasar S.A.:" Vector control of AC Drives", CRC Press, 1992.

[6] Kamper MJ, Mackay AT: "Optimum Control of the Reluctance Synchronous machine With a Cageless Flux barrier Rotor", SAIEE, Vol. 86, No. 2, 1995.

[7] Germishuizen J.J.: "Comparative Study of Reluctance Synchronous and Induction Machine Drives for Rail Traction", M.Eng dissertation, University of Stellenbosch, 2000.

[8] Bomela X.B, Kamper M.J.:"Effect of Stator Chording and Rotor skewing on Performance of Reluctance Synchronous Machine", IEEE Trans on Industry Applications, vol. 38, no.1, January/February 2002.

[9] Bose B.K, Modern Power Electronics and AC Drives

[10] Bianchi N, Bolognani S, Parasiliti F, Villani M: "Design of Interior PM Synchronous Motors for Flux-Weakening Characteristics", ICEM, 1998, pp 1178-1183.

[11] Shigeo M, Masayuki S, Yoji T: 'Performance of PM-Assisted Synchronous Reluctance Motor for High-Efficiency and Wide Constant-Power Operation', IEEE Trans on Industry Applications, vol. 37, no. 5, 2001

[12] Fratta A, Vagati A, Villata F: 'Permanent Magnet assisted Synchronous Reluctance Drives For Constant-Power Applications', Intelligent Motion Proceedings, 1992.

[13] Conti G, Parasiliti F, Vilani M: "Torque Ripple Analysis in Synchronous Reluctance Motors", Electromotion 3,1996, pp188-193.

[14] Salon SJ: "Finite Element Analysis of Electrical Machines", Kluiwer Academic Publishers, Boston, 1995.

[15] Wang RJW: " Design Aspects and Optimisation of an Axial Field Permanent Magnet Machine with an Ironless Stator", PhD Dissertation, University of Stellenbosch, 2003.

[16] Parasiliti F. and Bertold P. (ed), "Energy Efficiency in Motor Driven Systems", Springer-Verlag, Berlin, Germany, pp. 101-110, 2003.

[17] Schmidt E., Brandi W.: "Synchronous Reluctance Machines With Internal Rotor Flux Barriers – Efficient Performance Improvement by Means of Internal Permanent Magnets", IEE Power Electronics, Machines and Drives Conference, pp 546-550, April 2002.

[18] Jung H.L., Jung K., Dong S.H.:" Effect Analysis on Ld and Lq Inductance of Permanent Magnet Assisted Synchronous Reluctance Motor Using Finite Element Method", IEEE Trans on Magnetics, vol 35, No3, 1999.

[19] Xu L., Ye L., Zhen L., El-Antaby A.:" A new Design Concept of Permanent Magnet Machine for Flux Weakening Operation", IEEE Trans on Ind. App., Vol 31, No 2, 1995.

[20] Boldea I: "Reluctance Synchronous Machines and Drives", Clarendon press, Oxford, 1996.

[21] Fick P.D.: "Evaluation of the Constant Current Angle Controlled Reluctance Synchronous Machine Drive", M.Eng dissertation, University of Stellenbosch, 2002.

[22] Vagati A, Canova A, Chiampi M, Pastorelli M & Repetto M: "Design Refinement of Synchronous Reluctance Motors Through Finite-Element Analysis", IEE Trans. on Industry Applications, vol. 36, no. 4, 2000.

[23] Vas P.:"Sensorless Vector and Direct Torque Control", Oxford Science Publications, New York, 1998.

[24] Soong W.L, Miller T.J.E.:"Theoretical Limitations to the Field-Weakening Performance of the Five Classes of Brushless Synchronous AC Motor Drive", IEE Int. Conference on Electrical Machines and Drives, Oxford, September 1993,pp 127-132.

[25] Salon S.J.:"Finite element Analysis of Electrical Machines", Kluiwer Academic Publishers, 1995.

[26] Smuts J.L.:"Critical evaluation of a Position Sensorless Control Technique for the Reluctance Synchronous Machine Drive", M.Eng dissertation, University of Stellenbosch, 2001.

[27] Sen P.C.:"Principles of Electrical Machines and Power Electronics", John Wiley & Sons, Canada, 1997.

[28] Morgan A.T.:"General Theory of Electrical Machines", Heyden & Son, London, 1979.

[29] A Handbook on "A Guide to Effective Spoken & Written Communication", PCU department, UCT, 1993.

[30] N. Mohan, T.M. Underland, W.P. Robbins: "Power Electronics", John Wiley & Sons, Canada, 1995.

[31] Rekioua T., Meibody-Tabar M., Sargos F.M., Le Doeuff R.: " Modelling and Digital Simulation of Two Control Methods For a Permanent Synchronous Motor Supplied by PWM-VSI", IEEE EPE Firenze, pp 3-457 to 3-462, 1991.

[32] Pillay P., Krishan R.:"Modelling, Simulation, and Analysis of Permanent-Magnet Motor Drives, Part I: The Permanent Magnet Moror Drive", IEEE Trans on Ind Appl, Vol 25, No 2, pp 265-273, 1989.

[33] Rowan T.M., Kerkman R.J.:"A New Synchronous Current Regulator and an Analysis of Current Regulated PWM Inverters", IEEE Trans on Ind Appl, vol IA-22, No 4, pp 678-689, 1986.

[34] Lyshevski S.E., Nazarov A.:" Control and Analysis of synchronous Reluctance Motors", IEEE Proceedings of the American Control conference, pp 1682-1686, 1999.

[35] Jovanovic M.G., Betz R.E.:"Optimal Torque Controller for Synchronous Reluctance Motors", IEEE Trans on Energy Conversion, vol 14, no 4, pp 1088-1093, 1999.

[36] www.lem.com/ norma5000

Appendix A

Table of the induction machine characteristics based on a rated speed of 1500 rpm, maximum line voltage of 553 V and maximum speed of 3800 rpm.

Table A1: IM rated characteristics

Motor Parameters	**Rated Speed**	**Maximum Speed**
Number of poles	6	
Connection	Y	
Terminals	3	
Standards	IEC 349	
Air-gap	1.5 mm	
Insulation	200	
Cooling air	0.32 m^3/sec	
Frequency	75.47 Hz	191.66 Hz
Operation	Continuous	
Supply voltage	503 V	553 V
Supply current	205 A	187 A
Torque	700 Nm	360 Nm
Output power	110 kW	143 kW
Speed	1500 rpm	3800 rpm

Appendix B

Mechanical drawings of the PM-assisted RSM

This section presents the 2-dimention cross sectional diagram of the PM-assisted RSM.

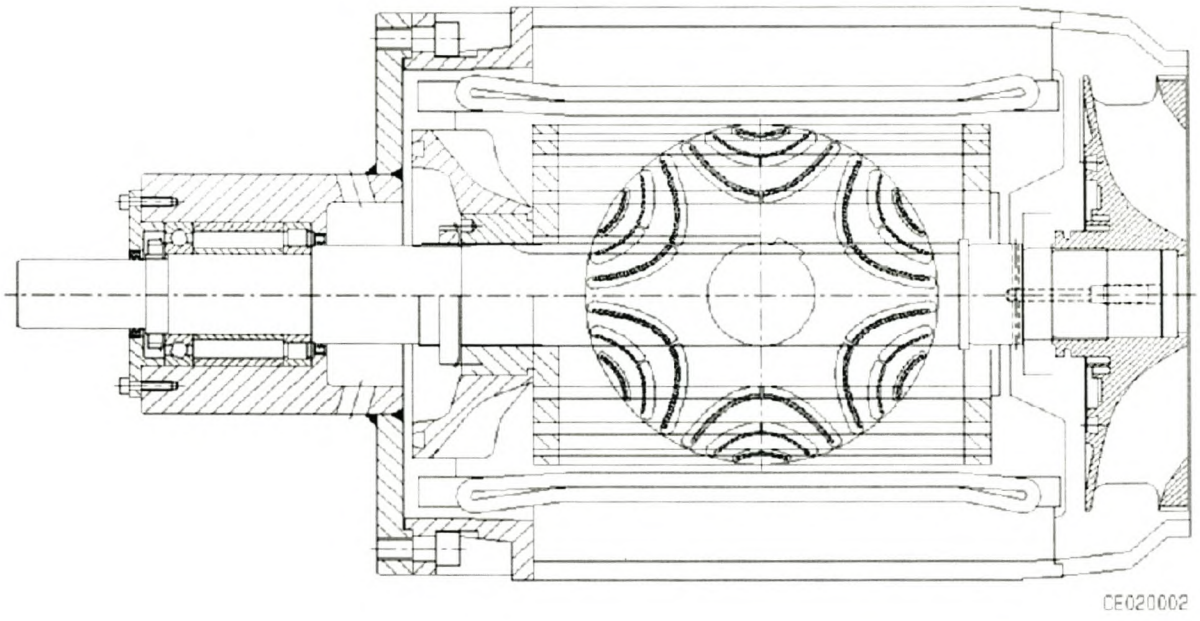

Figure B1: Stator and rotor cross sectional diagram of PM-assisted RSM

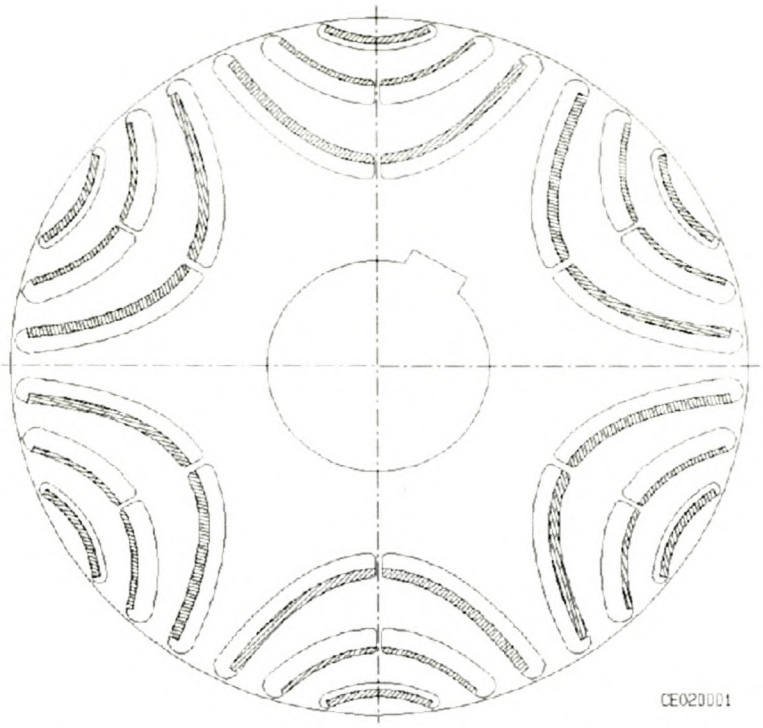

Figure B2: Rotor cross sectional drawing of PM-assisted reluctance rotor

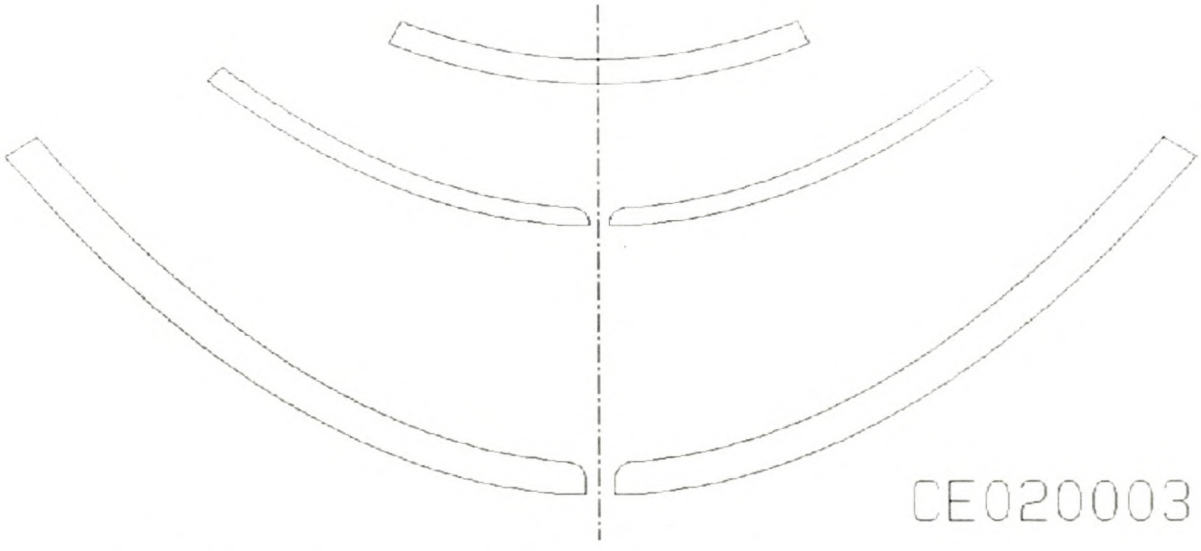

Figure B3: One pole cross sectional diagram of Epoxy bonded permanent magnet sheets

Appendix C

Induction machine data supplied by Siemens

This calculated induction machine data was supplied by Siemens. Siemens considers their calculated data to be the same as their measured results. It is on this basis that these results are considered to be measured results in this thesis. It is the optimal induction machine data based on the rated base speed of 1200 rpm, rated current of 200 A, maximum phase voltage of 220 V and the maximum speed of 2800 rpm (or else at the same conditions as those of the PM-assisted RSM and RSM described in Chapter 6). The important performance parameters of the induction machine are the fundamental voltage (U1), fundamental current (I1), Torque, speed, power factor, mechanical power and efficiency. These important parameters of the induction machine are also highlighted in bold.

```
|-V 2.43-------------------------------------------------------------------------|
| 1TB1921-0JJ03 | w1 =  30 |                          | 30/11/04  12:15:25  | MD076  |
|-------------------------------------------------------------------------------|
| LRV Portland 98                                                       Blatt 1 |
|                                                                               |
|-------------------------------------------------------------------------------|
| fp-max = 1838 Hz  tpuls-min =  15 us                                          |
|-------------------------------------------------------------------------------|
|                          |                    2p = 6   w =  30   l-Fe = 340.0 mm  |
|-------------------------------------------------------------------------------|
|Einsatzdaten        |      |      |      |      |      |      |      |      |
```

Betriebspunkte								
U1	**V**	**238**	**354**	**381**	**381**	**381**	**381**	**381**
I1	**A**	**200**	**200**	**199**	**199**	**199**	**199**	**200**
Torque	**Nm**	**700**	**700**	**642**	**587**	**514**	**410**	**358**
P-mechanical	**kW**	**59**	**88**	**101**	**103**	**105**	**105**	**105**
Frequenz	**Hz**	**40.7**	**60.7**	**76.0**	**85.0**	**98.5**	**124.1**	**141.7**
Schlupf	**%**	**1.64**	**1.09**	**1.09**	**1.12**	**1.16**	**1.22**	**1.26**
speed	**1/min**	**800.5**	**1200.7**	**1503.5**	**1680.9**	**1947.1**	**2452.1**	**2798.4**
power factor			**0.771**	**0.763**	**0.812**	**0.829**	**0.842**	**0.846**	**0.840**
Wirkungsgrad	**%**	**90.74**	**92.45**	**93.15**	**93.39**	**93.37**	**93.50**	**93.34**
Ges.Verluste	**kW**	**5.98**	**7.19**	**7.43**	**7.31**	**7.45**	**7.32**	**7.48**
R1 -150 Grd C	mOhm	23.608	23.608	23.608	23.608	23.608	23.608	23.608
R'2-150 Grd C	mOhm	13.608	13.610	13.615	13.618	13.625	13.639	13.652
L1 - sigma	mH	0.143	0.143	0.144	0.144	0.144	0.144	0.144
L'2- sigma	mH	0.314	0.314	0.318	0.319	0.319	0.319	0.319
L - sigma	mH	0.437	0.437	0.442	0.443	0.443	0.443	0.443
LDIFF	mH	0.000	0.000	0.000	0.000	0.000	0.000	0.000
LH	mH	4.592	4.575	4.815	4.845	4.860	4.867	4.868
RH	Ohm	56	76	87	94	103	117	126
R'2 - Stab	mOhm	11.34	11.34	11.35	11.35	11.36	11.37	11.39
R'2 - Ring	mOhm	2.27	2.27	2.27	2.27	2.27	2.27	2.27
L1 -sigma Lsp	mH	0.0147	0.0146	0.0154	0.0155	0.0155	0.0156	0.0156
L'2-sigma Lsp	mH	0.0779	0.0776	0.0816	0.0822	0.0824	0.0825	0.0825
L'2-sigma Nut	mH	0.0684	0.0684	0.0684	0.0684	0.0684	0.0683	0.0683
L'2-sigma Geo	mH	0.1682	0.1682	0.1682	0.1682	0.1682	0.1682	0.1682
R1 dom. OS	mOhm	349.249	297.562	285.251	345.324	251.545	374.352	323.069

R'2 dom. OS	mOhm	103.806	93.244	90.898	101.271	84.401	105.489	96.655	
L1-sig dom.OS	mH	0.133	0.133	0.133	0.133	0.133	0.133	0.133	
L'2-sig dom.OS	mH	0.202	0.203	0.204	0.204	0.204	0.204	0.204	
Reibung usw.	Nm	0.4	0.6	0.7	0.8	1.0	1.4	1.7	
E	V	208.3	312.4	336.0	334.3	331.5	324.8	319.0	
I-W	A	165.4	164.7	175.9	180.6	185.1	190.2	193.1	
I-B	A	-109.5	-110.5	-89.9	-79.5	-67.8	-52.6	-45.3	
cos-phi-i		0.834	0.831	0.890	0.915	0.939	0.964	0.974	
U-D	V	850.0	850.0	850.0	850.0	850.0	850.0	850.0	
I-D	A	75.5	111.3	126.9	129.3	131.2	133.0	132.6	
U-D / I-D	Ohm	11.3	7.6	6.7	6.6	6.5	6.4	6.4	
Spitzenstrom	A	318	336	336	328	337	322	327	
Vordrossel	mH	0.000	0.000	0.000	0.000	0.000	0.000	0.000	
M kipp / M	ca.	3.40	3.64	2.90	2.52	2.13	1.68	1.49	
Pulszahl		45	27	21	21	15	13	11	
Pulsfrequenz	Hz	1831.2	1638.8	1596.0	1785.0	1477.5	1613.5	1558.8	
Betriebsart		SupSin	SupSin	SupSin	SupSin	SupSin	13u1100	11u1100	

SIEMENS AG A&D LD T2 / BMASYN V 2.43 Name: Germishuizen 30/11/04

APPENDICE C – INDUCTION MACHINE DATA FROM SIEMENS

Programm	Datensatz	MLFB	ProjNr	Kennwort	Blatt
BMAPRIN2 0.18	R204	1TB1921-0JJ03	MD076	LRV Portland 98	1

Maschinendaten:

2P	N1	DA1	DI1	LFE	HN1	TN1	BN1	BCU1	HCU1
6.	54.	485.0	298.5	340.0	27.50	25.30	9.40	3.70	1.95
Y	ZNUE	ZNN	AZWEIG	ALEIT	THETA1	BLECH	KFE	ISOLSYS	WIKOPF
8.	10.	2.	3.	2.	130.0	330.00	1.000	1.50	0.00
N2	DELTAG	DI2	BZ2	HN2	HS2	BS2	BN2O	BN2U	DRUND
42.	1.50	90.0	10.50	25.50	3.00	2.00	0.00	0.00	2.00
THETA2	STABUE	KAPPAS	DARING	BRING	HRING	KAPPAR			
130.0	20.00	57.00	300.00	20.00	27.00	57.00			

ZLOCH1	DL1(1)	DLO1(1)	DL1(2)	DLO1(2)	DL1(3)	DLO1(3)	DM1	KFEJ1	KFEZ1
39.	25.0	450.	15.0	387.	0.0	0.	0.0	1.000	1.000
ZLOCH2	DL2(1)	DLO2(1)	DL2(2)	DLO2(2)	DL2(3)	DLO2(3)	DM2	KFE2	NSCH
12.	25.0	170.	0.0	0.	0.0	0.	0.0	1.000	0.00

Korrekturfaktoren fuer Erwaermungsrechnung

KWIKO	KDELTA	KRING	KKLOCH	KLAGERI	KLAGERA	KDRRING
1.000	1.000	1.000	1.000	1.000	1.000	1.000

Q-STAB = 203.37 mm2 Stdr.kaltwiderstand (20 Grd C) = 15.16 mOhm

Betriebspunkte								
U1	V	237.9	353.7	381.0	381.0	381.0	381.0	381.0
I1	A	200.1	200.3	199.5	199.2	198.8	198.8	199.7

Drehmoment	Nm	700	700	642	587	514	410	358	
P-mech	kW	59	88	101	103	105	105	105	
syn.Drehzahl	1/min	813.9	1213.9	1520.0	1700.0	1970.0	2482.4	2834.1	
Drehzahl	1/min	800.5	1200.7	1503.5	1680.9	1947.1	2452.1	2798.4	
U-D	V	850.0	850.0	850.0	850.0	850.0	850.0	850.0	
U1 - EFF	V	387.3	501.2	525.5	525.5	531.1	526.8	528.7	
I1 - EFF	A	201.0	202.0	201.3	200.7	201.0	201.2	202.1	
Magn.Strom	A	115.7	115.1	93.2	82.6	71.1	56.3	49.3	
Strombelag	A/cm	384.0	384.4	382.9	382.4	381.6	381.5	383.3	
Str.dichte Std	A/mm2	4.87	4.87	4.85	4.85	4.84	4.83	4.86	
Str.dichte Stb	A/mm2	3.08	3.07	3.28	3.37	3.45	3.55	3.60	
Str.dichte Rin	A/mm2	2.60	2.59	2.78	2.85	2.92	3.00	3.05	
Vcu 1	W	3224	3411	3403	3375	3423	3402	3456	
V-Fe 1 Zahn	W	304	481	487	447	412	349	324	
V-Fe 1 Joch	W	744	1218	1215	1131	1032	903	842	
Vcu 2	W	1319	1487	1632	1628	1780	1725	1787	
V-Fe 2 (Z.+J.)	W	41	49	40	29	30	14	12	
Gesamtverluste	W	5984	7191	7435	7310	7445	7317	7481	
Sinus-Verluste	W	4945	5656	5823	5791	5763	5818	5952	
B Grundwelle	T	0.746	0.750	0.644	0.574	0.493	0.388	0.336	
B Lsp. max.	T	0.732	0.735	0.642	0.573	0.493	0.387	0.336	
B Stdr. Joch	T	1.092	1.098	0.944	0.842	0.723	0.568	0.493	
B Lfr. Joch	T	0.648	0.651	0.560	0.499	0.429	0.337	0.292	
B Stdr. Zahn	T	1.571	1.578	1.377	1.230	1.057	0.830	0.721	
B Lfr. Zahn	T	1.562	1.568	1.368	1.222	1.050	0.825	0.717	

Kippmoment	Nm	2378	2550	1865	1477	1093	690	532
Stossmom. 3pKS	Nm	3851	4936	4035	3366	2634	1769	1399
Welligkeit	%	1.26	4.15	16.91	14.69	17.30	13.24	14.41
dom.Pendelfreq	Hz	1709	1457	3192	3570	2955	3724	3401
Std.Erwaermung	K	0	0	0	0	0	0	0
Lfr.Erwaermung	K	0	0	0	0	0	0	0
BSteg2 (magn.)	mm	2.001	2.001	2.001	2.001	2.001	2.001	2.001

SIEMENS AG A&D LD T2 / BMASYN V 2.43 Name: Germishuizen 30/11/04 12:15:25

Appendix D

Determining the offset position for the PM-assisted RSM and the RSM

This section describes how the offset position of the PM-assisted RSM and the RSM are determined.

Determining the offset position of the RSM

The zero position is defined as the position of the rotor where the *d*-axis of the rotor is aligned with the magnetic axis of phase *a*. This position is achieved by injecting DC stator currents in the coils shown in Fig. D1. The phase currents are injected as I_A = 0A, I_B = positive current and I_C = negative current. The magnetic flux lines and the rotor position are then aligned on the stator phase *a* coil as shown in the figure.

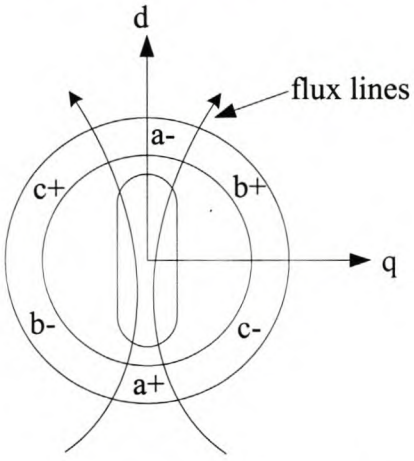

Figure D1. RSM flux-lines alignment with the injection of DC stator currents in the phases as

$$I_A = 0 \text{ A}, I_B = -I_C$$

The correct zero position means that when *iq* is zero and *id* is larger than zero, the system will not run when the position of the sensor is set at a correct position. This is due to the vector control principle, as with these current values, the machine will produce no torque. According to this principle, in the DSP control software *iq* is set to zero and *id* is set larger than zero. A low dc voltage is applied to the dc bus. The machine will run if the relative

position between the position sensor and the stator is not correct. If the machine is running, the rotor is manually clamped and the position sensor is adjusted till no torque is produced. Now, even under high DC bus voltage, there should be no rotation. This point is called a "zero point". After this, *iq* can be reset to its correct value and the system will run under vector control.

Determining the offset position of the PM-assisted RSM

The determination of the zero position for the PM-assisted RSM is rather less complex and more accurate as compared to that of the RSM. However, extra care must be taken to ensure that the magnet flux works against the main stator *q*-axis flux rather than with the stator *q*-axis flux. The correct offset position for the PM-assisted RSM is obtained by rotating the rotor of the machine by hand and observing the alignment of the rotor position and the induced voltage on the oscilloscope. The correct alignment of the rotor positionand the induced voltage is shown in Fig. D2.

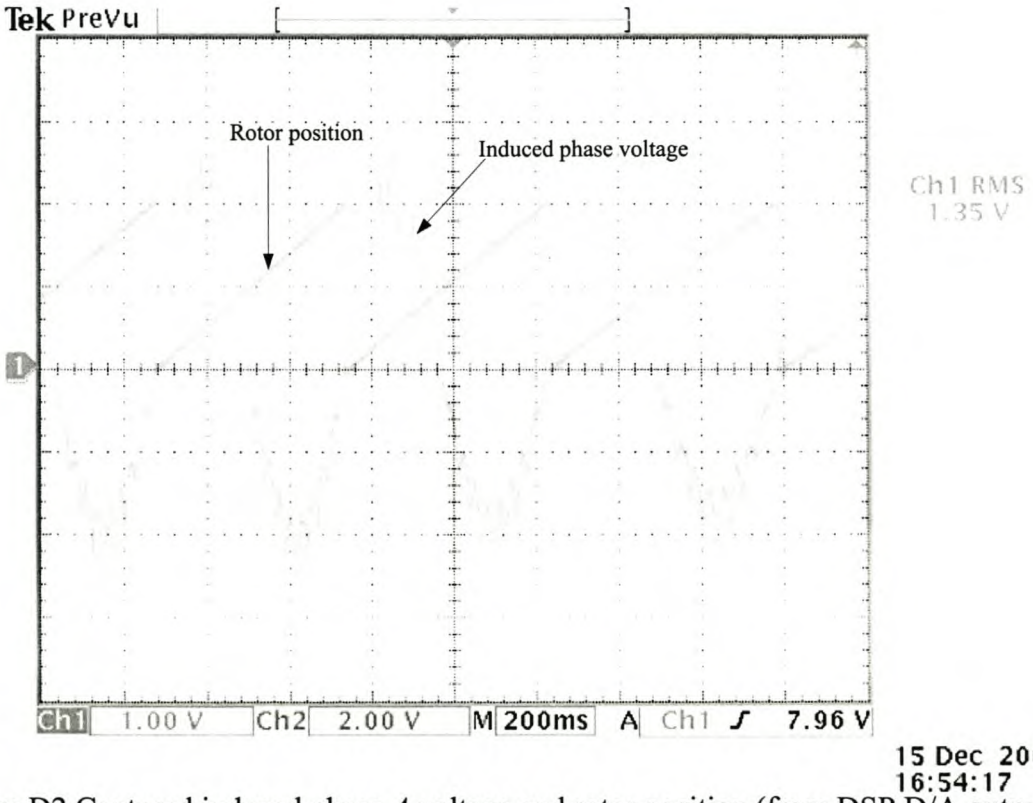

Figure D2 Captured induced phase *A* voltage and rotor position (from DSP D/A output port) to determine the zero position of the PM-assisted RSM

Appendix E

Photographs of the practical equipment

The photographs of the experimental equipments are presented in this section.

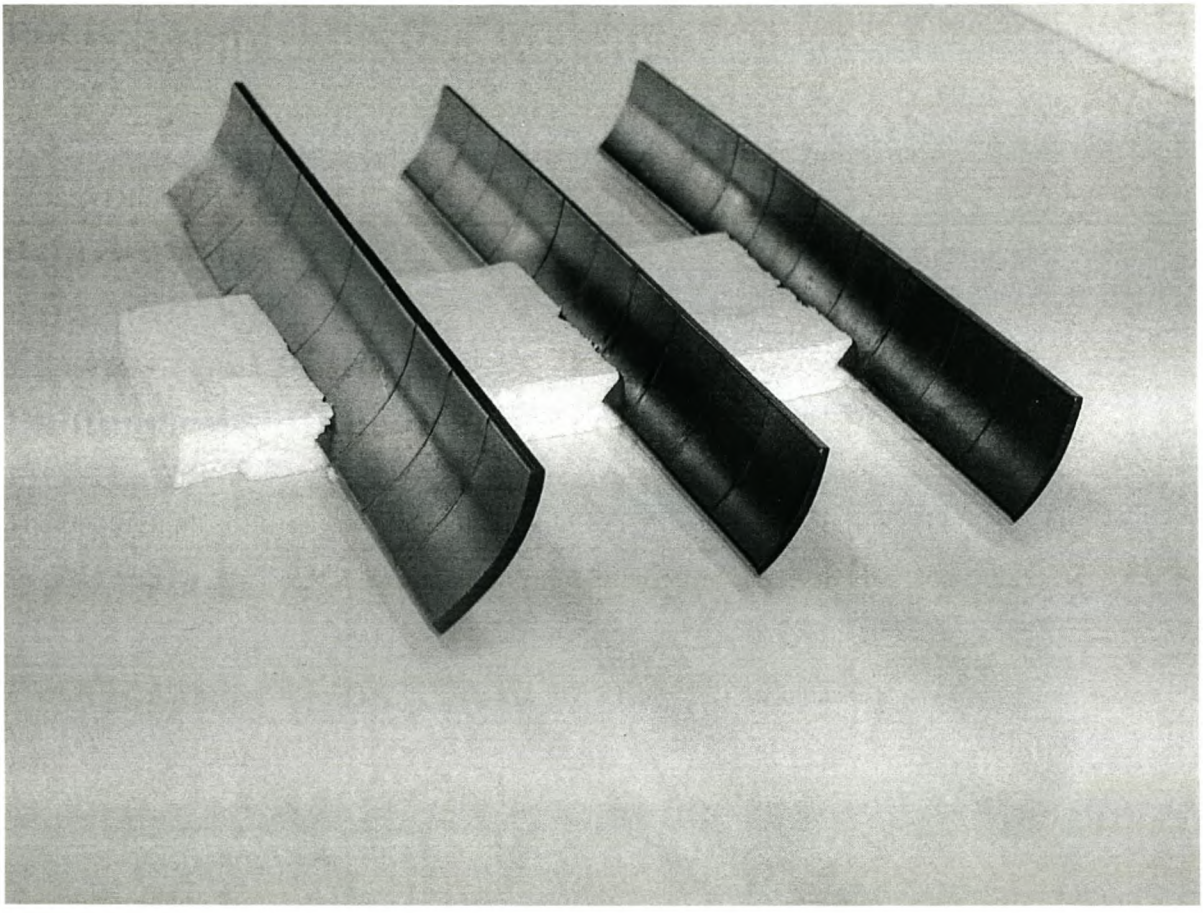

Figure E1. Permanent magnet sheets

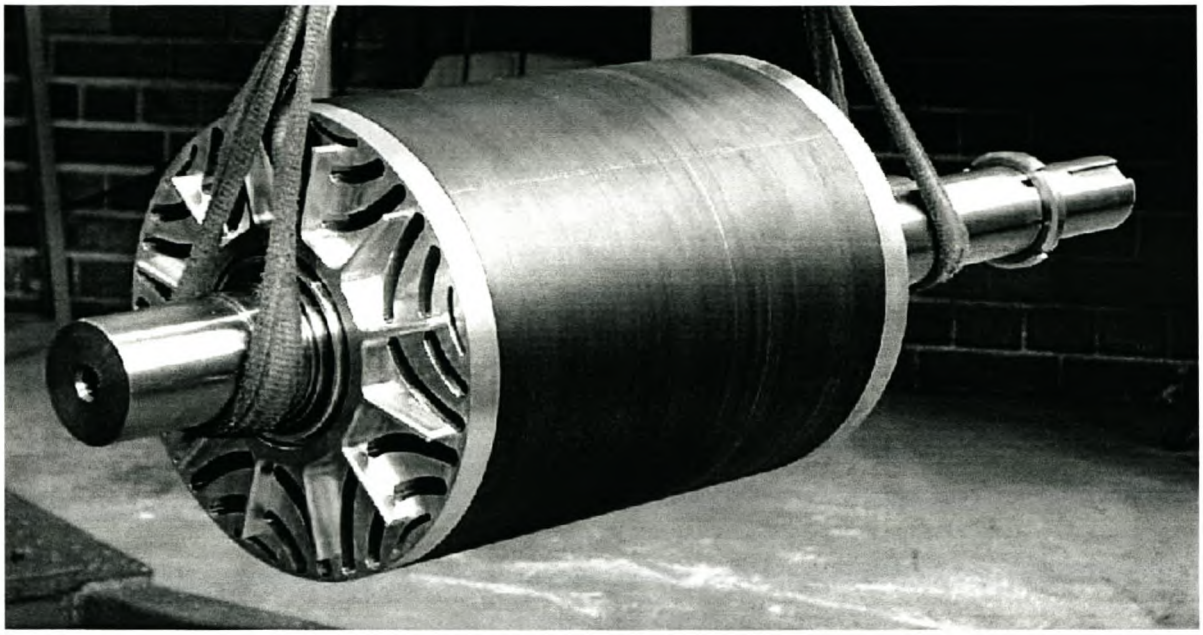

Figure E2. Assembled RSM rotor

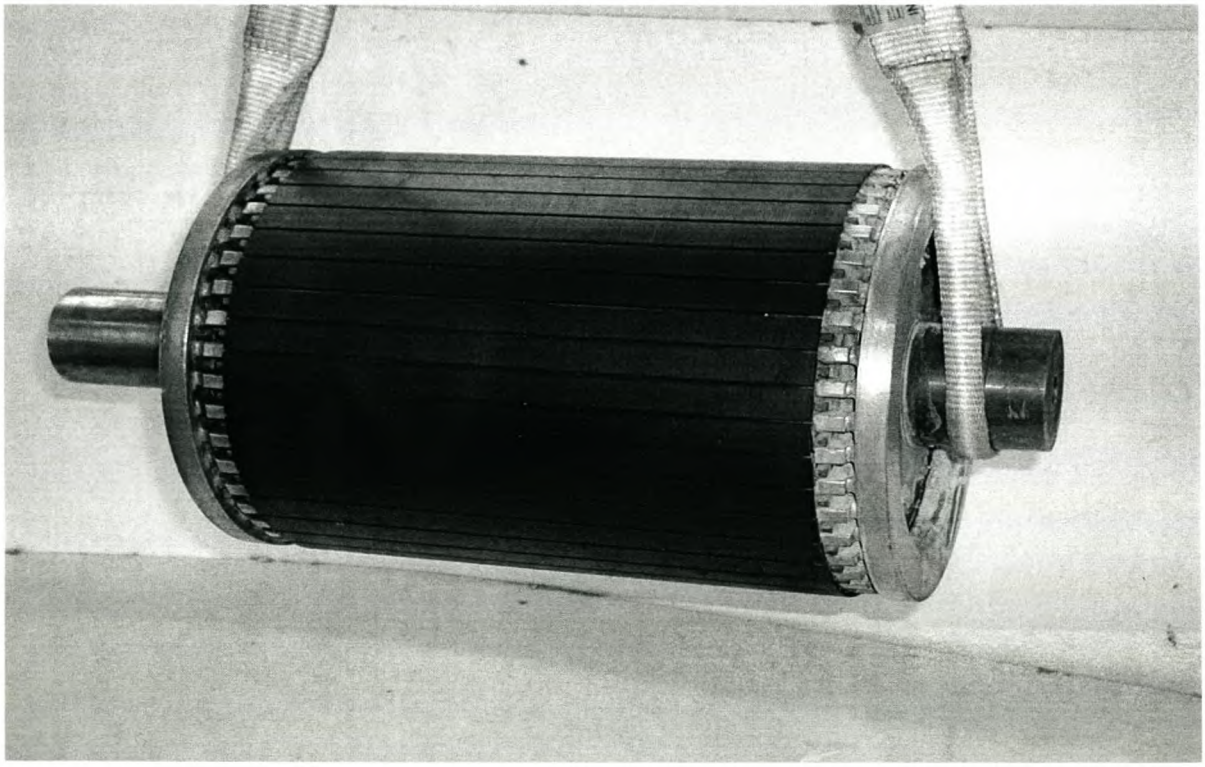

Figure E3. Assembled IM rotor

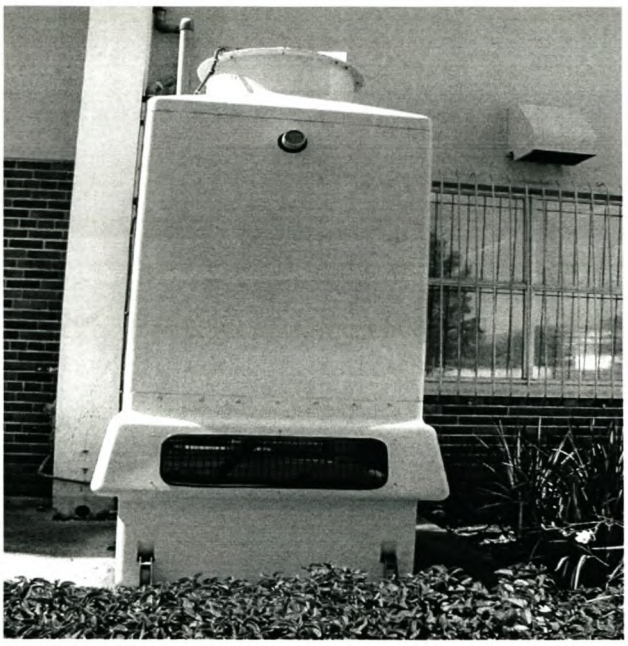

Figure E4. Cooling tower for cooling dynamometer outlet water

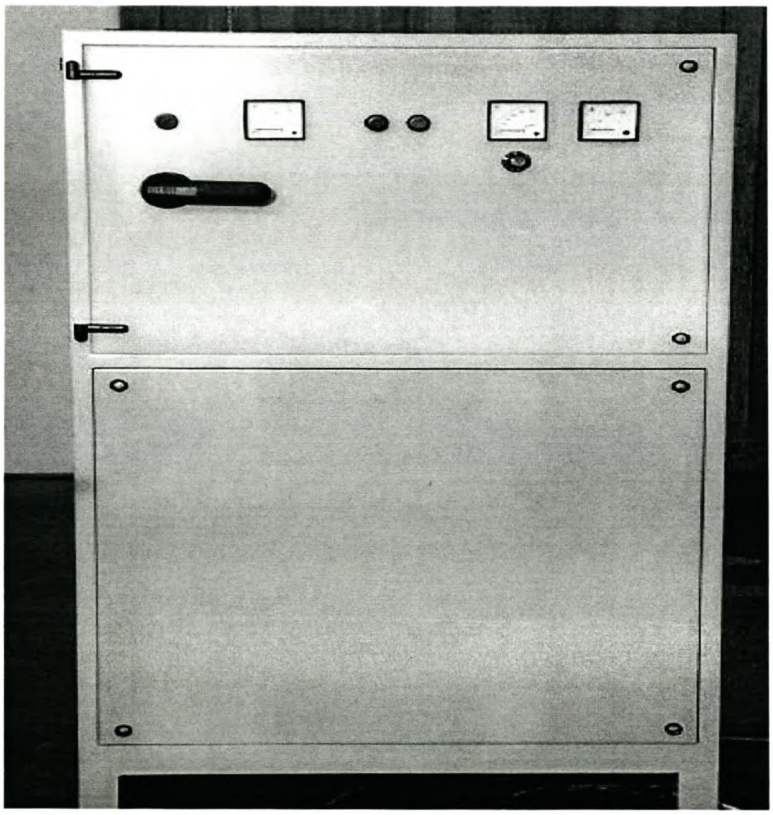

Figure E5. Rectifier

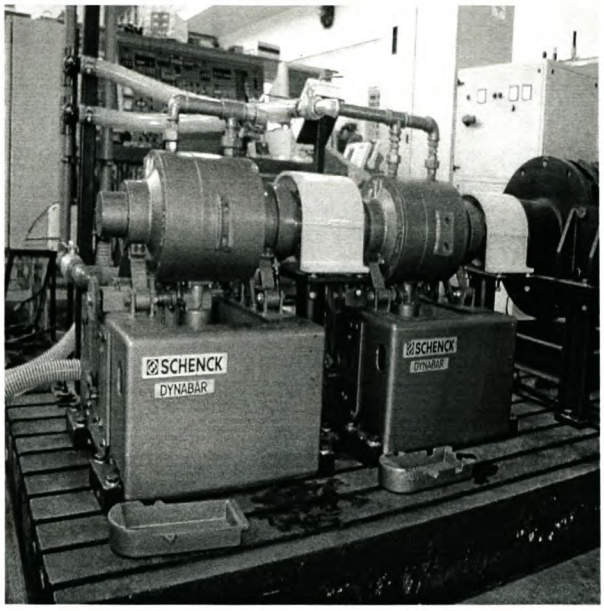

Figure E6: Schenk dynamometers coupled to the RSM

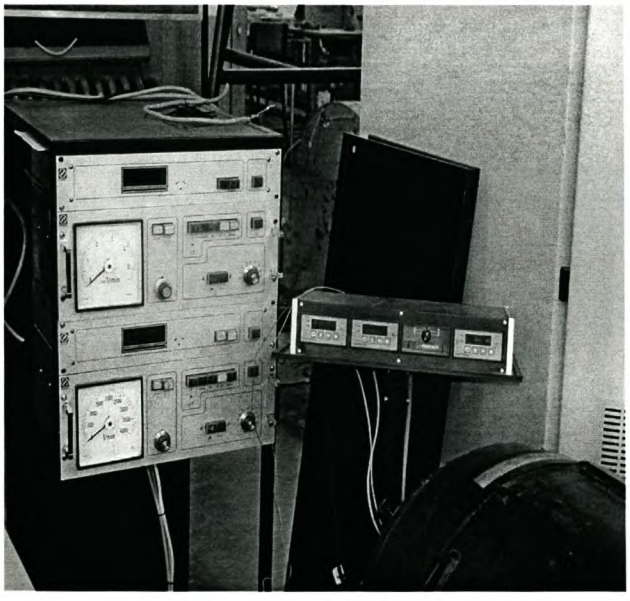

Figure E7. Dynamometer torque controllers (left) and speed and temperature displays (right)

Appendix F

Finite Element Solve.f algorithm

The finite element solve.f algorithim is used as a main program to calculate the performance parameters (torque, power factor, efficiency, e.t.c) of the machine during the design process. It contains sub-routines that it calls per iteration.

```
c 26 september 2003, Sguda
c-------------------------------------------------------------

      subroutine eesolv(xpar,ypar)

c ==================Varaible declaration=====================

c     Character
      character*25 bh_file,def_file,fname,ifile,ofile
      character*25 rl_file,rs_file,rs_type
      character*25 sl_file,ss_file,ss_type
      character*25 w_file

c     Double precision
      double precision T,T_out,Te,airg_l,alpha,angle,ar_slot,area_ar
      double precision area_rt,area_st,area_th,area_y,bp_air,bp_t
      double precision bp_y,c_angle,c_angle1,c_peak,cur_id,cur_id1
      double precision cur_iq,cur_iq1,den,d_slice,dtheta,current
      double precision e_d,e_q,e_rms,eff,f,fill_f,fl_a1,fl_a3,fl_b1
      double precision fl_b3,fl_c1,fl_c3,flux_pp,i_rms,fl_d,fl_q
      double precision i_s,i_s1,l_ce,l_d,l_end,l_q,length,mass_t
      double precision mass_y,num,omegas,gr,flinka(3),Ta,rot_ang
      double precision p_core,p_cu,p_fact,p_in,p_in2,p_out,p_wf,period
      double precision pi,qwn,relo,r_c,r_s
      double precision ro_od,ro_shfd,rr,rrad,sigma,sqrt2,srad
      double precision st_bw,st_gw,st_slh,stator_resis
      double precision st_id,st_od,st_shb,st_shs,st_sht,st_tw
      double precision st_yh,stack,step_angl,t_pitch,t_wid,temp
      double precision th_off,thao,theta_m,torq1,u0,v0,vm
      double precision v_d,v_q,v_s,vp,vs,w,pm_t,pm_w,v_0,weight,area_opt,area_pm

c     One dimensional double precision array
      double precision bcur(100),scoil(100),zp(100),ypar(12)
      double precision c_cur(14),xpar(10)
      double precision acoil(14),flink(3),fl(3),ro_bh(4)
      double precision ro_rw(4),ro_wh(4),ro_ww(4),ro_arc(4)
      double precision a(4000),ar(4000),grel(4000),rel(4000)
      double precision x(4000),y(4000),la(481),rthet(481),terms(481)
      double precision thetrot(481),thetstat(481),xbh(41),ybh(41)

      ! Two dimensional double precision array
      double precision ah(481,481),an(481,481),ap(481,481)
      double precision bh(481,481),bn(481,481),bp(481,481)
      double precision eqconst(40,4),gradcon(40,3)
      double precision se(3,3),sraz(481,481),ms(3,3)

c     Three dimensional double precision array
      double precision s(4000,3,3),pm_t1,pm_t2,pm_t3

c     Integer

      integer conv,i,ialpha,ithet_m,j,ks,n,n_ro_st,ikk
```

```
      integer n_st_rq,n_st_sp,n_st_st,nc_turns,ncoil
      integer nde,ne,nelm,neq,nfour,nlines,nnode,np,np_cir,nphase
      integer nppole,nprof,nraz,nrgn,nrs,ns,ns_pph,nsgn,nslots,nt
      integer nw_t,ro_nbp,testa,nsp,siemens

c     One dimensional integer array

      integer ic_typ(100),itype(4000),jdiag(4000),nd(4000)
      integer razind(481),razpnt(481),rgn(481),sgn(481)

c     Two dimensional integer array

      integer line(4000,2),neigh(4000,3),node(4000,3),nw_it(100,2)

      parameter (ns=3)
            common /int/ nsp
            common /const/ relo,gr
            common /rel/ eqconst,gradcon,xbh,ybh

c     direct and quadrature axis currents
      integer id,iq

c     permanent magnet strength
      double precision pm_strength

c ----------START of the routine----------

      open (23,file='results/performb.res')
      rewind 23
  132 format(F14.12)
  134 format(F14.12)
  151 format('1998/08/12 RSM Optimum Design')
  135 format(12F8.1)

c       constants not defined in FORTRAN

            pi   = 4.0d0*datan(1.0d0)
            sqrt2 = dsqrt(2.0d0)

      def_file = 'siemens.def'
      siemens  = 1

      call init(ss_type,rs_type,ro_nbp,airg_l,th_off,def_file,
     &   sl_file,w_file,rl_file,bh_file,ss_file,n_st_st,n_st_rq,
     &   rs_file,n_ro_st,st_od,length)

      if (ss_type.eq.'sso') then
        st_id  = 0.2983d0
        st_gw  = 0.0094d0
        st_sht = 0.0011d0
        st_tw  = 0.0120d0
        st_shs = 0.0011d0
        st_shb = 0.0253d0
        st_bw  = 0.0d0
      else if (ss_type.eq.'ssc') then
        st_id  = 0.21318d0
        st_gw  = 0.00570d0*st_id/0.309d0
        st_sht = 0.00064d0
        st_shs = 0.00100d0
        t_wid  = 0.00808d0
        st_yh  = 0.02991d0
        ! Calculate st_tw, st_bw and st_shb
        call slot(st_id,st_od,st_gw,st_sht,st_shs,n_st_st,t_wid,
     &     st_yh,st_tw,st_bw,st_shb)
      end if

      ro_od   = st_id-2.0d0*airg_l
      ro_shfd  = 0.09000d0
      ! These rotor parameters are fixed
      ro_ww(1) = 0.00150d0
```

```
      ro_ww(2) = 0.00100d0
      ro_ww(3) = 0.00075d0
      ro_ww(4) = 0.00075d0
      ro_rw(1) = 0.00150d0
      ro_rw(2) = 0.00125d0
      ro_rw(3) = 0.00125d0
      ro_rw(4) = 0.00100d0

      pm_w = 0.0005d0 ! current sheet width

c     These parameters are to be optimised
      ro_wh(1) = 0.00536d0
      ro_wh(2) = 0.00521d0
      ro_wh(3) = 0.00297d0
      ro_wh(4) = 0.00050d0
      ro_bh(1) = 0.57260d0*ro_od/2.0d0
      ro_bh(2) = 0.78650d0*ro_od/2.0d0
      ro_bh(3) = 0.92710d0*ro_od/2.0d0
      ro_bh(4) = 0.97070d0*ro_od/2.0d0
      ro_arc(1)= ro_wh(1)
      ro_arc(2)= ro_wh(2)
      ro_arc(3)= ro_wh(3)
      ro_arc(4)= ro_wh(4)

            pm_t1 = xpar(1)
            pm_t2 = xpar(2)
            pm_t3 = xpar(3)


c     pm_t = 0.0035d0 ! PM thickness

      !-------------------------------------------------------------
      ! The critical dimensions of the slots are now saved in the
      ! following files in the optim/menu/DATA directory:
      ! (i)  rotor slot  : <filename.dat>
      ! (ii) stator slot : <filename.dat>
      ! The data in this file are read by subroutine ee_pol.f.
      ! Therefore if the format is changed, it must be changed in
      ! in ee_pol.f as well.

      call save_rslot(rs_file,rs_type,ro_od,ro_shfd,ro_ww,ro_wh,
     &   ro_bh,ro_rw,ro_arc,ro_nbp,n_ro_st,pm_t1,pm_t2,pm_t3,pm_w)
      call save_sslot(ss_file,ss_type,st_od,st_id,st_gw,
     &   st_sht,st_tw,st_shs,st_shb,st_bw,n_st_st,t_wid,st_yh)

      ! With the dimensions of the slots saved only one pole is
      ! generated to optimum design the reluctance machine. The
      ! points that define the machine in the xy-plane is
      ! calculated by the subrourtine ee_as. The input of this
      ! subroutine is the .def definition file that contains
      ! the names of the slots and winding information to
      ! generate the pole. The output, .pol, is used as input
      ! for the subroutine ee_pmesh that generates the mesh.
      !
      ! ee_as:
      ! INPUT: <siemens.def>       OUTPUT: <mesh.pol>
      !
      ! ee_pmesh:
      ! INPUT: <mesh.pol>          OUTPUT: <mesh.fpl>
      !
      ! The .def and the .fpl files are in optim/menu/DATA and
      ! the .pol file is in optim/menu/temp.

      ofile  = 'mesh.pol'
      ifile  = 'mesh.fpl'

      !-------------------------------------------------------------
      ! The important files for the solver are now defined.
      ! (i)  fname    : file that contain the mesh information
      ! (ii) def_file : names of slot and winding files
```

```
! (iii) sl_file  : file with stator slot info
! (iv)  rs_file  : file with rotor slot info
! (v)   bh_file  : B-H charateristic for lamination
! (vi)  w_file   : winding info file

      fname   = 'mesh.fpl'

! While the solve.f subroutine is still tested the
! subroutines need not to be executed.

call ee_as(def_file,ofile)
call ee_pmesh(ofile,ifile,nelm,nnode)
call ee_pre(def_file,nprof)

! Other parameters:
! (i)   stack  : stack factor (laminations)
! (ii)  f      : frequency [Hz]
! (iv)  temp   : temperature (operating temp)
! (v)   fill_f : fill factor (stator slot)
! (vi)  w      : active core length
! (vii) p_cu   : copper losses
! (viii) p_wf  : wind and friction losses
! (ix)  l_ce   : lenght of the end windings
! (xi)  period : time of one cycle
! (xii) omegas : sinchronous speed [rad/sec]

stack  = 0.97d0
f      = 145.0d0
       period  = 1.0d0/f
temp   = 130.0d0
fill_f = 0.5d0
w      = length*stack
p_wf   = 5000.0d0
p_cu   = 7500.0d0
l_ce   = 0.185d0
omegas = f*pi*2.0d0

! omegas is the synchronous speed of the rotating magnetic
! in rad/s.  To convert it to rpm it must be multiplied by 60
! and divide by 2pi, because one revolution is 2pi radians.
! The speed of the rotor is then the above value times 2/p,
! where p is the number of poles.

! Now read the mesh and winding information.
! (i) fname  : the <filename.fpl> file in optim/menu
! (ii) w_file : the <filename.dat> in optim/menu/DATA

call sreadmesh(fname,nde,nelm,nnode,x,y,node,itype,testa,
&   nlines,line,neigh)
call read_sw(w_file,n_st_sp,nw_it,nw_t)

! Load turns-info. First the stator.
! (i) nc_turns : number of turns of each coil
nc_turns = nw_t

! Now read the following information:
! (i)   np     : number of poles
! (ii)  nppole  : number of pole pairs
! (iii) nslots  : number of stator slots per pole
! (iv)  ns_pph  : number of stator slots per pole phase
! (v)   qwn     : windingfactor
! (vi)  n_st_sp : number of stator slots per pole
! (viii) n_st_rq : number of slots to be meshed

np    = n_st_st/n_st_sp
nppole = np/2
nslots = n_st_sp
ns_pph = n_st_sp/3
qwn   = 0.925d0
```

```
! Curve fitting for stator lamination BH-data. The data for
! the curve is read from the stator info file. The firts
! line in the file is the filename, <filename.bh>

      call acs_spline(bh_file)

!-------------------program main body----------------------
! DATA read in from mesh & prepro
! The following files are now read from the optim/menu/temp
! directory:
! (i)  age.ren
! (ii)  age.age
! (iii) age.res
! (iv)  age.rtm

call age_ren(neq,nprof,nd,jdiag,ar,nnode,nelm)
call age_age(rrad,srad,rr,nrs,nt,nraz,rthet,razind)

do i = 1,nraz
  razpnt(i) = nd(razind(i))
end do

! include calculation at point (nt+1)
! remember this will change with a new mesh. So far correct

razind(nt+1) = razind(nt)+1
rthet(nt+1)  = pi - 2*pi/np

! razpnt() now contains the variable numbers of the razek
! element i.e. that associated with nd(var)

call age_res(sraz,nt)
call age_rtm(nfour,nt,thao,terms,la,ah,ap,bh,bp,an,bn)

! The value u is the permeability of a meduim. u0 is the
! absolute permeability [H/m] of a meduim.  The reluctance
! of a material is defined as:
!         R = lenght/(u*area of cross section)
! The reluctivity is defined as 1/u.  The value v0 is the
! absolute reluctivity of air.

u0   = 4.0d0*pi*1.0d-7
v0   = 1.0d0/u0
       sigma = 44.573d6
vp   = 78.0d0
vs   = 78.0d0
! for NdFeB N35H (Br=1.18T, Hcb=880kA/m, density=7.45g/cm^3)
! withhold temperature to 120 degC, mu=1.06706
vm=1.0d0/(1.1616d0*u0)


! Circuit numbering convention
! 1.  phase a       1
! 2.  phase b       2
! 3.  phase c       3

! The detail information on how the actual winding looks is
! not given here.  The stator windings are considered as
! three coils only.

! ncoil  : number of coils - 3 phases which imply 3 coils
! scoil  : surface area of a coil per pole
! acoil  : surface area of a single coil
! ic_typ : the type of a winding - there are  three  phases

      ic_typ(1) = 1
      ic_typ(2) = 2
ic_typ(3) = 3
ic_typ(4) = 4
ic_typ(5) = 5
```

```
      ic_typ(6) = 6

      ncoil    = 6

      call area(ncoil,scoil,nelm,rel,grel,itype,vs,ar,vp,ic_typ,
     &   v0,vm,area_st,area_ar,area_rt,area_pm,acoil,ns_pph,st_id,
     &   ro_od,np,st_od)

      call airgapnode(rgn,sgn,nrgn,nsgn,rrad,srad,x,y,nnode,
     &   thetstat,thetrot)

      ! stiffness term for elements
      do ne=1,nelm
       call dos(nelm,nnode,x,y,node,ne,ar,se)
            do i=1,3
             do j=1,3
              s(ne,i,j) = se(i,j)
             end do
            end do
           end do

      ! l_end  : calculate the endwinding L (Dr. Kamper)
      ! r_s    : stator winding resistance
      ! np_cir : number of parallel circuits per winding
      ! nphase : number of series turns per phase (double layer)

      np_cir = 3
      nphase = 2*nc_turns*ns_pph*nppole/np_cir
      l_end  = 57.83d0*st_id*(dble(nphase)**2)*1.0d-8
      r_s    = stator_resis(fill_f,scoil(1),temp,nphase,
     &   np_cir,ns_pph,nppole,w/stack,l_ce)

      call test(def_file,ss_type,rs_type,sl_file,w_file,
     &   rl_file,bh_file,ss_file,rs_file,ofile,ifile,fname,airg_l,
     &   th_off,st_od,length,ro_nbp,n_st_st,n_st_rq,n_ro_st,nelm,
     &   nnode,nprof,n_st_sp,nw_t,np,nppole,nslots,ns_pph,np_cir)

      !  PROGRAM: Calculate flux linkages with skew.
      !
      ! Calculate flux linkages without skew
      ! alpha     : current angle (radians) in dq reference frame
      ! theta_m   : rotor position in mechanical radians
      ! th_off    : offset rotor angle (radians)
      ! ks        : number of slice(s) over slot pitch
      ! d_slice   : displacement between slices
      ! T         : calculated torque from subroutine torque
      ! step_angl : if the machine is rotated
      ! dtheta    : absolute rotor position in radians


      pm_strength = 4.350d0   ! 0.0d0
      v_0 = 550.0d0
      weight = 40.0d0
      ks = 1.0d0
           ka = 1.0d0
      d_slice = 2.0d0*pi/dble(n_st_st)/dble(ks)

      do id = 1,1

!       cur_id = dble(id) + 0.0000000001d0

*       make current angle vary for Torque vs current angle plot

        do ialpha = 79,79
         c_peak = sqrt2*101.0d0/dble(np_cir)

c          alpha  = 78.9999644d0*pi/180.0d0
          alpha  = dble(ialpha)*pi/180.0d0 +0.1d0*pi/180.0d0
!         print*,alpha*180/pi
```

```
!       do iq = 240,240
!         cur_iq = dble(iq) + 0.0000000001d0
!               print *, cur_iq
!          c_peak = sqrt(cur_id**2+cur_iq**2)/dble(np_cir)
!         alpha = datan(dble(cur_iq)/dble(cur_id))

!    Initialisations of torque and flux linkages

              Ta = 0.0d0
              Ttot = 0.0d0
              fl_d = 0.0d0
              fl_q = 0.0d0

              do i=1,3
                flinka(i)=0.0d0
              end do


        rot_ang = 35.0d0*pi/180.0d0 ! rotor offset angle

*       step_angl = 0.667d0
        do ithet_m = 1,ka

!         theta_m  = dble(ithet_m)*pi/180.0d0
                        if(ka.eq.5) then
                                theta_m=dble(ithet_m-ka+2)*d_slice+rot_ang
                                else if (ka.eq.1) then
                                 theta_m=rot_ang
                                end if


*         Calculate the currents in the abc reference frame.

          c_cur(1) = c_peak*dsin(nppole*theta_m+alpha)
          c_cur(2) = c_peak*dsin(nppole*theta_m+alpha-2*pi/3)
          c_cur(3) = c_peak*dsin(nppole*theta_m+alpha+2*pi/3)


*         define magnet current sheet values: nI=Hc*(r2-r1), where r2-r1
*         is the thickness of PM in magnetization direction; for bonded magnet
*         DGPM-6 Hcb=440kA/m Br=550mT Mur=0.9947184d0

          c_cur(4) = pm_strength*1.0d5*pm_t1/dble(nc_turns)
          c_cur(5) = pm_strength*1.0d5*pm_t2/dble(nc_turns)
          c_cur(6) = pm_strength*1.0d5*pm_t3/dble(nc_turns)

          angle = theta_m*nppole
          call park(c_cur(1),c_cur(2),c_cur(3),angle,cur_iq,cur_id)
          cur_id = cur_id*dble(np_cir)
          cur_iq = cur_iq*dble(np_cir)
                print *,cur_iq,cur_id

!                       stop

*         Initialise torque,T, and total flux linkage of each phase

          T_out = 0.0d0
          do i=1,3
           flink(i) = 0.0d0
          end do

*         Accounting for skew

          do i=1,ks
           if (ks.eq.1) then
             dtheta  = theta_m+th_off
           else if (ks.eq.5) then
             dtheta  = dble(i-ks+2)*d_slice+theta_m+th_off
           end if
```

```
      call step(dtheta,sraz,nfour,terms,an,bn,nrs,nt,
     &     ah,ap,bh,bp,la,thao)

*     a is magnetic vector potensial - p94

 10    call nonlinear(neq,nelm,nnode,nprof,nraz,v0,ar,nd,
     &     node,razpnt,itype,jdiag,s,sraz,rel,c_cur,a,x,y,
     &     razind,nppole,acoil,nc_turns,w,ms,np,ns,zp,nlines,
     &     line,neigh,bcur,conv)


*     Recall nonlinear if solution did not converge

      if (conv.eq.0) then
       goto 10
      end if

      call torque(rrad,srad,torq1,1,nppole,nrs,nraz,w,
     &     a,an,bn,razind)
      T_out = T_out + torq1

*     call airgap_flux(st_id,nrs,nt,razind,rthet,a,bgap)

      do n=1,3
       call flux_linkage(fl(n),n,itype,node,a,ar,acoil,
     &     nelm,nppole,w,np_cir,nc_turns)
      end do

      do n=1,3
       flink(n) = fl(n) + flink(n)
                end do

     end do


*     End of Ks

     Ta  = T_out/dble(ks)+Ta

          print *,"TA", Ta

     do i=1,3
      flinka(i) = flink(i)/dble(ks)+flinka(i)
     end do

                ! END of ithet_m  (Ka)
          end do

                ! Get the average values
                Ta = Ta/dble(ka)

                do ikk=1,3
                flink(ikk)=flinka(ikk)/dble(ka) ! /dble(np_cir)
                end do


*     Co-phasal 3rd harmonic flux linkages can be obtained
*     from the actual three phase flux linkages p. 15
*     phase a : 1 / phase b : 2 / phase c : 3



     fl_a3 = (flink(1)+flink(2)+flink(3))/3.0d0
     fl_b3 = (flink(1)+flink(2)+flink(3))/3.0d0
     fl_c3 = (flink(1)+flink(2)+flink(3))/3.0d0


*     Calculate the fundamental flux linkages

     fl_a1 = flink(1)-fl_a3
```

```
      fl_b1 = flink(2)-fl_b3
      fl_c1 = flink(3)-fl_c3


*     calculate the dq axis flux

      angle = rot_ang*nppole !theta_m*nppole


            print *,"angle",angle
      call park(fl_a1,fl_b1,fl_c1,angle,fl_q,fl_d)


*     Calculate the speed voltages using dq-axis flux linkage

      e_d = -fl_q*omegas
      e_q = fl_d*omegas
      e_rms = dsqrt(e_d**2.0d0 + e_q**2.0d0)/sqrt2

            print *,"RMS", e_rms

*     Calculate the dq-axis inductance, including the
*     stator slot leakage inductance

      l_d = fl_d/(cur_id)
      l_q = fl_q/(cur_iq)
      Te  = 3.0d0*dble(nppole)*(l_d-l_q)*cur_id*cur_iq/2.0d0
            print*," Torque = ",Te,T_out



*     Calculate the flux per pole
      flux_pp = e_rms/(4.44d0*f*nphase*qwn)

*     Calculate the flux density in the airgap

      bp_air = flux_pp*dble(np)/(2.0d0*st_id*w)

      if (ss_type.eq.'sso') then
       st_slh   = st_sht+st_shs+st_shb
       ar_slot  = st_sht*st_gw+st_shs*st_tw+st_shb*st_gw
       area_th  = pi/4.0d0*((st_id+2.0d0*st_slh)**2.0d0-
     &    st_id**2.0d0)-n_st_st*ar_slot
       area_y   = pi/4.0d0*(st_od**2.0d0-(st_id+2.0d0*
     &    st_slh)**2.0d0)
       if (siemens.eq.1) then
        area_y = area_y - 39.0d0*(0.025d0**2.0d0+
     &      0.015d0**2.0d0)/4.0d0
       end if
       mass_y   = 7880.0d0*w*area_y
       mass_t   = 7880.0d0*w*area_th
      else if (ss_type.eq.'ssc') then
       st_slh   = st_sht+st_shs+st_shb+st_bw/2.0d0
       ar_slot  = 0.5d0*(st_gw+st_tw)*st_shs + st_gw*st_sht +
     &    0.5d0*(st_tw+st_bw)*st_shb + pi*st_bw**2.0d0/8.0d0
       area_th  = pi/4.0d0*((st_id+2.0d0*st_slh)**2.0d0-
     &    st_id**2.0d0)-n_st_st*ar_slot
       area_y   = pi/4.0d0*(st_od**2.0d0-(st_id+2.0d0*
     &    st_slh)**2.0d0)
       mass_y   = 7880.0d0*w*area_y
       mass_t   = 7880.0d0*w*area_th
      end if

*     Calculate the maximum flux density in the teeth and yoke
      t_pitch  = pi*st_id/dble(n_st_st)
      if (siemens.eq.1) then
       st_yh = 0.036d0
       t_wid = st_gw
      end if
      bp_t     = bp_air*t_pitch/t_wid
```

```
      bp_y    = flux_pp/(2d0*st_yh*w)

*     Calculate the core loss
      num   = (bp_t**2.0d0)*mass_t+(bp_y**2.0d0)*mass_y
      p_core = 0.0337d0*(f**1.32d0)*num

*     Core loss resistance and supply current, id1 and iq1
      r_c    = 3d0*e_rms**2d0/p_core
      cur_id1 = cur_id + e_d/r_c
      cur_iq1 = cur_iq + e_q/r_c
            alpha = datan(dble(cur_iq1)/dble(cur_id1))

*     Calculate the copper loss

      i_rms = dsqrt(cur_id1**2.0d0+cur_iq1**2.0d0)/sqrt2
      p_cu  = 3.0d0*(i_rms**2.0d0)*r_s

*     Calculate the effiency in terms of losses

      p_out = omegas*Ta/nppole - p_wf
      p_in  = p_out + p_core + p_cu + p_wf

!     print *, "P_in=", p_in, " p_out=",p_out

      !eff  = p_out/p_in

*     Calculate the terminal voltage

      v_d    = e_d - omegas*cur_iq1*l_end + r_s*cur_id1
      v_q    = e_q + omegas*cur_id1*l_end + r_s*cur_iq1

            print *,e_d,e_q,omegas,cur_id1,cur_iq1,r_s


      v_s    = dsqrt(v_d**2.0d0+v_q**2.0d0)/sqrt2


      num    = dabs(v_d/v_q)
      den    = cur_id1/(cur_iq1+1.0d-12)
      p_fact = dcos(datan(num)+datan(den))

      c_angle1 = datan(cur_iq1/(cur_id1+1.0d-12))
      c_angle  = datan(cur_iq/(cur_id+1.0d-12))
      i_s1 = dsqrt(cur_id1**2d0+cur_iq1**2d0)/sqrt2
      i_s  = dsqrt(cur_id**2d0+cur_iq**2d0)/sqrt2

      call save_parameters(e_d,e_q,e_rms,l_d,l_q,Te,flux_pp,
     &     bp_air,ar_slot,area_th,area_y,mass_y,mass_t,t_pitch,
     &     bp_t,bp_y,p_core,i_rms,p_cu,p_out,p_in,eff,r_c,
     &     cur_id1,cur_iq1,v_d,v_q,v_s,p_fact,i_s1,i_s,nphase,
     &     qwn,f,w,r_s,c_angle,c_angle1)

*     Write results to file: /optim/menu/results/performb.res

      area_pm = 0.0d0
      area_opt = 0.0d0
      do i=1,nelm
       if (abs(itype(i)).eq.12) then
         rel(i)  = vm
         area_pm = area_pm + ar(i)
       end if
            end do


      area_opt=1.0d0/(area_pm)-weight*(Ta-362.0d0)**2-
     &     weight*(v_s-550.0d0)**2


    print*,'Resutls =',Ta,alpha*180.0d0/pi,v_s,i_s1,p_fact
      ypar(1) = fl_d
```

```
      ypar(2) = fl_q
      ypar(3) = cur_iq
      ypar(4) = cur_id
      ypar(5) = area_opt
      ypar(6) = eff
      ypar(7) = ithet_m
      ypar(8) = e_q
      ypar(9) = v_d
      ypar(10)= v_q
      ypar(11)= fl_q
      ypar(12)= fl_d

      write(23,131) ypar(1),ypar(2),ypar(3),ypar(4),ypar(5),
     &     ypar(6),ypar(7),ypar(8),ypar(9),ypar(10),ypar(11),
     &     ypar(12)
  131 format(12F9.3)
```

Appendix G

Finite Element Obtimb.f algorithm

This is an optimization sub-routine that is called by the main algorithm (solve.f) during finite element optimization.

```
! ndim  - number of dimensions
      ! xk(i)   - i-th value of xk in the equation [X]=[P]+xk*[XI]
      ! idiv    - xk range, from xk(1) to xk(idiv)
      ! ik       - number where xk value start in above equation
      ! dim(i,j)- boundary values (i=1 lower; i=2 upper) of each
      !                                                  dimension j
      ! kdir    - k-th direction
      ! xi(j,kdir) - direction value of dimen. j in direction kdir
      ! fk(i)   - function value for xk(i)
      ! po(i)   - starting point of dimension i

      program eeoptmb

      ! variable declarations

      double precision tol
      parameter(ndim=3,tol=5.0d-5)

      ! integer m,time
      double precision xpar(3),ypar(12),xk(30),fk(3)
      double precision pvar(10),po(10),xi(ndim,ndim),pe(10)
      double precision xn,fn,fo,fe,fmp,del,dim(2,ndim)
      double precision avdir(ndim),a,b,p_old(10)

      character*1 esc,bot*20,cls*20,mes*20
      esc = CHAR(27)
      bot = esc//'[23;01H'//esc//'[2K'//esc//'[23;01H'
      cls = esc//'[2J'
      mes = esc//'[19;46H'//esc//'[2K'//esc//'[19;46H'

      print *,cls

      ! ---------------------------------------------------------------
      ! start program                                                 |
      ! ---------------------------------------------------------------

      open (22,file="results/perform.res", form='formatted')
      rewind 22
      write(22,100)
  100 format(' ')
  131 format(d20.9,5F10.6)
  133 format('Optimum',2I3,d20.9,5F10.6)

      ! initialise

      idiv=40.0d0
      nsol=0


      dim(1,1) = 0.0005d0
      dim(2,1) = 0.005d0
      po(1) = 0.00455d0 !dim(1,1) + (dim(2,1) - dim(1,1))/2.0d0
      dim(1,2) = 0.0005d0
      dim(2,2) = 0.005d0
      po(2) =  0.00307d0! dim(1,2) + (dim(2,2) - dim(1,2))/2.0d0
      dim(1,3) = 0.0005d0
      dim(2,3) = 0.003d0
```

```
      po(3) = 0.00363d0 !0.003068505d0!dim(1,3) + (dim(2,3) - dim(1,3))/2.0d0

      do j=1,ndim
        pvar(j)=po(j)
        xpar(j)=po(j)
      end do

      print *, 'here...',xpar(1),xpar(2),xpar(3),ypar(4)



      ! initial directions
      do i=1,ndim
        do j=1,ndim
          xi(i,j)=0.0d0
        end do
        xi(i,i)=1.0d0
      end do

      ! start optimisation
      write(22,151)
  151 format('Start Optimisation: AFPM Machine ...')

      nsol=nsol+1

      call eesolv(xpar,ypar)
        stop


      write(22,131) ypar(4),xpar(1),xpar(2),xpar(3),
     &  xpar(4),xpar(5)

      fn=ypar(4)

      ! start with iterations
      ! ---------------------

      lfinish=1
      nnn=1
      iter=0
    7 if (lfinish.eq.1) then
        write(22,100)
        iter=iter+1
        fo=fn
        ibig=0
        del=0.0d0
        print *,' '

        ! start with each direction
        ! -------------------------
        do kdir=nnn,ndim
          fmp=fn
          call maximum(nsol,idiv,kdir,ndim,dim,fn,pvar,xi)

          !   test for largest decrease (del is always <= to zero)
          if (fmp-fn.lt.del) then
            del=fmp-fn
            ibig=kdir
          end if

          write(22,133) iter,kdir,fn,pvar(1),pvar(2),pvar(3),
     &      pvar(4),pvar(5)
          write(22,100)

          print *,' '
        end do
        ! end of kdir
        ! -----------
        nnn=1

        ! test for convergence
```

```
      if (2.0d0*abs(fo-fn).le.tol*(abs(fo)+abs(fn))) then
        lfinish=0
        print *,'finished: iterations =, solutions =',iter,nsol
        go to 7
      end if

      ! get pe and calculate fe
      do j=1,ndim
        pe(j)=2.0d0*pvar(j)-po(j)
        xpar(j)=pe(j)
        avdir(j)=pvar(j)-po(j)
        p_old(j)=po(j)
        po(j)=pvar(j)
      end do

      !      print *,'Calculate fe'
      nsol=nsol+1
      call eesolv(xpar,ypar)
      write(22,131) ypar(4),xpar(1),xpar(2),xpar(3),
     &   xpar(4),xpar(5)
      fe=ypar(4)

      write(22,141) ibig,del,fo,fn,fe
141   format('ibig,del,fo,fn,fe =',I3,F10.5,3d20.9)
      write(22,100)

      a=2.0d0*(fo-2.0d0*fn+fe)*(fo-fn-del)**2
      b=del*(fo-fe)**2


      ! first test
      ! --->
      !go to 7
      if (fe.le.fo) go to 7

      ! second test
      if (a.le.b) go to 7

      ! move to maximum in new direction
      xk(1)=0.0d0
      xk(2)=1.0d0
      xk(3)=2.0d0
      fk(1)=fo
      fk(2)=fn
      fk(3)=fe
      ik=1
      fmp=fn
      call newton(ik,xk,fk,xn,fn)
      do j=1,ndim
        pvar(j)=p_old(j)+xn*avdir(j)
        po(j)=pvar(j)
        xpar(j)=pvar(j)
      end do

      ! Newton is only estimation of fn: make thus sure of fn.
      ! (but this step is not strictly necessary)
      !      print *,'Optimum new direction: run number',nsol
      nsol=nsol+1
      call eesolv(xpar,ypar)
      fn=ypar(4)

      ! check if valid: if not, retain old fn and pvar.
      if (fn.lt.fmp) then
        if (fe.gt.fn) then
          do j=1,ndim
            pvar(j)=p_old(j)+2.0d0*avdir(j)
            po(j)=pvar(j)
          end do
          fn=fe
        else
          do j=1,ndim
```

```
            pvar(j)=p_old(j)+1.0d0*avdir(j)
            po(j)=pvar(j)
          end do
          fn=fmp
        end if
      end if

      ! adjust boundary values if po(j) is outside boundaries
      do j=1,ndim
        if (po(j).lt.dim(1,j)) dim(1,j)=po(j)
        if (po(j).gt.dim(2,j)) dim(2,j)=po(j)
      end do

      ! drop direction 'ibig' and add new direction to bottom of list
      !      print *,'ibig=',ibig
      do i=ibig,ndim
        if (i.eq.ndim) then
          do j=1,ndim
            xi(j,i)=avdir(j)
          end do
        else
          do j=1,ndim
            xi(j,i)=xi(j,i+1)
          end do
        end if
      end do

      ! write results
      do i=1,ndim
        write(22,143) i,xi(1,i),xi(2,i),xi(3,i),
     &    xi(4,i),xi(5,i),xi(6,i),xi(7,i),xi(8,i)
143     format('direction',I3,8F10.5)
      end do
      write(22,100)
      write(22,135) iter,fn,pvar(1),pvar(2),pvar(3),
     &   pvar(4),pvar(5)
135   format('Optimum new direction',I3,d20.9,5F10.5)
      write(22,100)

      go to 7

    end if
    ! end of iteration (lfinish=0)
    ! ----------------------------

    write(22,137) nsol,iter,fn,pvar(1),pvar(2),pvar(3),
   &  pvar(4),pvar(5)
137 format('Final:nsol,iter',2I4,d20.9,5F10.5)

    call eesolv(pvar,ypar)
    write(22,100)
    write(22,149) ypar(4)
149 format('Performance',d20.9,6F10.5)

    close (22,status='keep')
    end

    ! end of main program
    ! -------------------

    ! ------------------------------------------------------------
    subroutine maximum(nsol,idiv,kdir,ndim,dim,fn,pvar,xi)

    ! get pvar(j) where f is a maximum, by line maximisation in
    ! the direction of xi - return optimum pvar and fn

    ! variable declarations
    double precision xpar(10),ypar(10),xk(30),fk(3)
    double precision pvar(10),xi(ndim,ndim)
    double precision xn,fn,fmp,dim(2,ndim)
    double precision a,b,deldiv,xka(4),fka(4),xna
```

```
131 format(d20.9,5F10.6)
136 format('Out=',10F9.3)
138 format('Newton3',6F9.3)

    ! calculate xk values
    call kvalue(idiv,kdir,ndim,dim,pvar,xi,ik,xk)
    xk(ik+1)=0
    fk(2)=fn

    ! calculate fk for each value of xk
    ! ---------------------------------
    do i=1,3,2

      ! calculate xpar values
      do j=1,ndim
        xpar(j)=pvar(j)+xk(ik-1+i)*xi(j,kdir)
      end do

      print *,'xpar(1-3.1)=',xpar(1),xpar(2),xpar(3)


      ! calculate fk with func
      nsol=nsol+1
      call eesolv(xpar,ypar)
      write(22,131) ypar(4),xpar(1),xpar(2),xpar(3),
     &    xpar(4),xpar(5)

      fk(i)=ypar(4)
      print *,'fn = ',ypar(4)

    end do
    ! end of i in one direction
    ! -------------------------

    ! test if another run is required
    ! -------------------------------
    deldiv=(xk(idiv)-xk(1))/(idiv-1.0d0)
  3 if (fk(1).gt.fk(2)) then
      ik=ik-1
      if (ik.lt.1) then
        do j=idiv,2,-1
          xk(j)=xk(j-1)
        end do
        xk(1)=xk(1)-deldiv
        ik=1
        do j=1,ndim
          a=pvar(j)+xk(1)*xi(j,kdir)
          if (a.lt.dim(1,j)) then
            dim(2,j)=dim(2,j)-(dim(1,j)-a)
            dim(1,j)=a
          else if (a.gt.dim(2,j)) then
            dim(1,j)=dim(1,j)+(a-dim(2,j))
            dim(2,j)=a
          end if
        end do
      end if
      fk(3)=fk(2)
      fk(2)=fk(1)
      do j=1,ndim
        xpar(j)=pvar(j)+xk(ik)*xi(j,kdir)
      end do

      nsol=nsol+1
      print *,'Another run required: decrement ik'
      call eesolv(xpar,ypar)

      write(22,131) ypar(4),xpar(1),xpar(2),xpar(3),
     &    xpar(4)
      fk(1)=ypar(4)
      go to 3
```

```
      else if (fk(3).gt.fk(2)) then
        ik=ik+1
        if (ik.gt.idiv-2) then
          do j=1,idiv-1
            xk(j)=xk(j+1)
          end do
          xk(idiv)=xk(idiv)+deldiv
          ik=idiv-2
          do j=1,ndim
            b=pvar(j)+xk(idiv)*xi(j,kdir)
            if (b.lt.dim(1,j)) then
              dim(2,j)=dim(2,j)-(dim(1,j)-b)
              dim(1,j)=b
            else if (b.gt.dim(2,j)) then
              dim(1,j)=dim(1,j)+(b-dim(2,j))
              dim(2,j)=b
            end if
          end do
        end if
        fk(1)=fk(2)
        fk(2)=fk(3)
        do j=1,ndim
          xpar(j)=pvar(j)+xk(ik+2)*xi(j,kdir)
        end do
        nsol=nsol+1
        print *,'Another run required: increment ik'
        call eesolv(xpar,ypar)
        write(22,131) ypar(4),xpar(1),xpar(2),xpar(3),
     &    xpar(4),xpar(5)
        fk(3)=ypar(4)
        go to 3
      end if
      ! end of test
      ! ------------

      ! get maximum with Newton:
      fmp=fn
      call newton(ik,xk,fk,xn,fn)

      ! save point for next direction:
      do j=1,ndim
        pvar(j)=pvar(j)+xn*xi(j,kdir)
        xpar(j)=pvar(j)
      end do

      ! Newton is only estimation of fn: make thus sure of fn.
      ! (but this step is not strictly necessary)
      print *,'optimum/direction: run number',nsol,xpar(1),xpar(2)
      nsol=nsol+1
      call eesolv(xpar,ypar)
      fn=ypar(4)

      ! check if valid: if not, retain old fn and pvar.
      if (fn.lt.fmp) then
        if (xn.eq.xk(ik+1)) go to 5
        xka(1)=xk(ik)
        fka(1)=fk(1)
        xka(4)=xk(ik+2)
        fka(4)=fk(3)
        if (xn.gt.xk(ik+1)) then
          xka(2)=xk(ik+1)
          fka(2)=fk(2)
          xka(3)=xn
          fka(3)=fn
        else
          xka(2)=xn
          fka(2)=fn
          xka(3)=xk(ik+1)
          fka(3)=fk(2)
        end if
        print *,'call newton3'
```

```
      call newton3(xka,fka,xna)
      do j=1,ndim
        pvar(j)=pvar(j)+(xna-xn)*xi(j,kdir)
      end do
      nsol=nsol+1
      call eesolv(pvar,ypar)
      fn=ypar(4)
      write(22,138) fn,pvar(1),pvar(2),pvar(3),pvar(4),pvar(5)
      if (fn.lt.fmp) then
        print *,'no improvement!'
        do j=1,ndim
          pvar(j)=pvar(j)-xna*xi(j,kdir)
        end do
        fn=fmp
      end if
    end if

  5 print *,'ypar',ypar(4)
    write(22,136) ypar(4)

    return
    end

    !------------- End of subroutine maximum ---------------------


    subroutine kvalue(idiv,kdir,ndim,dim,pvar,xi,ik,xk)

    ! calculate the 'ndiv' amount of xk-values according to the     *
    ! direction 'xi' using the boundary values 'dim'.               *

    double precision xk(30),dim(2,ndim),pvar(10),xi(ndim,ndim)
    double precision a,b,del

    ! check if direction is zero
    do j=1,ndim
      if (xi(j,kdir).eq.0.0) xi(j,kdir)=1.0d-14
    end do

    ! bracket xk(1) and xk(idiv)
    xk(1)=(dim(1,1)-pvar(1))/xi(1,kdir)
    xk(idiv)=(dim(2,1)-pvar(1))/xi(1,kdir)
    do j=2,ndim
      a=pvar(j)+xk(1)*xi(j,kdir)
      b=pvar(j)+xk(idiv)*xi(j,kdir)
      if (a.lt.dim(1,j)) then
        xk(1)=(dim(1,j)-pvar(j))/xi(j,kdir)
      else if (a.gt.dim(2,j)) then
        xk(1)=(dim(2,j)-pvar(j))/xi(j,kdir)
      end if
      if (b.lt.dim(1,j)) then
        xk(idiv)=(dim(1,j)-pvar(j))/xi(j,kdir)
      else if (b.gt.dim(2,j)) then
        xk(idiv)=(dim(2,j)-pvar(j))/xi(j,kdir)
      end if
    end do

    ! calculate remainder xk()
    del=(xk(idiv)-xk(1))/(idiv-1)
    do j=2,idiv-1
      xk(j)=xk(j-1)+del
    end do

    ! calculate ik [linear equation with xk(a) = del*a + b = 0]
    b=xk(1)-del
    a=-b/del
    n=a*1.0

    if (a-n.gt.0.5) then
      ik=n
    else
```

```
  ik=n-1
end if

if (ik.gt.idiv-2) then
  do j=1,idiv-1
    xk(j)=xk(j+1)
  end do
  xk(idiv)=xk(idiv)+del
  ik=idiv-2
end if

if (ik.lt.1) then
  do j=idiv,2,-1
    xk(j)=xk(j-1)
  end do
  xk(1)=xk(1)-del
  ik=1
end if

return
end

! ------------------- End of subroutine kvalue ------------


subroutine newton(ik,xk,fk,xn,fn)

! Use interpolating polinomial of the newton form: second degree.
! Inputs are 3 variables of 'xk' and 3 function values 'fk'.     .
! Outputs are maximum of curve 'fn' at position 'xn'.            .

double precision xk(30),fk(3),const(3)
double precision xn,fn,a

! calculate constants
const(1)=fk(1)
const(2)=(fk(1)-fk(2))/(xk(ik)-xk(ik+1))
a=(fk(2)-fk(3))/(xk(ik+1)-xk(ik+2))
const(3)=(const(2)-a)/(xk(ik)-xk(ik+2))

xn=0.5d0*(xk(ik+1)+xk(ik)-const(2)/const(3))
a=const(3)*(xn-xk(ik))*(xn-xk(ik+1))
fn=const(1)+const(2)*(xn-xk(ik))+a

return
end

! ----------------- End of subroutine newton -----------------


subroutine newton3(x,f,xn)

! Use interpolating polinomial of the newton form: third degree.
! Inputs are 4 variables of 'x' and 4 function values 'f'.      .
! Output is position 'xn' at maximum of curve.                  .

double precision x(4),f(4),const(4)
double precision xn,a,b,c,d,xe,xt

const(1)=f(1)
const(2)=(f(1)-f(2))/(x(1)-x(2))
a=(f(2)-f(3))/(x(2)-x(3))
const(3)=(const(2)-a)/(x(1)-x(3))
b=(f(3)-f(4))/(x(3)-x(4))
c=(a-b)/(x(2)-x(4))
const(4)=(const(3)-c)/(x(1)-x(4))

a=3.0d0*const(4)
b=2.0d0*(const(3)-const(4)*(x(1)+x(2)+x(3)))
c=const(4)*(x(1)*x(2)+x(1)*x(3)+x(2)*x(3))
c=const(2)-const(3)*(x(1)+x(2))+c
```

```
d=b**2-4.0d0*a*c
if(d.le.0.0d0) then
  d=1.0d-16
  print *,'Fault in Newton3: square root'
end if
xe=(-b+dsqrt(d))/(2.0d0*a)
xt=(-b-dsqrt(d))/(2.0d0*a)

if(x(1).lt.x(4)) then
  if(xe.ge.x(1).and.xe.le.x(4)) then
    xn=xe
  else
    xn=xt
  end if
else
  if(xe.le.x(1).and.xe.ge.x(4)) then
    xn=xe
  else
    xn=xt
  end if
end if

return
end

! ------------ End of subroutine newton3 ------------
```

Appendix H

DSP control algorithm (Constant angle current control)

This is the DSP code used to control the PM-assisted RSM and the RSM. The difference between the RSM and PM-assisted RSM code is the decoupling as described in Chapter 3.

```
/*****************************************************************/
/*      controllers.c        (27 February 2004)                  */
/*                ******          *****                          */
/*  (Control program for PI current control of the 110kW RSM)  */
/*                                                               */

/* This program is the control program for a DSP controller     */
/* which implements 2-phase PI current control using constant */
/* current angle current control.                               */

/* This program decouples the mutual inductances.               */
/* The switching is bipolar with a switching frequency          */
/* of 2.5kHz.                                                   */

/*****************************************************************/

#include "F240.h"

volatile unsigned int *EVIMRA     = (volatile unsigned int *) 0x742C;
volatile unsigned int *ACTR       = (volatile unsigned int *) 0x7413;
volatile unsigned int *SACTR    = (volatile unsigned int *) 0x7414;
volatile unsigned int *DBTCON     = (volatile unsigned int *) 0x7415;
volatile unsigned int *COMPR1     = (volatile unsigned int *) 0x7417;
volatile unsigned int *COMPR2     = (volatile unsigned int *) 0x7418;
volatile unsigned int *COMPR3     = (volatile unsigned int *) 0x7419;
volatile unsigned int *SCOMPR1  = (volatile unsigned int *) 0x741A;
volatile unsigned int *SCOMPR2  = (volatile unsigned int *) 0x741B;
volatile unsigned int *SCOMPR3  = (volatile unsigned int *) 0x741C;
volatile unsigned int *COMCON     = (volatile unsigned int *) 0x7411;
volatile unsigned int *GPTCON     = (volatile unsigned int *) 0x7400;
volatile unsigned int *T1CON      = (volatile unsigned int *) 0x7404;
volatile unsigned int *Datain   = (volatile unsigned int *) 0x8000;
volatile unsigned int *DataOut    = (volatile unsigned int *) 0x8001;

int     IaBack, IbBack, IcBack, IdBack, IqBack, DC, steps;
int     IsRef, IdRef, IqRef, Wait;
int     Va, Vb, Vc, Vd, Vq, limit, IsRefZ;
int     DAC1, DAC2, DAC3, DAC4, MdInd, MqInd, MrotorAngleZ, SpeedBack,SpeedRefZ;
int     MrotorAngle, ErotorAngle, CurrentAngle, CurrentAngle2, AddedAngle;
int     angleA1, angleB1, angleB2, angleC1, angleC2, Speed, GSBus, SpeedBack;
int     QOut, DOut, Time, TimeTemp, PITemp, Inductance, SpeedTemp;
int     dIq_dt, dId_dt, IqBackZ, IdBackZ, MdDec, MqDec;
int     PISpeed, PISpeedIn, PISpeedInZ, SpeedRef, ESpeedBack, SpeedVolD, SpeedVolQ;
```

```
int    average1,average2,average3,average4,average5,count,ErotorAngleZ;
float  PISpeedOut, PISpeedOutZ;
float     PIqOutZ, PIqOut, PIqInZ, PIqIn, PIdOutZ, PIdOut, PIdInZ, PIdIn;
extern int          sine(), md(), mq(), fluxd(), fluxq();

void main(void)
{
            /* Inisialize the interupt roetines */

      *EVIMRA |= 0x0001;      /* Enable the PDPINT interupt roetine */

      /* Inisialize the PWM  and deadtime roetines */

      *ACTR   = 0x0666;       /* Make PWM1, PWM3 and PWM5 active low */
                              /* Make PWM2, PWM4 and PWM6 active high */
      /* *DBTCON = 0x80E0;   Deadtime = 6.4us */
      *DBTCON = 0xAAE0;       /* Deadtime = 6.4us */
    *COMCON = 0x0207;         /* Inisialize Compare PWM mode */
      *COMCON = 0x8207;       /* Inisialize Compare PWM mode */

      /* Inisialize the counters */

      *T1PR  = 4000;          /* Period = 2*(50ns x 4000) = 400us */
      *T1CNT = 0;             /* Starting value for counter = 0 */
      *T1CON = 0x0A802;       /* Inisialize Counter #1 */
      *T1CON = 0x0A842;       /* Inisialize Counter #1 */

            /* Inisialize the ADs */

      *OCRA |= 0x070F;              /* Make ADC0, ADC1, ADC8 and ADC9 active */
      ADCTRL2 -> ADCPSCALE = 0;     /* Prescale value = 0 */
      ADCTRL2 -> ADCEVSOC = 0;
      ADCTRL2 -> ADCEXTSOC = 0;
      ADCTRL1 -> suspend_free = 0;
      ADCTRL1 -> suspend_soft = 1;
      ADCTRL1 -> ADCIMSTART = 0;
      ADCTRL1 -> ADCINTEN = 0;      /* Disable interrupt */
      ADCTRL1 -> ADCCONRUN = 0;     /* Single conversion */
      ADCTRL1 -> ADC2EN = 1;                /* Enable ADC2 */
      ADCTRL1 -> ADC1EN = 1;                /* Enable ADC1 */

      /* Resolver inisializing */

      *SYSCR &= 0xFF3F;             /* Make IOPC1 a IO Pin */
      *PCDATDIR = 0x0303;           /* Make IOPC1 (FREEZE) = 1 */
                                    /* Make IOPC0 (ENABLE) = 1 */

      /* Set the COMPR registers for 50% duty cicle */

      *COMPR1  = 2000;
      *COMPR2  = 2000;
      *COMPR3  = 2000;

      /* Inisialize the DACs */

      *PBDATDIR |= 0x7878;          /* Making IOPB3..6 high and outputs */
```

```
        /* Inisialize starting values */

        PIqOutZ = 0;
        PIqInZ  = 0;
        PIdOutZ = 0;
        PIdInZ  = 0;
        IqBackZ = 0;
        IdBackZ = 0;
        Wait    = 0;
        SpeedVolQ = 0;
        SpeedVolD = 0;
        IsRef   = 0;
        IsRefZ  = 0;
        limit   = 700;
        count = 0;
        average1 = 0;
        average2 = 0;
        average3 = 0;
        average4 = 0;
        average5 = 0;
        PISpeedInZ  = 0;
        PISpeedOutZ = 0;
        MrotorAngleZ = 0;
        SpeedRefZ = 0;
        steps = 0;
    MrotorAngle = 0;
        ErotorAngleZ = 0;
        *OCRB &= 0xFF0F;                    /* Making IO1, IO2, IO3, IO4 active */
        *PCDATDIR |= 0xF000;

/*=========================================================*/
/*                    Start of Main Programloop                    */
/*=========================================================*/

        do
                {
                } while (*T1CNT > 5);

        for(;;)

                {
                *PCDATDIR |= 0x0080;

/*-------------------------------------------------------------------------*/
                /* Read data in from ADC5 (Current Ic) and ADC10 (Current Ib) */

                ADCTRL1 -> ADC1CHSEL = 5;           /* Select ADC5 to be read */
                ADCTRL1 -> ADC2CHSEL = 2;           /* Select ADC10 to be read */
                ADCTRL1 -> ADCSOC = 1;                      /* Begin convertion */
                while (ADCTRL1 -> ADCINTFLAG == 0); /* Wait for completion of convertion */
                ADCTRL1 -> ADCINTFLAG = 1;          /* Reset vlag */
                IcBack = *ADCFIFO1;                 /* Read in data */
                IbBack = *ADCFIFO2;

                IcBack = IcBack >> 6;               /* Scaling data to 16 bit value */
```

```
IcBack &= 0x03FF;
IcBack = IcBack - 512;

IbBack = IbBack >> 6;
IbBack &= 0x03FF;
IbBack = IbBack - 512;

/* Read data in from ADC6 (Current Ia) and ADC15 (Rotor speed) */

ADCTRL1 -> ADC1CHSEL = 6;              /* Select ADC5 to be read */
ADCTRL1 -> ADC2CHSEL = 7;              /* Select ADC15 to be read */
ADCTRL1 -> ADCSOC = 1;                          /* Begin convertion */
while (ADCTRL1 -> ADCINTFLAG == 0); /* Wait for completion of convertion */
ADCTRL1 -> ADCINTFLAG = 1;             /* Reset vlag */
IaBack = *ADCFIFO1;                    /* Read in data */
Speed  = *ADCFIFO2;

IaBack = IaBack >> 6;                  /* Scaling data to 16 bit value */
IaBack &= 0x03FF;
IaBack = IaBack - 512;

IaBack = -IcBack - IbBack;

Speed = Speed >> 6;                    /* Scaling data */
Speed &= 0x03FF;
Speed = -(Speed - 512) + 2;            /* From 5V to 2.5V max. */

/* Read data in from ADC1 (Is reference) and ADC11 (DC Bus-voltage)*/

ADCTRL1 -> ADC1CHSEL = 1;              /* Select ADC5 to be read */
ADCTRL1 -> ADC2CHSEL = 3;              /* Select ADC10 to be read */
ADCTRL1 -> ADCSOC = 1;                          /* Begin convertion */
while (ADCTRL1 -> ADCINTFLAG == 0); /* Wait for completion of convertion */
ADCTRL1 -> ADCINTFLAG = 1;             /* Reset vlag */
IsRef = *ADCFIFO1;                     /* Read in data */
GSBus = *ADCFIFO2;

IsRef = IsRef >> 6;                    /* Scaling of data */
IsRef &= 0x03FF;
IsRef = IsRef;                         /* From 5V to 2.5V max. */
SpeedRef = IsRef;

ADCTRL1 -> ADC1CHSEL = 0;              /* Select ADC0 to be read */
ADCTRL1 -> ADC2CHSEL = 7;              /* Select ADC15 to be read */
ADCTRL1 -> ADCSOC = 1;                          /* Begin convertion */
while (ADCTRL1 -> ADCINTFLAG == 0); /* Wait for completion of convertion */
ADCTRL1 -> ADCINTFLAG = 1;             /* Reset vlag */
DC = *ADCFIFO2;                        /* Read in data */
AddedAngle  = *ADCFIFO1;
DC = DC >> 6;                  /* Scaling data to 16 bit value */
DC &= 0x03FF;
DC = DC;
AddedAngle = AddedAngle >> 6;                   /* Scaling data */
AddedAngle &= 0x03FF;
AddedAngle = AddedAngle/100;
```

```
            /* Reading the position of the rotor */

            /* The machanical rotor angle is 0 - 1023 to give an electrical rotor   */
            /* angle of 3*(0 - 1023) per mechanical rotor cycle. The sine table     */
            /* will have a max. magnitude of 255 */

            *PCDATDIR &= 0xFFFD;                    /* Make IOPC1 (FREEZE) = 0 */
            *PCDATDIR &= 0xFFFE;                    /* Make IOPC0 (ENABLE) = 0 */
            MrotorAngle = *Datain;
            *PCDATDIR |= 0x0003;                    /* Make IOPC1 (FREEZE) = 1 */
                                                    /* Make IOPC0 (ENABLE) = 1 */
            MrotorAngle = MrotorAngle >> 6 ;/* Make position a 16-bit value */
      MrotorAngle &= 0x03FF;
            MrotorAngle = MrotorAngle + 405;        /* Zero angle by adding a constant */
            if (MrotorAngle > 1023)
                  {MrotorAngle = MrotorAngle -1023;}
            ErotorAngle = 3*MrotorAngle;
             if (ErotorAngle > 3071)
                  {ErotorAngle = ErotorAngle - 3071;}
            if (ErotorAngle > 2047)
                  {ErotorAngle = ErotorAngle - 2047;}
            if (ErotorAngle > 1023)
                 {ErotorAngle = ErotorAngle - 1023;}

/*-------------------------------------------------------------------------------*/
            /* Calculating the speed of the rotor */

            if ((ErotorAngleZ > 750) & (ErotorAngle < 250))
                  {ErotorAngle = ErotorAngle + 1023;}
            if ((ErotorAngleZ < 250) & (ErotorAngle > 750))
                  {ErotorAngleZ = ErotorAngleZ + 1023;}
            SpeedBack = 1.7*(ErotorAngle - ErotorAngleZ);          /* Convert position to speed */
            count = count + 1;
            if(count = 1)
                  {average1 = SpeedBack;}
            if(count = 2)
                  {average2 = SpeedBack;}
            if(count = 3)
                  {average3 = SpeedBack;}
            if(count = 4)
                  {average4 = SpeedBack;}
            if(count = 5)
                  {average5 = SpeedBack;
                   count = 0;}
            SpeedBack = (average1+average2+average3+average4+average5)/5;


            DAC2 = SpeedBack;
            if (ErotorAngle > 1023)
                  {ErotorAngle = ErotorAngle - 1023;}
            if (ErotorAngleZ > 1023)
                  {ErotorAngleZ = ErotorAngle - 1023;}
            ErotorAngleZ = ErotorAngle;

            ESpeedBack = (32 * SpeedBack) ;
```

```
/*-------------------------------------------------------------------------*/
        /* Calculation of angles for the Park-transformaton */

        angleA1 = ErotorAngle + 256;
        if (angleA1 >1023)
                {angleA1 = angleA1 - 1023;}
        angleB1 = ErotorAngle - 341;
        if (angleB1 < 0)
                {angleB1 = angleB1 + 1023;}
        angleB2 = ErotorAngle - 85;
        if (angleB2 < 0)
                {angleB2 = angleB2 + 1023;}
        angleC1 = ErotorAngle + 341;
        if (angleC1 > 1023)
                {angleC1 = angleC1 - 1023;}
        angleC2 = ErotorAngle +597;
        if (angleC2 >1023)
                {angleC2 = angleC2 - 1023;}

/*-------------------------------------------------------------------------*/
        /* Speed Controller */


        PISpeed = SpeedRef - SpeedBack;          /* Calculating the error */

        if (Wait < 8000)
                {Wait = Wait + 1;
                 PISpeed = 0;}

        PISpeedIn = PISpeed;
        if ((IsRefZ >= limit) || (IsRefZ <= -limit))    /* Stop integrator in limit */
                {PISpeedIn = 0;}

        PISpeedOut = PISpeedOutZ + 5*(PISpeedIn - PISpeedInZ) + 0.00021*PISpeedIn;
                /* U = U(Z-1) + Kp*[I - I(Z-1)] + Ki*T*I */
        PISpeedInZ  = PISpeedIn;
        PISpeedOutZ = PISpeedOut;
        IsRef = (int) PISpeedOut;

        /* IsRef = SpeedRef;  */

        if ((IsRefZ >= limit) || (IsRef <= -limit))
                {IsRef = IsRef + 5*PISpeed ;}
        IsRefZ = IsRef;

        if (IsRef >= limit)
                {IsRef = limit;}
        if (IsRef <= -limit)
                {IsRef = -limit;}

/*-------------------------------------------------------------------------*/
        /* Transforming Is and the angle to Id and Iq */

        if (Wait < 4000)
                {IsRef = 0;}
```

```
                CurrentAngle  = 201 + AddedAngle*1023/360;
                CurrentAngle2 = 457 + AddedAngle*1023/360;
                if (IsRef < 0)
                        {CurrentAngle  = 822 + AddedAngle*1023/360;
                         CurrentAngle2 = 55 + AddedAngle*1023/360;
                         IsRef = IsRef * -1;}


                IsRef = IsRef / 4;
                IqRef = 4 * ((IsRef * sine(CurrentAngle )) / 256);
                IdRef = 4 * ((IsRef * sine(CurrentAngle2)) / 256);

/*--------------------------------------------------------------------------*/
                /* abc-to-qdo transformation (Park-1) */

                IaBack = IaBack/4;
                IbBack = IbBack/4;
                IcBack = IcBack/4;
                IqBack = (IaBack*sine(angleA1)    )/256 + (IbBack*sine(angleB2))/256 +
(IcBack*sine(angleC2))/256;
                IdBack = (IaBack*sine(ErotorAngle))/256 + (IbBack*sine(angleB1))/256 +
(IcBack*sine(angleC1))/256;
                IqBack = 4*(IqBack*2/3);
                IdBack = 4*(IdBack*2/3);


/*--------------------------------------------------------------------------*/
                /* PI Controllers */

                PIdIn = IdRef - IdBack;                 /* D-as Current error */
        PIdOut = PIdOutZ + 7.992*(PIdIn - PIdInZ) + 0.008*PIdIn;
                        /* U = U(Z-1) + Kpd*(I - I(z-1)) + Kid*T*I */
                PIdOutZ = PIdOut;                       /* Saving data for next loop */
                PIdInZ = PIdIn;
                Vd = (int)PIdOut;

                PIqIn = IqRef - IqBack;                 /* Q-as Current error */
                PIqOut = PIqOutZ + 4.995*(PIqIn - PIqInZ) + 0.0005*PIqIn;
                /* U = U(Z-1) + Kpq*(I - I(z-1)) + Kiq*T*I */
                PIqOutZ = PIqOut;                       /* Saving data for next loop */
                PIqInZ = PIqIn;
                Vq = (int)PIqOut;
/*--------------------------------------------------------------------------*/
                /* Decoupling of Speed Voltages */
                if (IdBack < 0)
                        {SpeedVolD = (-1*fluxd(-1*IdBack) * ESpeedBack/28) / 100;}
                else
                        {SpeedVolD = (fluxd(IdBack) * ESpeedBack/28) / 100;}

                if (IqBack < 0)
                        {SpeedVolQ = (-1*fluxq(IqBack)* ESpeedBack/40) / 100;}
                else
                        {SpeedVolQ = (fluxq(IqBack)* ESpeedBack/40) / 100;}

/*--------------------------------------------------------------------------*/
                /* Decoupling of terms */
```

```
                Vd = Vd - SpeedVolQ;  /*  Decouple the Md inductance */
                Vq = Vq +  SpeedVolD; /*   Decouple the Mq inductance */

/*--------------------------------------------------------------------------*/
                /* qdo-to-abc transformation (Park) */

                Vd = Vd / 16;
                Vq = Vq / 16;
                Va = (Vd*sine(ErotorAngle))/256 + (Vq*sine(angleA1))/256;
                Vb = (Vd*sine(angleB1)   )/256 + (Vq*sine(angleB2))/256;
                Vc = (Vd*sine(angleC1)   )/256 + (Vq*sine(angleC2))/256;
                Va = 16*Va;
                Vb = 16*Vb;
                Vc = 16*Vc;

                DAC1 = AddedAngle*50;
                DAC2 = SpeedBack;
                DAC3 = Vq;
                DAC4 = steps;
/*--------------------------------------------------------------------------*/
                /* Giving the values to the PWM part of the DSP */

                *COMPR1  = 2000 - Va;
                *COMPR2  = 2000 - Vb;
                *COMPR3  = 2000 - Vc;

/*--------------------------------------------------------------------------*/
                /* Write to the DACs */

                *PBDATDIR &= 0xFFF7;            /* Select DAC 1 */
                *DataOut  = DAC1*4 + 1000;
                *PBDATDIR |= 0x0008;

                *PBDATDIR &= 0xFFEF;                    /* Select DAC 2 */
                *DataOut  = DAC1*4 + 1000;
                *PBDATDIR |= 0x0010;

                *PBDATDIR &= 0xFFDF;                    /* Select DAC 3 */
                *DataOut  = Vc + 1000;
                *PBDATDIR |= 0x0020;

                *PBDATDIR &= 0xFFBF;                    /* Select DAC 4 */
                *DataOut  = SpeedRef;
                *PBDATDIR |= 0x0040;

                *PCDATDIR &= 0xFF7F;

                do
                        {
                        } while (*T1CNT > 5);

                        }

}
```

Appendix I

LEM

Current Transducer LT 505-S

I_{PN} = 500 A

For the electronic measurement of currents : DC, AC, pulsed..., with a galvanic isolation between the primary circuit (high power) and the secondary circuit (electronic circuit).

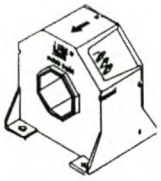

Electrical data

I_{PN}	Primary nominal r.m.s. current			500			A
I_P	Primary current, measuring range			0 .. ± 1200			A
R_M	Measuring resistance @		T_A = 70°C		T_A = 85°C		
			$R_{M\,min}$	$R_{M\,max}$	$R_{M\,min}$	$R_{M\,max}$	
	with ± 15 V	@ ± 500 A_{max}	0	65	0	60	Ω
		@ ± 800 A_{max}	0	15	0	12	Ω
	with ± 24 V	@ ± 500 A_{max}	0	145	15	140	Ω
		@ ± 1200 A_{max}	0	22	15	18	Ω
I_{SN}	Secondary nominal r.m.s. current			100			mA
K_N	Conversion ratio			1 : 5000			
V_C	Supply voltage (± 5 %)			± 15 .. 24			V
I_C	Current consumption			30 (@±24V) + I_S			mA
V_d	R.m.s. voltage for AC isolation test, 50 Hz, 1 mn			6			kV
V_b	R.m.s. rated voltage [1], safe separation			1750			V
	basic isolation			3500			V

Accuracy - Dynamic performance data

X_G	Overall accuracy @ I_{PN}, T_A = 25°C		± 0.6		%
ε_L	Linearity		< 0.1		%
			Typ	Max	
I_O	Offset current @ I_P = 0, T_A = 25°C			± 0.4	mA
I_{OT}	Thermal drift of I_O	- 10°C .. + 85°C	± 0.3	± 0.5	mA
t_r	Response time [2] @ 90 % of $I_{P\,max}$		< 1		µs
di/dt	di/dt accurately followed		> 50		A/µs
f	Frequency bandwidth (- 1 dB)		DC .. 150		kHz

General data

T_A	Ambient operating temperature		- 10 .. + 85		°C
T_S	Ambient storage temperature		- 25 .. + 100		°C
R_S	Secondary coil resistance @	T_A = 70°C	65		Ω
		T_A = 85°C	69		Ω
m	Mass		400		g
	Standards [3]		EN 50178		

Features

- Closed loop (compensated) current transducer using the Hall effect
- Insulated plastic case recognized according to UL 94-V0.

Advantages

- Excellent accuracy
- Very good linearity
- Low temperature drift
- Optimized response time
- Wide frequency bandwidth
- No insertion losses
- High immunity to external interference
- Current overload capability.

Applications

- AC variable speed drives and servo motor drives
- Static converters for DC motor drives
- Battery supplied applications
- Uninterruptible Power Supplies (UPS)
- Switched Mode Power Supplies (SMPS)
- Power supplies for welding applications.

Notes : [1] Pollution class 2. With a non insulated primary bar which fills the through-hole
[2] With a di/dt of 100 A/µs
[3] A list of corresponding tests is available

980708/